

Wright State University

CORE Scholar

[Browse all Theses and Dissertations](#)

[Theses and Dissertations](#)

2016

Determination of Atmospheric Particulate Matter Composition in the Dayton Metro Area

Saagar Mahendra Patel
Wright State University

Follow this and additional works at: https://corescholar.libraries.wright.edu/etd_all



Part of the [Chemistry Commons](#)

Repository Citation

Patel, Saagar Mahendra, "Determination of Atmospheric Particulate Matter Composition in the Dayton Metro Area" (2016). *Browse all Theses and Dissertations*. 1533.
https://corescholar.libraries.wright.edu/etd_all/1533

This Thesis is brought to you for free and open access by the Theses and Dissertations at CORE Scholar. It has been accepted for inclusion in Browse all Theses and Dissertations by an authorized administrator of CORE Scholar. For more information, please contact library-corescholar@wright.edu.

Determination of Atmospheric Particulate Matter Composition in the Dayton Metro Area

A Thesis Submitted in Partial Fulfillment of the Requirements for the Degree of Master of
Science

By

Saagar Mahendra Patel

B.S. Chemistry & B.A. Psychology, Wright State University, 2013

2016

Wright State University

WRIGHT STATE UNIVERSITY

GRADUATE SCHOOL

June 8, 2016

I HEREBY RECOMMEND THAT THE THESIS PREPARED UNDER MY SUPERVISION BY Saagar Mahendra Patel ENTITLED Determination of Particulate Matter Composition in the Dayton Metro Area BE ACCEPTED IN PARTIAL FULFILLMENT OF THE REQUIREMENTS FOR THE DEGREE OF Master of Science.

Audrey McGowin, Ph. D.
Thesis Director

David Grossie, Ph. D.
Department Chair

Committee on Final Examination

Audrey McGowin, Ph. D.

Steven Higgins, Ph. D.

Rachel Aga, Ph. D.

Robert E. W. Fyffe, Ph. D.
Vice President for Research and
Dean of the Graduate School

Abstract

Patel, Saagar Mahendra. M.S., Department of Chemistry, Wright State University, 2016.
Determination of Atmospheric Particulate Matter Composition in the Dayton Metro Area

Quartz filters from high-volume air samplers of particulate matter of a size less than 10 micrometers in diameter (PM_{10}) located in Moraine and Yellow Springs, Ohio, were obtained from the Regional Air Pollution Control Agency and analyzed for levoglucosan, metals, and the EPA 16 priority polycyclic aromatic hydrocarbons (PAHs). Average concentration of levoglucosan increased as ambient temperature decreased. Winter concentrations of levoglucosan for Moraine and Yellow Springs were $39.41 \pm 31.58 \mu\text{g/g}$ and $51.52 \pm 27.44 \mu\text{g/g}$, respectively, which is due to a greater amount of residential wood burning in the colder months. The concentration of biomass burning marker potassium correlated with levoglucosan greater in Moraine ($R^2=0.6097$) than in Yellow Springs ($R^2=0.4035$), indicating the presence of other, most likely agricultural, inputs of potassium in Yellow Springs. The mean concentrations of aluminum in Moraine and Yellow Springs were $184.6 \pm 96.67 \text{ ng/m}^3$ and $138.6 \pm 84.94 \text{ ng/m}^3$, respectively. The mean concentrations of silicon in Moraine and Yellow Springs were $529.1 \pm 228.4 \text{ ng/m}^3$ and $547.4 \pm 203.6 \text{ ng/m}^3$, respectively. Aluminum and silicon represent two commonly found elements in road dust, and their variability indicates the lack of predictability that road dust has on air quality. The quantity of PAHs in Yellow Springs on average was greater than that of Moraine ($2075 \pm 660 \mu\text{g/g}$ vs. $1620 \pm 1324 \mu\text{g/g}$). An incredibly large amount of PAHs measured on 2/16/14 (142.322 ng/m^3), coupled with high $PM_{2.5}$ values, low wind speeds, variable wind direction, low temperature and high humidity around the same date express the possibility that a temperature inversion occurred in Yellow Springs during the middle of February 2014. When compared to the $PM_{2.5}$ & PM_{10} data obtained by RAPCA and this study's analysis, the occurrence of an inversion was supported; however, low levoglucosan and potassium concentrations indicate a minimal contribution from wood smoke. The combined use of three analytical methods allowed for a more comprehensive understanding of atmospheric particulate matter in the Dayton metro area to be achieved.

Table of Contents

INTRODUCTION	1
EXPERIMENTAL	11
Materials.....	11
Sampling	11
Filter Selection.....	12
Workup & Analysis - Levoglucosan	14
Workup & Analysis - PAHs.....	15
Workup & Analysis - Metals	16
Data Analysis	17
RESULTS & DISCUSSION	21
Levoglucosan	21
Potassium	24
Other Metals	26
Dust Metals	31
Trace Metals.....	33
PAHs	34
Weather Analysis.....	41
CONCLUSIONS	49
REFERENCES	51
APPENDIX A – Yellow Springs News Article – February 20th, 2014.....	58
APPENDIX B – Table of Polycyclic Aromatic Hydrocarbons.....	62
APPENDIX C – Filter Choice Data	64
APPENDIX D – Weather and Radiosonde Data	68
APPENDIX E – Standard Operating Procedures	81
APPENDIX F – Levoglucosan Data.....	97
APPENDIX G – Metals Data	99
APPENDIX H – PAH Data	107
APPENDIX I – Discussion on Experimental Issues.....	114

List of Figures

Figure 1. Levoglucosan Synthesis Mechanism.....	5
Figure 2. Sample Radiosonde Plot	19
Figure 3. Potassium Concentration for both Moraine & Yellow Springs.....	24
Figure 4. Potassium Concentration vs. Levoglucosan Concentration in Moraine.....	25
Figure 5. Potassium Concentration vs. Levoglucosan Concentration in Yellow Springs	25
Figure 6. Concentration of PAHs in Moraine	35
Figure 7. Concentration of PAHs in Yellow Springs.....	35
Figure 8. Bivariate plot of $IcdP/(IcdP+BghiP)$ vs. $Flt/(Flt+Pyr)$ for Moraine and Yellow Springs	41
Figure 9. Bivariate plot of $BaA/(BaA+Chr)$ vs. $Flt/(Flt+Pyr)$ for Moraine and Yellow Springs.....	42
Figure 10. Radiosonde Data for 2/9-13/14.....	44
Figure 11. Radiosonde Data for 5/16-17/13.....	47

List of Tables

Table 1. PM₁₀ Filter Choice Dates & PM_{2.5} Spike Dates.....	13
Table 2. Average Concentrations of Levoglucosan.....	21
Table 3. Calculated Contributions wood smoke to PM for Moraine	23
Table 4. Calculated Contributions wood smoke to PM for Yellow Springs	23
Table 5. Concentration of Metals in Moraine per air volume	27
Table 6. Concentration of Metals in Yellow Springs per air volume	29
Table 7. Dust Metal Ranges	32
Table 8. ΣPAH concentrations per sample volume for each date in Moraine.....	37
Table 9. ΣPAH concentrations per sample volume for each date in Yellow Springs	38
Table 10. February 16th 2014 Filter Data	46

Acknowledgments

I would like to acknowledge and thank the following people for their contributions and support for my research. I would first like to thank Dr. Audrey McGowin for guiding me through this difficult process, keeping me focused, and reminding me to always think “big picture.” I would like to thank Andy Roth from RAPCA for providing the filters and answering all of my questions regarding air monitoring. I would like to thank Dr. Steven Higgins, Dr. Rachel Aga, & Dr. Roger Gilpin for serving on my committee. I would also like to Garret van Ness & Joe Solch for providing much appreciated expertise in the use of instrumentation. Finally, I would like to thank my family for their support in all of my endeavors.

Introduction

On December 14th and 15th, 2014, the hourly atmospheric PM_{2.5} (particulate matter that is 2.5 microns or less in diameter) sampler in Yellow Springs registered values in excess of 150 µg/m³, well above the 12 µg/m³ maximum established by the Environmental Protection Agency (Andy Roth, personal communication, Feb 2, 2014). This aberrant event sparked concerns about air quality and the determination of air pollution sources (Yellow Springs News, February 20, 2014, see Appendix A). Although there are no official criteria for establishing when a temperature inversion occurs, it has been accepted that these inversion events adversely affect air quality due to improper interference with air pollution dispersion (Manahan, 2009). The Ohio EPA Regional Air Pollution Control Agency (RAPCA) maintains a network of 30 monitors in 11 locations in southwestern Ohio to measure ozone, carbon monoxide, sulfur and nitrogen oxides, lead, and particulate matter (PM_{2.5} & PM₁₀). The PM_{2.5} samplers monitor the air continuously, and therefore do not produce lasting samples of the air it monitors. However, RAPCA operates two PM₁₀ samplers, one in Yellow Springs and one in Moraine, that collect air samples on quartz fiber filters, which are weighed and kept in secure storage but not routinely chemically analyzed. It is believed that analysis of the PM₁₀ filters will generate data that can be related to the aberrant PM_{2.5} sample data. While no physical samples exist that relate to the PM_{2.5} monitors, the potential exists for the particles on the PM₁₀ filters to provide chemical evidence showing the conditions that existed at times when the high PM_{2.5} readings occurred, and that is the subject of this thesis.

Atmospheric Particulate Matter Sources

Particulate matter is defined by the United States Environmental Protection Agency as a complex mixture of extremely small particles and liquid droplets in the air (USEPA, 2015). PM can vary in size but two classes are considered by the EPA to be most deleterious to human health: PM₁₀, which includes particles equal to or smaller than 10 µm in diameter but larger than 2.5 µm in diameter and PM_{2.5}, which includes particles equal to or smaller than 2.5 µm in diameter. They exist either as solids or liquid droplet aerosols. PM can be in the form of dust or can be derived through incomplete combustion reactions from both natural and anthropogenic sources. Natural sources for PM include volcanoes and forest fires; however, the amount of PM from anthropogenic sources is increasing. Anthropogenic sources include coal-fired power plants, internal combustion engines, and other industrial processes, particularly those that use fossil fuels (Harrison, 2010). In rural areas, residential heating through biomass burning has also been found to contribute substantially to PM (Rick, 2010).

Composition of Atmospheric Particulate Matter

Particulate matter can be composed of metals, inorganic salts, elemental carbon (EC), and organic carbon (OC) compounds. Typically, the largest portion of PM consists of ammonium salts, such as NH₄NO₃ and (NH₄)₂SO₄, and EC/OC (Yin, 2010). Some particles are released directly from the source, while others, particularly ≤ PM_{2.5}, are produced from a gas to particle conversion through chemical reactions (Engel-Cox, 2013). Elemental carbon is released in the form of soot while organic carbon consists of hundreds of different individual compounds (Yin, 2010). A third form of carbon is known as inorganic or carbonate carbon, and is often overlooked as it is found in low quantities in PM_{2.5}. It is mostly associated with calcium and

magnesium salts found in mineral dust which is found in measurable quantities in PM₁₀ (Jankowski, 2008). As it pertains to this study, two forms of organic carbon were selected for analysis: polycyclic aromatic hydrocarbons (PAHs) and anhydrosugars.

Particulate Matter Effects on Human Health

PM₁₀ and PM_{2.5} exposure has been shown to be deleterious to human health.

Particulate matter aerosols that are ≤ 2.5 micrometers in diameter are able to pass through the lining of the lungs and cause serious health problems to the cardiovascular and pulmonary systems. The primary danger of PM pollution is the incredibly small size of the particles. They are easily inhaled, and once inside the human body, are able to pass through the mucosal lining of the trachea and lungs. At this point PM_{2.5} is quickly transported throughout the body via the bloodstream. Concentrations of only 100-200 $\mu\text{g}/\text{m}^3$ can lead to alveolar inflammation, exacerbation of lung disease, an increase in blood coagulability, and an increase in acute cardiovascular events, among other maladies (Seaton, 1995). As the inhalation of PM increases, so does the rate at which asthma attacks, nonfatal heart attacks, arrhythmia, decreased lung function, and respiratory symptoms increase. In addition to these primarily physical effects, the actual chemistry of particulate matter components may pose their own set of dangerous health effects (USEPA, 2000).

The organic carbon portion of PM is made up of hundreds of different compounds of varying degrees of toxicity. Of particular interest are the presence, type, and abundance of polycyclic aromatic hydrocarbons (PAHs). PAHs are a class of molecules made up of two or more fused benzene rings. There exists over 200 of these types of molecules as their ring size, number of rings, and presence of additional functional groups allow for a diverse library of

molecules. They are also considered the most toxic of the hydrocarbon families. PAHs that have greater than 4 rings (e.g. pyrene, fluoranthene) are considered to be more toxic than those with 2-3 rings (e.g. naphthalene, fluorine). The majority of PAH toxicity is associated with disrupting cellular membrane function and membrane-associated enzyme systems. This occurs via the biotransformation of molecules through redox reactions with PAHs (Moyo, 2013). PAHs can be carcinogenic, mutagenic, and teratogenic, and therefore the identification of their sources is of great interest to public health. The EPA has designated 16 PAHs as “priority PAHs” based upon their toxicological profiles. These 16 were chosen because more information is known about them than others; they are suspected to be more harmful than others, they exhibit harmful effects that are representative of PAHs in general, there is greater chance for exposure to these than others, and of all PAHs analyzed, these 16 exhibited the highest concentrations (Ravindra, 2008). A table of the EPA 16 priority PAHs can be found in Appendix B.

PM Sampling Methods

PM₁₀ in the air is monitored by passing large volumes of air through quartz filters. These filters can be subjected to analytical methods that will help discern the types of material comprising the PM, indicating the sources from which they originate. For instance, ratios of certain polycyclic aromatic hydrocarbons (PAHs), often referred to as molecular diagnostic ratios (MDRs), can indicate whether the source was a diesel truck or a coal-fired power plant (Tomashuk, 2012). This method works well with larger PAHs (> 4 rings) and provides pretty reliable information about whether the source was mobile or immobile. Unfortunately, PAHs are reactive in the atmosphere, especially those with 4 or fewer rings, so many PAHs can chemically degrade or transform before they are collected on the filter giving misleading results

(Zhang, 2015). The lower molecular weight PAHs will volatilize at a higher rate from filters than the heavier weight PAHs, which will lead to a skewing of concentrations obtained in samples.

Molecular diagnostic ratios of certain PAHs cannot discriminate well between particles produced by burning coal, wood, or grass. Therefore, the use of other markers, such as anhydrosugars and metals, will help provide a more comprehensive idea of source apportionment. Levoglucosan is a product of the incomplete combustion of cellulose and has been widely accepted as a biomarker for wood burning (Bari, 2009). It is atmospherically stable and shows little or no acid-catalyzed degradation. The proposed mechanism for levoglucosan synthesis is shown below.

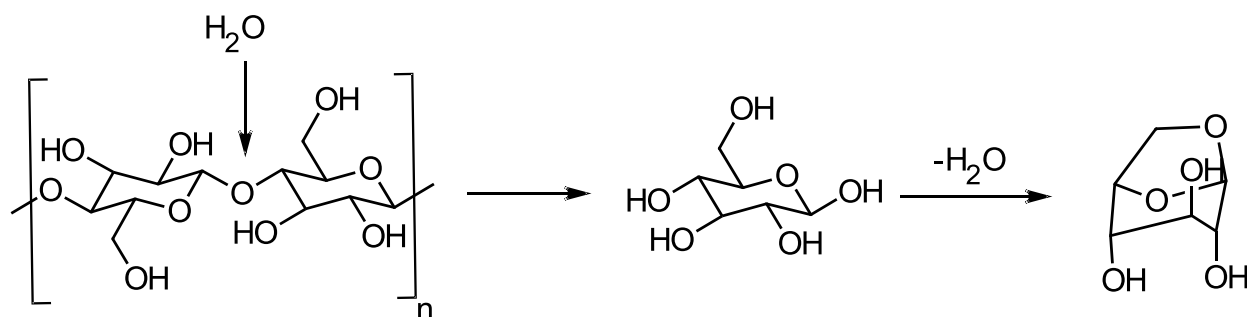


Figure 1: Levoglucosan produced from the combustion of cellulose (Zhang, 2013)

Levoglucosan is the most abundant anhydrosugar measured in PM samples relative to its isomers, galactosan and mannosan (Caseiro, 2009). The amount of levoglucosan relative to total organic matter can be used to quantify the contribution of wood burning to PM (Schmidl, 2008). In addition, potassium has also been utilized as a tracer for biomass burning. As a significant mineral component in plant life, it has been shown to correlate strongly with levoglucosan. However, in PM, the ratio of potassium to levoglucosan changes with the seasons, with higher values in the summer than the winter (Caseiro, 2009). This is hypothesized

to be due to the presence of other potassium sources, including soil resuspension and fertilization (Ward, 2006).

Analysis of Particulate Matter

Analytical methods for the determination of PAHs predominantly use gas chromatography-mass spectrometry (GC/MS) (Ravindra, 2008). Li et al analyzed the concentration of 21 PAHs from stack flue gas to determine the relative contributions of 2-ring, 3-ring, and 4-ring PAHs in industrial boilers using GC/MS. It was determined that the fuel source correlated highly with ring number (Li, 1999). Using GC/MS, Fabbri et al determined the concentration of PAHs in the combustion of Miocene lignites and corroborated previous studies' findings that lignite smoke emits PAHs at low concentrations, with phenanthrene, fluoranthene, and pyrene exhibiting the highest concentrations (Fabbri, 2009).

Levoglucosan has been successfully quantified using GC/MS; however, derivitization with trimethylchlorosilane is required when using GC (Caseiro, 2009). Bari et al quantified the concentration of levoglucosan and its isomers in wood smoke using the derivitization method with GC/MS and observed that levoglucosan was observed in high concentrations in all ambient PM₁₀ samples (Bari, 2010). Simpson and coworkers developed a comprehensive method to determine levoglucosan concentrations in PM using GC/MS. Using a surrogate standard for quality control purposes, the method developed exhibited robust reproducibility in the quantification of levoglucosan in both PM_{2.5} and PM₁₀ (Simpson, 2004). By comparing the quantity of PM and levoglucosan produced from different woods, multiplicative constants that convert levoglucosan concentration to wood-fire contributions to PM₁₀ were developed (Schmidl, 2008). It is important to note that the percentages of levoglucosan in PM ranged from

4-15% w/w, and therefore the constants derived should be cautiously applied and should only provide estimates for source apportionment (Schmidl, 2008).

Kolker et al analyzed polytetrafluoroethylene (PTFE) sample filters using Inductively Coupled Plasma-Mass Spectrometry (ICP-MS) and were able to attribute metals to different PM generating sources (Kolker, 2013). The concentration of metals in fireplace combustion was determined by Alves et al, finding that potassium, lead, aluminum, manganese, and strontium were present in all samples, with potassium composing the majority of the metals found (Alves, 2011). Van der Merwe et al utilized ICP-MS to quantify the amount of iron being delivered to the Kerguelen Plateau and associated higher iron concentrations in air samples to the dissolution of shelf sediments (van der Merwe, 2015). Kabir et al measured the concentration of trace metals in various charcoal products using Inductively Coupled Plasma – Atomic Emission Spectrometry (ICP-AES) and determined that concentrations varied widely across metal types and charcoal products, which was due to differences in the manufacturers' choice of raw materials and production processes (Kabir, 2011). The effect of urban, natural, and mixed metal contributions to street dust has been investigated via ICP-AES by de Miguel et al, who were able to point to soil resuspension and/or mobilization as the most important source for natural elements, such as aluminum, manganese, and sodium, while urban traffic and corrosion of building materials are the primary source for 'urban' metals, such as barium, cadmium, lead, and titanium (de Miguel, 1997). Amato et al measured the impact of road dust emissions on PM₁₀ and PM_{2.5} in rural, urban, and industrial sites using ICP-AES to quantify metals. It was discovered that road dust increased PM₁₀ levels on average by 21-35% at traffic

sites, 29-34% at urban background sites, 17-22% at urban industrial sites, and 9-22% at rural sites (Amato, 2014).

Meteorological Effects on Atmospheric Particulate Matter

Periods of high particulate matter concentrations have been previously linked to certain meteorological factors, namely wind speed, temperature, and humidity (Zhang, 2015). Low wind speed allows for pollutants to accumulate near the Earth's surface, which leads to high concentrations of PM. (Chaloulakou, 2003). Though higher atmospheric temperatures contribute to convective mixing of the air, it also can increase the rate at which secondary aerosols are formed (Papanastasiou, 2007). Humid air allows for the adsorption of water on a particle's surface, thereby increasing its size – this has the added effect of reducing the particle's lifetime (Nilsson, 1994). By comparing weather parameters to criteria air pollutant concentrations, Zhang and coworkers observed that wind speed was inversely correlated to PM concentration, relative humidity positively correlated with PM concentration, and temperature correlated with PM concentration, though the direction and strength of the relationship varied between cities in China (Zhang, 2015). Though a similar study in Abu Dhabi found the same strong correlation between PM₁₀ and temperature, it also found a weak positive correlation between PM₁₀ and wind speed, and also found a strong positive correlation between PM₁₀ and humidity, but only when humidity was below 25% (Al Jallad, 2013).

Another form of PM analysis compares air quality to weather data to determine the existence of temperature inversion events. A temperature inversion occurs when a layer of colder air is trapped below a layer of warmer air. The convective mixing of air allows for the circulation and dilution of particulate matter; however, when cold and dense air is unable to

mix with warmer air above it, any PM trapped in the colder layer will remain there (Wallace, 2006). Inversions can exist anywhere in the troposphere but are more likely to be harmful as the inversion layer approaches altitudes of population centers. Surface temperature inversions are common and frequently extend at least 100 meters up in the atmosphere (Eagleman, 1985). Inversions frequently occur at night when the earth loses heat in the form of infrared radiation to the lower atmosphere and typically last until 10-11 a.m., when the heat from solar radiation restarts the mixing of air (Eagleman, 1985). Inversions also occur more frequently in colder climates because they radiate off more heat than they absorb, leading to stratification in the troposphere (Lutgens, 1986).

The cold dense layer of air in an inversion can remain in an area for as little as a few hours or as long as a few weeks (Jacob, 1999). The mass of cold air and particulate matter tends to remain for longer periods of time in valleys and lowlands, so it is unfortunate that valleys are favored for manufacturing due to their easy access to water transport because it also contributes greatly to air pollution in those areas (Lutgens, 1986).

The atmosphere generally cools as altitude increases; the mathematical relation for this is given by the lapse rate and is expressed as temperature loss per altitude increase (Lutgens, 1986). For the troposphere, the average lapse rate is 6.5 °C/km. Classical inversion parameters include both the intensity, ΔT (the increase of temperature between the bottom and top of the inversion layer), and the depth, ΔH (the thickness of the inversion layer) (Kassomenos, 2014). An inversion is present when the lapse rate falls below 0 °C/km (Eagleman, 1985). High humidity, low temperatures, low wind speed with changing direction, and clear skies are positively correlated with temperature inversions (Enz, 2014). As stated before, inversions are

naturally present and may exist at multiple regions of the troposphere; however, the presence of a negative lapse rate at low altitudes coupled with high humidity, low temperatures, weak and variable winds represent clues to the presence of an inversion event (Vihma, 2011).

Present Study

This study endeavors to determine a relationship between the air quality in the Dayton, Ohio area by determining the chemical composition of particulate matter that is $\leq 10 \mu\text{m}$ in diameter. It involves the analysis of 25 filters obtained by RAPCA over a period of two years in two distinct locations: the village of Yellow Springs, a small, rural town with low industrial activity and the city of Moraine, a suburb with a greater degree of traffic and industrialization. It is theorized that analysis of PAHs, levoglucosan, and metals can help elucidate the cause behind the high $\text{PM}_{2.5}$ spike events in Yellow Springs. The concentrations of the 16 priority PAHs and the biomass burning marker levoglucosan were quantified using GC/MS. The concentrations of 16 metals, including trace, dust-related, and biomass burning-related metals, were quantified using ICP-OES. The detection of chemical and meteorological patterns were observed using a combination of: the concentrations determined via instrumentation, radiosonde data obtained from the National Oceanic and Atmospheric Administration, weather data obtained from The Weather Underground, and $\text{PM}_{10}/\text{PM}_{2.5}$ measurements from the Regional Air Pollution Control Agency. This study will also provide a holistic view of the differences in the chemical characteristics of particulate matter between Moraine and Yellow Springs.

Experimental

Materials

A set of calibration standards composed of the EPA 16 priority PAHs (naphthalene, acenaphthene, acenaphthylene, fluorene, phenanthrene, anthracene, fluoranthene, pyrene, benz[a]anthracene, chrysene, benzo[b]fluoranthene, benzo[k]fluoranthene, benzo[a]pyrene, dibenz[a,h]anthracene, benzo[ghi]perylene, indeno[1,2,3-cd]pyrene) and six deuterated standards (acenaphthene-d10, chrysene-d12, 1,4-dichlorobenzene-d4, naphthalene-d8, perylene-d12, phenanthrene-d10) were prepared from a 200 ppm ($\mu\text{g/L}$) (Accustandard, New Haven, CT) mixed standard and 4000ppm ($\mu\text{g/L}$) (Accustandard, New Haven, CT) mixed standard in a 1:1 hexane:dichloromethane solution mixture by volume. A set of calibration standards of levoglucosan was prepared using solid 1,6-Anhydro- β -D-Glucose (Sigma-Aldrich Co., St. Louis, MO) dissolved in ethyl acetate. For the PAH analysis, the internal standard used was p-terphenyl (Sigma-Aldrich Co., St. Louis, MO). All solvents were GC-grade and were purchased from Sigma-Aldrich or Thermo Fisher Scientific.

Sampling

Particulate matter sampling was performed in two locations: Moraine, OH [39° 42' 52.21" N, 84° 13' 04.93" W] and Yellow Springs, OH [39° 48' 29.96" N, 83° 53' 13.53" W]. An Anderson instruments model 1200 high-volume sampler (Anderson Instrument Company, Fultonville, NY) placed on top of the Moraine firehouse and a Wedding & Associates model 600 high-volume sampler (Wedding & Associates, Fort Collins, CO) placed on top of the Yellow Springs Government office were used to perform the sampling. The Moraine sampler is located near both Interstate-75 and a large train junction, while the Yellow Springs sampler is located

between a light-traffic road and State Highway 68. Adjacent to the Yellow Springs sampler is a wood-fired pottery kiln that is typically fired once a month for 24 hours. There is also a cement kiln 5 miles west of the Yellow Springs sampler.

Both samplers were equipped with EPM 2000 grade high purity quartz microfiber filters (Whatman Inc., Picataway, NJ). To measure PM_{10} , both samplers use a gravimetric filter-based technique. Each filter is allowed to run for 6 days, after which a mass of PM_{10} deposited and volume of air filtered is recorded. Before inserting the filters into the samplers, the clean filters were dried in desiccators for 24 hours, after which they were weighed on a Mettler type H balance. The tare weight was recorded and after use were folded so that the particle-covered side was facing itself, re-dried in a desiccator, and re-weighed to record the mass of PM_{10} . The filter was then stored in a dry envelope in a cool and dark place until further use. Once the folders were obtained, one 3.2-cm by 20.4-cm and one 3.0-cm x 20.4-cm portion of the filter were cut and placed in separate pre-cleaned and labeled 120-mL amber jars and stored in the refrigerator for ICP and PAH analysis, respectively. For levoglucosan analysis, a 2.5-cm x 20.4-cm portion was cut instead. The relative sizes chosen were expected to result in adequate sensitivities for the methods selected.

Filter Selection

In order to select filters for analysis and validate the use of PM_{10} filters for information on $PM_{2.5}$, air quality data was obtained from the RAPCA website for $PM_{2.5}$ and PM_{10} in both Yellow Springs and Moraine. Overlaying the plot of PM_{10} and $PM_{2.5}$ for each site showed that there was some association between particulate matter size and concentration. By visual observation, there appears to be similar trends in Yellow Springs $PM_{2.5}$ and PM_{10}

concentrations; this relationship is weaker in the Moraine data. One important deviation between Yellow Springs PM_{2.5} & PM₁₀ data can be observed for the December 14th, 2014 spike event. As the samples are collected by different methods (a six-day sample for PM₁₀ and a continuous monitor for PM_{2.5}), the data cannot be analyzed through direct means. The PM₁₀ samplers operate on a six-day run-cycle so appropriate dates were chosen that bracketed spike events. Certain PM₁₀ filters without PM_{2.5} spike events were purposefully chosen to determine differences in PM₁₀ composition when PM_{2.5} values were within USEPA limits.

Table 1. PM₁₀ Filter Date Ranges and PM_{2.5} Spike Dates. M and YS indicate the sample filter the sample filter location of Moraine and Yellow Springs, respectively.

PM ₁₀ Date Ranges	PM 2.5 Spike Dates & Locations & Concentrations (µg/m ³)
1/22/13-1/27/13	*
2/3/13-2/8/13	2/5 - 25.7 (M)
5/16/13-5/21/13	5/17 - 26.2 (M)
8/20/13-8/25/13	*
12/6/13-12/11/13	*
12/18/13-12/23/13	*
12/24/13-12/29/13	12/27 - 25.5 (M)
2/10/14-2/15/14	2/10 - 40.3 (YS), 2/11 - 26.3 (YS), 2/12 - 38.8 (YS), 2/13 - 32.9 (YS), 2/10 - 32.7 (M), 2/12 - 33.5 (M), 2/13 - 38.9 (M)
2/16/14-2/21/14	2/16 - 25.4 (YS), 2/16 - 26.2 (M)
3/12/14-3/17/14	*
7/10/14-7/15/14	7/12 - 27.0 (YS), 7/12 - 25.8 (M)
8/5/14-8/20/14	8/18 - 26.8 (YS)
12/13/14-12/18/14	*

*No PM_{2.5} spikes occurred during these ranges

The overlaid PM₁₀ and PM_{2.5} figures can be found in Appendix C. The PM_{2.5} spike can be clearly seen in Appendix C - Figure 1.

The 25 filters were evenly split over two years between Moraine and Yellow Springs. They represented a collection of both 'aberrant' weather periods and 'normal' weather periods.

Abnormally high PM_{2.5} concentrations in December-February and July-August indicated seasonal trends, and as such, filters were chosen during those months. Filters were chosen to encompass the entire year for comparison. Three individual portions of each filter were cut and placed into separate 150-mL amber jars for levoglucosan, PAH and metals analysis.

Sample Work-Up & Analysis - Levoglucosan

To the filter portions assigned for levoglucosan GC/MS analysis, 50 mL of ethyl acetate was added to 150-mL amber jars and the jar lids were tightened. The jars were placed in a 150 W FS14H ultrasonicator (Fisher Scientific, Fairlawn, NJ) for 10 minutes. The supernatant in the amber jar was pipetted into a 250-mL round bottom flask using a Pasteur pipette and the extraction process was repeated once more using fresh solvent aliquots. The combined volumes were reduced to ~5 mL by rotary evaporation. The samples were then filtered using a 10-mL syringe and a 0.45- μ m PTFE filter into a graduate centrifuge tube. With N₂ vapor, the samples were reduced to a final volume of 2.0 mL. An aliquot of 500 μ L was transferred to a silitated GC vial and reduced to dryness with N₂ vapor. The sample was then re-dissolved in 500 μ L pyridine and a 100- μ L aliquot of bistrifluoroacetamide (BSTFA) with 1% trimethylchlorosilane (TMCS) was added to each. Samples were vortexed for 1 minute and then heated for 1 hour at 78 °C on a heating block. The samples were allowed to cool, after which they were brought to dryness with N₂ vapor and re-dissolved in 500 μ L toluene. Samples were analyzed on the Agilent Technologies 7820A GC System & 5975 Series MSD. The program used to analyze the data was MS Data Review 7.0.1. The Gas Chromatograph was run on split-less mode with a flow rate of 1 mL/min and an injection volume of 1 μ L. The carrier gas was helium. Samples on the GC/MS were run in Selective Ion Monitoring (SIM) mode. The following ions were selected: 73,

129, 147, 204, 217, and 333. These represent the predominant peaks for the triple silylated derivative of levoglucosan. Each sample was injected in duplicate. The GC oven temperature ramp procedure went as follows: the initial temperature was 50 °C and was held for 5 min. The temperature was raised to 300 °C at a rate of 15 °C/min and was held for 15 min. The coefficient of determination obtained from the calibration curve of levoglucosan was 0.978. The limit of detection was established as the lowest standard concentration for derivitized levoglucosan. The lowest standard concentration was 1 ppm, which converts into 1 µg/kg of PM mass and 1 ng/m³ of air. The Standard Operation Procedure can be found in Appendix E.

Sample Work-Up & Analysis - PAHs

To the filter portions assigned for PAH GC/MS analysis, 5 µL of the deuterated standard was spiked onto the dirty side of each filter and allowed to air dry for 20 minutes. Afterwards, 60 mL of a 1:1 hexane:dichloromethane mixture was added to the jars and the lids were tightened. The jars were placed in an ultrasonicator for 10 minutes, and then the supernatant was pipetted into a 250-mL round bottom flask. This extraction was repeated once more and the combined volumes were reduced to ~5 mL using rotary evaporation. The samples were then filtered into a graduated centrifuge tube using a 10-mL syringe and a 0.45-µm PTFE filter and the volume was brought to 2.0 mL using N₂ gas. Five hundred microliters were transferred to a GC vial for analysis while the remainder was transferred to a storage vial. To each sample, 50 µL of a 10-ppm p-terphenyl solution was added as an internal standard. Samples were analyzed on the Agilent Technologies 7890B GC & 240 Ion Trap GC/MS. The program used to analyze the data was MSD Chemstation E.02.01.1177. The Gas Chromatograph was run on splitless mode with a flow rate of 1 mL/min and an injection volume of 1 µL. The carrier gas was

helium. Samples on the GC/MS were run in Selective Ion Monitoring (SIM) mode. Each sample was injected in duplicate. The GC oven temperature ramp procedure was as follows: the initial temperature was 40 °C and was held for 5 min. The temperature was raised to 180 °C at a rate of 10 °C/min and was held for 5 min. The temperature was then raised to 250 °C at a rate of 10 °C/min and was held for 5 min. The temperature was then raised to 320 °C at a rate of 10 °C/min and was held for 15 minutes, giving a final runtime of 58 minutes. The coefficients of determination obtained from the 16 PAH calibration curves were 0.8583 to 0.9980 with two outliers of 0.6876 & 0.6968. The two outliers represent benzo[b]fluoranthene and dibenz[a,h]anthracene, two PAHs that elute towards the end of the column run and therefore provide variable peak areas. The limits of detection were established as the lowest standard concentration for each PAH. The lowest standard concentration for each PAH was 100 ppb, which converts into 100 µg/kg of PM mass and 100 ng/m³ of air. The Standard Operation Procedure can be found in Appendix E.

Sample Work-Up & Analysis - Metals

To the filter portions assigned to ICP analysis, samples were placed in individual beakers with 15 mL ASTM Type I water and 15 mL of concentrated Trace Metal Grade nitric acid (Fisher Scientific). Samples were heated at 95±5 °C for one hour to digest the filter until 5 mL of supernatant remained. Once cooled, the supernatant was decanted into a glass funnel with a Whitman #42 filter into a 100-mL volumetric flask. The filter contents were diluted to the mark with ASTM Type I water. A portion of each sample was then transferred to test tubes for ICP analysis. Samples were analyzed on the Varian Instruments 710-ES ICP-OES. The software used to analyze the data was ICP Expert II 1.1.2. The ICP samples were analyzed in triplicate with a

read time of 10 s and a dilution factor of 1. All other values remained unchanged. A total of 16 analytes were measured, which are as follows: aluminum, arsenic, calcium, cadmium, chromium, copper, iron, potassium, magnesium, manganese, sodium, nickel, lead, silicon, strontium, and zinc. The wavelengths associated with each can be found in appendix C. The coefficients of determination obtained from the 16 calibration curves were 0.9849 to 0.9999. The limits of detection were established as the lowest standard concentration for each analyte. The lowest standard concentration for aluminum, arsenic, cadmium, chromium, copper, iron, manganese, nickel, lead, strontium and zinc was 10 ppb, which converts into 10 $\mu\text{g}/\text{kg}$ of PM mass and 10 ng/m^3 of air. The lowest standard concentration for silicon was 20 ppb, which converts into 20 $\mu\text{g}/\text{kg}$ of PM mass and 20 ng/m^3 of air. The lowest standard concentration for calcium, potassium, magnesium, and sodium was 100 ppb, which converts into 100 $\mu\text{g}/\text{kg}$ of PM mass and 100 ng/m^3 of air. The Standard Operation Procedure can be found in Appendix E.

Data Analysis

Calibration curves were generated for each of the 16 EPA priority PAHs, deuterated PAHs, levoglucosan, and metals. Deuterated standards were not used to correct the priority PAH concentrations. The range of coefficients of determination for the six deuterated standards was 0.03 – 0.56, therefore the poor quality of data as a result of experimental error was not adequate enough to use for recovery calculations. As such, reported PAH values represent those obtained directly from the filter sample, giving concentrations that would be less than corrected concentrations.

Bivariate graphs were generated by plotting the ratios of different isomeric PAHs. Concentrations of metals were compared to concentrations of organic compounds to

determine if any correlation exists. Once all sample analyte concentrations were calculated, a series of comparisons were made based upon previous studies as well as weather-related comparisons.

Weather data (temperature, humidity, wind speed and direction) was obtained from Weather Underground, which obtains its data from Automated Surface Observation System (ASOS) systems located at regional airports. The weather data obtained for Moraine and Yellow Springs came from the Dayton-Wright Brothers Airport (KMGY) and the Springfield-Beckley Municipal Airport (KSGH). Radiosonde data were obtained from the National Oceanic and Atmospheric Association (NOAA) and Earth System Research Laboratory (ESRL) Database. The radiosonde balloon is located in Wilmington, Ohio (KILN-72426) and provides readings at 0000 UTC and 1200 UTC (Coordinated Universal Time), which correlate to 8 p.m. and 8 a.m. local time. Temperature, dew point and winds with altitude are recorded and presented in the form of a skew-t plot.

In order to determine the existence of an inversion during the selected filter dates, radiosonde data was analyzed for the presence of the textbook definition of a negative lapse rate, which is defined as an increase in temperature with respect to an increase in height.

Mathematically, it is given by the following equation:

$$\text{Eqn 1: } \Upsilon = -\frac{dT}{dz}$$

where the lapse rate Υ is given in temperature (T) units divided by height (z) units. Visually, it can be seen on NOAA radiosonde figures as a red line directed towards the top right of the chart. An example of a positive and negative lapse rate are shown below, with the positive and negative lapse rates circled in green and purple, respectively.

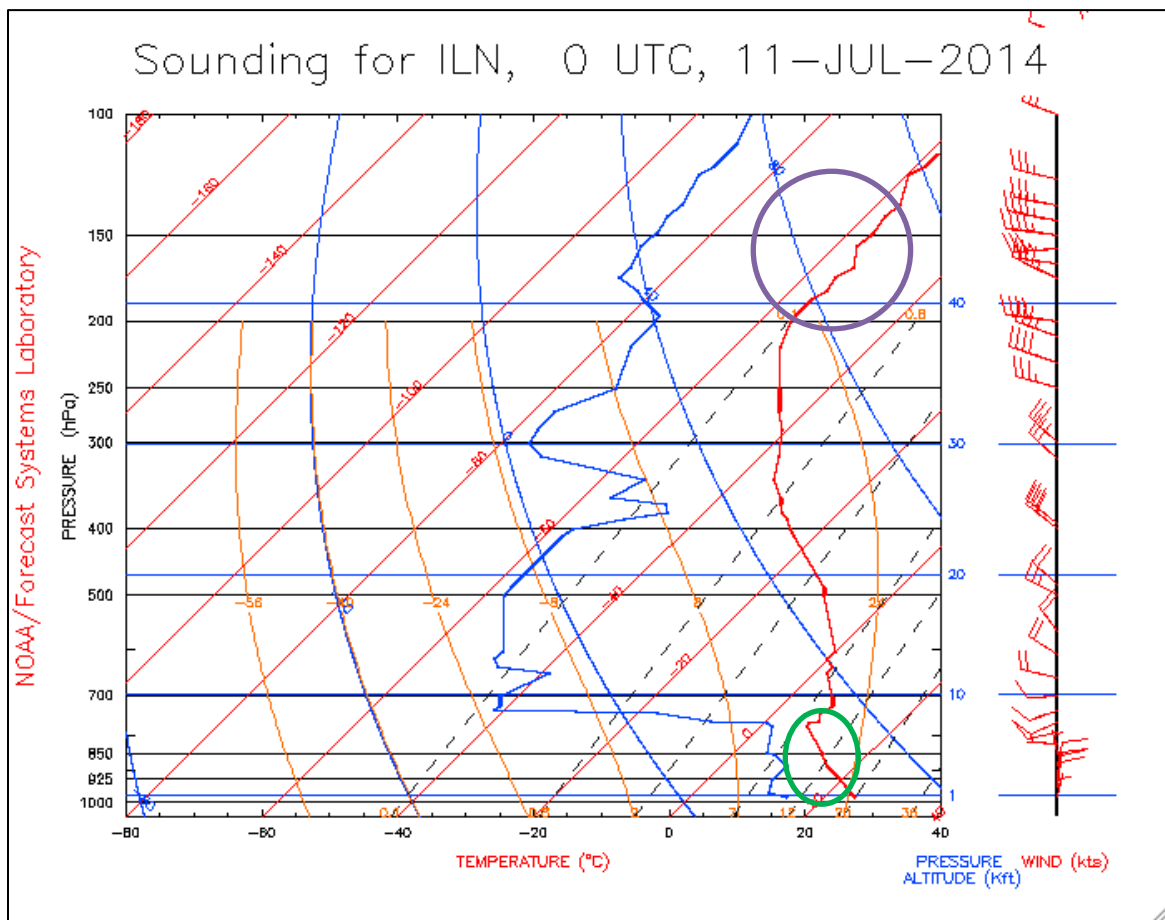


Figure 2. Sample Radiosonde data depicting a positive (green circle) and negative (purple circle) lapse rate. Figure was obtained from the NOAA/ESRL Radiosonde Database. Accessed on 9/3/2015

On July 11th, 2014 a positive lapse rate was observed at low altitudes – this is to be expected as it was a warm summer day and therefore the earth was radiating excess heat to the atmosphere. At high altitudes, a negative lapse rate is observed, which is also common, as the effect of solar radiation on atmospheric temperature becomes more pronounced at higher altitudes. Once a negative lapse rate at low altitudes was confirmed via visual observation, the temperature, humidity, wind speed, wind direction, PM_{2.5} concentration, PM₁₀ concentration, and the concentrations of the PAHs, levoglucosan, and metals during that time period were

cross-referenced to either to substantiate or weaken the claim that a true inversion had taken place during that given time. If a true inversion event occurred, the concentrations of all analytes would be high, the temperature would be generally lower than usual, the humidity would be high, and the wind speed and direction would be weak and variable.

Results & Discussion

Levoglucosan Analysis

The levoglucosan concentrations in the air filters are given below and can also be found in Appendix F.

Table 2. Levoglucosan Average Concentrations for Moraine and Yellow Springs, separated by season. Winter was defined as all dates within November-February. Summer was defined as all dates with May-August.

	Average (μg levoglucosan/ g PM_{10})	Standard Deviation (μg levoglucosan/ g PM_{10})
Moraine	39.4	31.6
Yellow Springs	46.9	27.1
	Summer Average ($\mu\text{g/g}$)	Summer Standard Deviation ($\mu\text{g/g}$)
Moraine	29.7	23.5
Yellow Springs	37.6	24.9
	Winter Average ($\mu\text{g/g}$)	Winter Standard Deviation ($\mu\text{g/g}$)
Moraine	39.4	31.6
Yellow Springs	51.5	27.4

For Moraine, concentrations ranged from 10.2 $\mu\text{g/g}$ to 110 $\mu\text{g/g}$, while for Yellow Springs, concentrations ranged from 15.8 $\mu\text{g/g}$ to 88.2 $\mu\text{g/g}$ (levoglucosan mass/ PM_{10} mass). The total and seasonal averages and standard deviations for each site are given in Appendix F, Table E2. The average concentrations for Moraine and Yellow Springs are 39.4 ± 31.6 $\mu\text{g/g}$ and 46.9 ± 27.1 $\mu\text{g/g}$, respectively. For the summer, which was defined as April to September, the average concentrations for Moraine and Yellow Springs are 29.7 ± 23.5 $\mu\text{g/g}$ and 37.6 ± 24.9 $\mu\text{g/g}$, respectively. For the winter, which was defined as October to March, the average concentrations for Moraine and Yellow Springs are 39.4 ± 31.6 $\mu\text{g/g}$ and 51.5 ± 27.4 $\mu\text{g/g}$, respectively. Although the concentration of levoglucosan in Yellow Springs was consistently

greater than that of Moraine, the high standard deviations indicate a high level of variance between sampling dates. The PM concentration of levoglucosan in rural areas such as Yellow Springs was expected to be greater than that of an urban area like Moraine, especially during winter months due to the greater amount of wood burning in rural areas compared to urban areas (Caseiro, 2009 & Bari, 2009). However, the highest concentration observed for either location was on the filter date of 12/24/13 in Moraine (for the dates 12/24-12/29) where the concentration of levoglucosan was measured to be 110 µg/g. As there was no known large-scale fire event between the dates of 12/24 and 12/30, the cause for this anomalous value is unknown. It should be noted, however, that that filter encompasses air quality for 12/24 to 12/29, and the increase may be related to the Christmas holiday. Isolated events such as grass fires can also affect levoglucosan concentrations in area- and time-specific ways, further increasing variability and decreasing predictability in the analysis.

Caseiro et al developed multiplier constants to calculate relative contributions of wood smoke to the total particulate matter (PM) from wood smoke utilizing levoglucosan concentrations (Caseiro, 2009). The equation, followed by the calculated concentrations in mass per volume units, are given below.

$$\text{Eq 1: Wood smoke PM} = \text{levoglucosan} * 10.7$$

Table 3. Calculated concentrations of levoglucosan and wood smoke contributions to particulate matter (PM) for Moraine.

Dates	Original concentration of levoglucosan (ng/m ³)	Concentration of wood smoke contribution to PM (ng/m ³)	Percent of wood smoke in PM sample (%)
01/22/13	0.34	3.60	0.026
02/03/13	0.34	3.59	0.046
05/16/13	0.35	3.76	0.013
08/20/13	0.41	4.44	0.013
12/06/13	0.59	6.29	0.031
12/18/13	0.60	6.43	0.040
12/24/13	1.10	11.77	0.118
02/10/14	0.38	4.09	0.011
02/16/14	0.36	3.84	0.014
03/12/14	< 0.06	< 0.64	< 0.003
07/10/14	0.59	6.28	0.035
08/15/14	1.04	11.18	0.066
12/13/14	0.85	9.09	0.051

Table 4. Calculated concentrations of levoglucosan and wood smoke contributions to particulate matter (PM) for Yellow Springs.

Dates	Original concentration of levoglucosan (ng/m ³)	Concentration of wood smoke contribution to particulate matter (ng/m ³)	Percent of wood smoke in PM sample (%)
01/22/13	0.72	7.71	0.094
02/03/13	0.39	4.12	0.027
05/16/13	0.34	3.64	0.018
08/20/13	0.34	3.67	0.017
12/06/13	0.81	8.69	0.077
12/18/13	0.40	4.25	0.033
12/24/13	0.38	4.09	0.044
02/10/14	*	*	*
02/16/14	< 0.06	< 0.64	< 0.003
03/12/14	0.33	3.54	0.032
07/10/14	0.63	6.73	0.070
08/15/14	0.59	6.31	0.039
12/13/14	†	†	†
* No filter was received from RAPCA			
† Sample was lost during workup			

The multiplier constants were derived empirically by Caseiro by calculating concentrations of levoglucosan, OC, OM & PM from controlled burns. They are dependent upon the type of wood, as softer woods such as spruce skew the constants downward while harder woods such as beech skew them upward. Even taking into account that these represent conservative values, the small initial concentration of levoglucosan indicates that overall, wood burning did not contribute significantly to the particulate matter load in neither Moraine nor Yellow Springs.

Potassium Analysis

The concentration for potassium, a marker for wood burning, which ranged from 9960 $\mu\text{g/g}$ to 30600 $\mu\text{g/g}$ (analyte mass/ PM_{10} mass), is plotted against time in Figure 3.

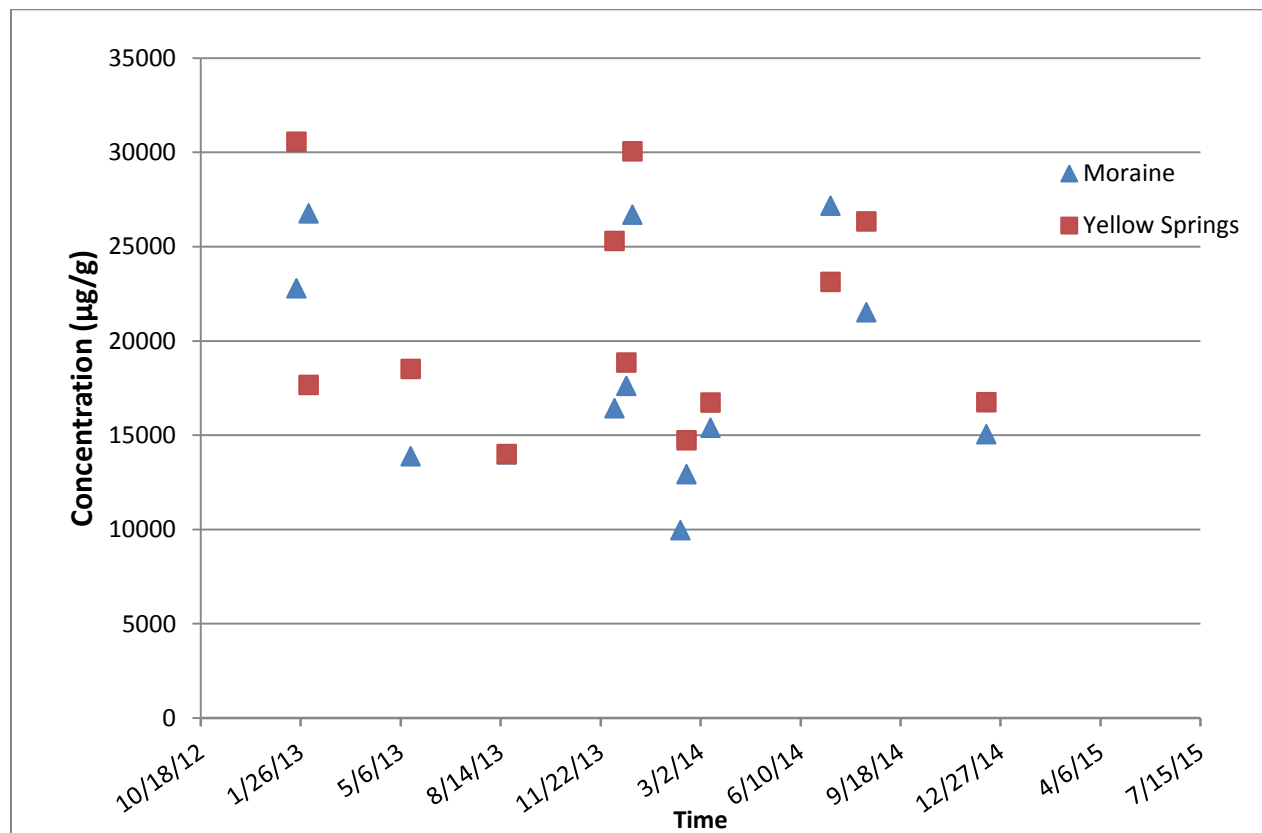


Figure 3. Plot of concentration of potassium vs. time

At both sites, peaks can be observed during winter months and during the fall-to-winter transition. During colder months, the potassium concentration is expected to increase due to the influx of wood burning (Urban, 2012). To determine the relationship between potassium and levoglucosan, a linear regression was performed between the two concentrations at both sites which is shown below and can also be found in Appendix G.

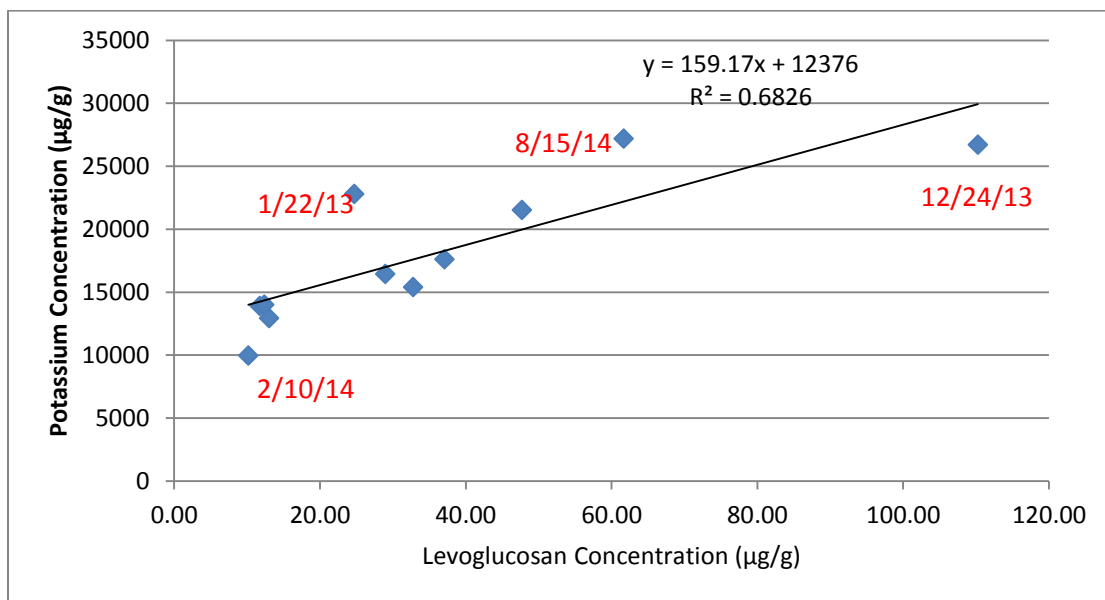


Figure 4. Plot of potassium concentration versus levoglucosan concentration in Moraine.

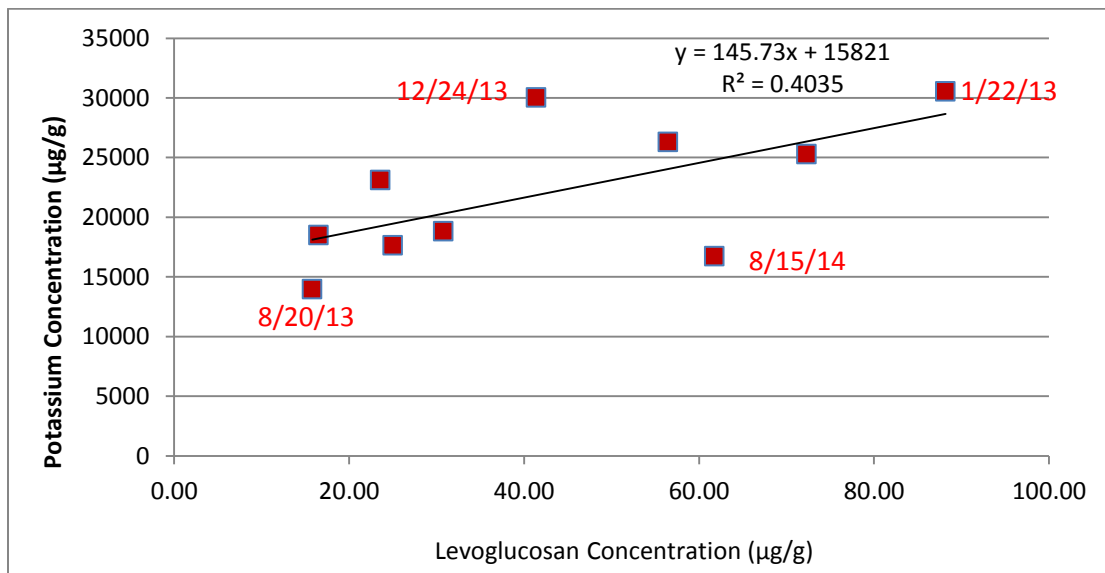


Figure 5. Plot of potassium concentration versus levoglucosan concentration in Yellow Springs.

In Moraine, a moderate linear correlation ($R^2 = 0.610$) was observed while a weaker correlation in Yellow Springs ($R^2 = 0.404$) was observed. The difference in sampling site location and correlation is indicative of other sources of potassium in the Yellow Springs. The most common sources are agrarian techniques used to increase soil fertility. Fertilization, the application of natural or synthetic products to increase the nutrient content of soil, and soil resuspension, the process of mixing soil to circulate nutrients would therefore have a confounding effect on the linearity of potassium-levoglucosan relationship (Urban, 2014).

Individually, neither location exhibited seasonal differences with respect to the potassium/levoglucosan ratio. There was no clustering or skewing of values when compared to the date of filter acquisition, indicating that the relationship between these two analytes is not affected by time. By comparing the ratio of potassium to levoglucosan on specific dates and determining whether both sites had a similar value, a possible situational or regional effect could be demonstrated. Once again, this was not found in the data, indicating a high degree of variability between the two sample sites.

Other Metals Analysis

Tables 2 and 3 represent the Moraine and Yellow Springs concentrations of metal analyte per cubic meter of air that passed through the filter. This conversion was necessary to compare with previous studies on metal concentration in PM_{10} . The concentrations of trace metals in the air were well below EPA national air quality standards. Metals that contribute to the formation of dust, such as aluminum, silicon, iron, and calcium were detected at measureable levels; their concentrations and suggested sources are given below.

Table 5. Concentration of Metals in Moraine per air volume

	Analytes (ng/m ³)												
	Al	As	Ca	Cu	Fe	K	Mg	Mn	Na	Pb	Si	Sr	Zn
01/22/13	> 10239.4	> 10	4579	149.0	554.3	309.7	386.7	> 10	3316	> 10	693.2	> 10	55.03
02/03/13	102.6	> 10	12460	33.59	212.5	207.5	> 100	> 10	4090	> 10	388.7	> 10	33.05
05/16/13	20.5	> 10	2492	6.7	42.49	41.49	> 100	> 10	818	> 10	77.73	> 10	6.61
08/20/13	377.6	> 10	3958	259.9	2215	468.1	604.0	22.60	1921	> 10	569.3	> 10	200.5
12/06/13	112.8	> 10	848.4	78.34	342.0	333.0	> 100	> 10	5413	> 10	450.0	> 10	60.77
12/18/13	213.7	> 10	1554	100.3	677.0	285.3	> 100	23.00	6669	> 10	533.9	> 10	76.69
12/24/13	129.0	> 10	1173	86.1	240.9	266.3	> 100	> 10	2340	> 10	229.5	> 10	52.68
02/10/14	198.2	> 10	1343	116.6	563.8	373.9	> 100	14.48	6874	> 10	910.2	> 10	78.59
02/16/14	177.6	> 10	900.7	84.81	322.7	355.1	> 100	> 10	4544	> 10	677.0	> 10	55.78
03/12/14	178.1	> 10	825.9	41.27	316.9	260.6	> 100	> 10	3777	> 10	383.6	> 10	42.07

Table 5 (continued)

	Analytes (ng/m3)										
	Standard Deviation	Mean	12/13/14	08/15/14	07/10/14						
	92.67	184.6	112.7	284.3	253.0	Al					
	> 10	> 10	> 10	> 10	> 10	As					
	3156	2855	858.3	3292	2832	Ca					
	62.57	98.04	79.96	129.3	108.6	Cu					
	580.5	619.4	328.2	1179	1058	Fe					
	113.7	309.2	267.9	364.5	486.3	K					
	208.2	400.0	> 100	491.6	117.6	Mg					
	7.888	13.46	> 10	> 10	> 10	Mn					
	1902	3550	1866	2095	2427	Na					
	> 10	> 10	> 10	> 10	> 10	Pb					
	228.4	529.1	496.1	689.1	780.2	Si					
	19.69	20.88	> 10	> 10	> 10	Sr					
	138.1	103.0	53.56	537.1	86.05	Zn					

Table 6. Concentration of Metals in Yellow Springs per air volume

	Analytes (ng/m ³)									
02/16/14	12/24/13	12/18/13	12/06/13	08/20/13	05/16/13	02/03/13	01/22/13			
102.6	121.2	153.7	115.5	124.5	397.3	116.2	157.3	Al		
> 10	> 10	> 10	> 10	> 10	57.22	> 10	> 10	As		
483.5	640.2	967.9	575.3	765.4	1204	661.2	1684	Ca		
> 10	> 10	> 10	> 10	> 10	> 10	> 10	> 10	Cr		
103.9	85.89	30.08	119.5	93.40	121.1	25.29	49.63	Cu		
180.4	133.1	254.8	201.6	306.7	587.7	166.4	178.5	Fe		
361.9	277.5	243.4	284.2	303.9	382.1	272.4	249.8	K		
> 10	> 10	> 10	> 10	> 10	> 10	> 10	> 10	Mn		
2544	2469	3801	1975	1692	2078	2181	2534	Na		
> 10	> 10	> 10	> 10	11.45	1.116	> 10	> 10	Pb		
893.0	144.4	831.9	554.9	560.7	518.9	556.7	350.9	Si		
62.45	68.60	72.92	54.93	72.68	45.50	39.97	33.79	Zn		

Table 6 (continued)

Standard Deviation	Mean	12/13/14	08/15/14	07/10/14	03/12/14	Analytes (ng/m ³)											
						Al	As	Ca	Cr	Cu	Fe	K	Mn	Na	Pb	Si	Zn
84.94	138.6	86.13	111.4	104.2	72.63												
N/A	57.22	> 10	> 10	> 10	> 10												
335.5	822.6	682.3	795.5	854.2	557.9												
	62.50	> 10	> 10	> 10	> 10												
34.0	69.52	55.43	41.54	63.26	45.18												
123.6	227.7	175.3	209.3	212.0	126.8												
46.07	282.6	271.2	251.5	257.8	235.1												
> 10	2.735	> 10	> 10	> 10	> 10												
550.2	2328	2097	1786	2188	2595												
	> 10	> 10	> 10	> 10	> 10												
203.6	547.4	521.2	390.3	714.8	531.2												
17.61	50.21	59.07	24.64	23.37	44.56												

Dust Metals Analysis

The mean concentrations of aluminum in Moraine and Yellow Springs were 185 ± 96.7 ng/m^3 and 139 ± 84.9 ng/m^3 , respectively (analyte mass/ volume of air sampled). Aluminum has been used previously as a marker for soil/road dust materials in the modeling of $\text{PM}_{2.5}$ (Harrison, 2010). The reported values were much smaller than those reported by Harrison et al ($100\text{--}200$ ng/m^3 vs. $400\text{--}600$ ng/m^3).

The mean concentrations of silicon in Moraine and Yellow Springs were 529 ± 228 ng/m^3 and 547 ± 204 ng/m^3 , respectively. Silicon has also been used previously as a marker for soil/road dust materials in the modeling of $\text{PM}_{2.5}$ (Harrison, 2010). The values obtained here were much larger than those reported by Harrison et al ($500\text{--}600$ ng/m^3 vs. $200\text{--}400$ ng/m^3).

The concentration of iron, linked to crustal/dust materials, in Moraine and Yellow Springs were 619 ± 581 ng/m^3 and 22.7 ± 124 ng/m^3 , respectively. The difference between the two concentrations is similar to, though much greater than, Harrison et al's finding of higher iron concentration in urban areas (102 ng/m^3) relative to rural areas (87.1 ng/m^3) (Harrison, 2010).

The wide range in aluminum, silicon, and iron demonstrates elements originating from dust materials can vary widely, even within the same location (Karanasiou, 2009).

The mean concentrations of calcium for Moraine and Yellow Springs were 2860 ± 3160 ng/m^3 and 822 ± 335 ng/m^3 , respectively. Concentrations reported by Argyropoulos and coworkers were in the range of $900\text{--}3300$ ng/m^3 , indicating that the values reported here are comparable to literature values (Argyropoulos, 2013). The abnormally large standard deviation for the Moraine site is due to the sample obtained on February 3rd, 2013, where calcium

concentration was 12,500 ng/m³. Calcium is considered a crustal/dust element which explains the magnitude and variations in its concentrations; however, it has also been linked to more anthropogenic sources such as calcium soaps in automotive lubricating oils (Harrison, 2003). Thus, the higher calcium concentration in Moraine is likely due to anthropogenic inputs into the atmosphere. The presence of a cement kiln in Yellow Springs was expected to increase the concentration of calcium in PM as it is a primary component of cement (Naik, 2003). Galindo and colleagues reported PM_{2.5}-derived calcium concentrations near a cement works at 1,030 ng/m³, indicating that the additional contributor to calcium concentration in the Moraine area dwarfs the cement kiln's contribution (Galindo, 2011).

A table of the maximum, minimum and range for aluminum, calcium, iron and silicon is given below.

Table 7. Dust Metal Maxima, Minima & Range for Moraine & Yellow Springs

Moraine (ng/m ³)	Al		Ca		Fe		Si	
Max	377.6	1/22/13	4579.3	1/22/13	2214.9	2/16/14	910.2	1/22/13
Min	20.5	2/10/14	825.9	2/16/14	42.5	8/15/14	77.7	8/20/13
Mean	184.6		2055		619.4		529.1	
Yellow Springs (ng/m ³)	Al		Ca		Fe		Si	
Max	397.3	2/16/14	1683.7	1/22/13	587.7	2/16/14	893.0	12/18/13
Min	72.6	5/16/13	483.5	2/16/14	126.8	5/16/13	144.4	12/24/13
Mean	138.6		822.6		227.7		547.4	

Seasonal effects can be observed in both Moraine and Yellow Springs for iron as maximum values were obtained in colder months and minimum values were observed in warmer months. The higher relative maxima for iron in Moraine can be attributed to the higher degree of industrialization in the city; the presence of freight rail and the continuous highway

construction in the area are significant contributors to iron dust in the air (Harrison, 2010). The range in calcium concentrations is very large indicating that contributors to calcium concentration in PM can vary greatly. Galindo's reported mean for calcium (1030 ng/m^3) is similar to what was observed in Yellow Springs; this similarity is reflected by both sites being located near cement works (Galindo, 2011). There is no direct explanation as to why Moraine's calcium concentration is much greater; it is likely that the cause may be similar to that of iron – higher degrees of industrialization will lead to higher concentrations of calcium in PM (Harrison, 2010). The aluminum range is similar in both sites, signifying similarities in aluminum contribution to PM between Moraine & Yellow Springs. The concentration of each element was plotted with respect to time (Figure G4-G9) to determine the existence of any seasonal effects in PM_{10} . For aluminum (Figure G4), concentrations peaked during mid-December in both Moraine and Yellow Springs. Relative maxima were observed for both sites during the summer months as well. This was also observed in silicon (Figure G7) and sodium (Figure G8).

Trace Metals Analysis

In Moraine, concentrations of cadmium and chromium were below the limit of detection and were therefore not reported. Similarly in Yellow Springs, the concentrations for cadmium, chromium, magnesium, and strontium were below the limit of detection and were not reported. Neither cadmium nor chromium was detected at either site.

Trace metal concentrations for Moraine were in the order of $\text{Zn} (103 \text{ ng/m}^3) > \text{Cu} (98.0 \text{ ng/m}^3) > \text{Sr} (20.9 \text{ ng/m}^3) > \text{Mn} (13.5 \text{ ng/m}^3) > \text{Pb} (3.21 \text{ ng/m}^3) > \text{As} (0.461 \text{ ng/m}^3)$. Trace metal concentrations for Yellow Springs were in the order of $\text{Cu} (98.0 \text{ ng/m}^3) > \text{Cr} (62.5 \text{ ng/m}^3) > \text{Zn} (50.2 \text{ ng/m}^3) > \text{Pb} (6.29 \text{ ng/m}^3) > \text{Mn} (2.74 \text{ ng/m}^3)$. These values are similar in magnitude to

those obtained by Brown et al, which summarized the PM₁₀ contribution from metals in urban, industrial, roadside, and rural sites from 1980-2005 (Brown, 2008). However, the detection of a trace amount of arsenic occurred on May 16th 2013 represented the only amount greater than the limit of detection.

The regulations enforced by the National Ambient Air Quality Standards (NAAQS) lists lead as the only heavy metal of concern in ambient air, with concentrations not to exceed 150 ng/m³ (OhioEPA, 2014). As the reported concentrations of lead and the other heavy metals fall far below that, it is reasonable to assume the air quality with respect to the reported metals analysis falls within EPA acceptable limits. The concentration of metals that can adversely affect health, such as lead or cadmium, were either so low that they fell below the limit of detection, or low enough that they pose no health risk. The presence of moderate concentrations of dust-contributing metals represents an obvious but minimal concern to health quality as the concentrations are not threatening. The high variability in their concentrations with respect to location denotes the difficulty to which source apportionment can be applied to dust metals, as particulate matter that is formed in one location can spread to far distances. This is known as fugitive dust.

PAH Analysis

Moraine and Yellow Springs filter concentrations are shown below for the sixteen EPA 'priority PAHs' analyzed.

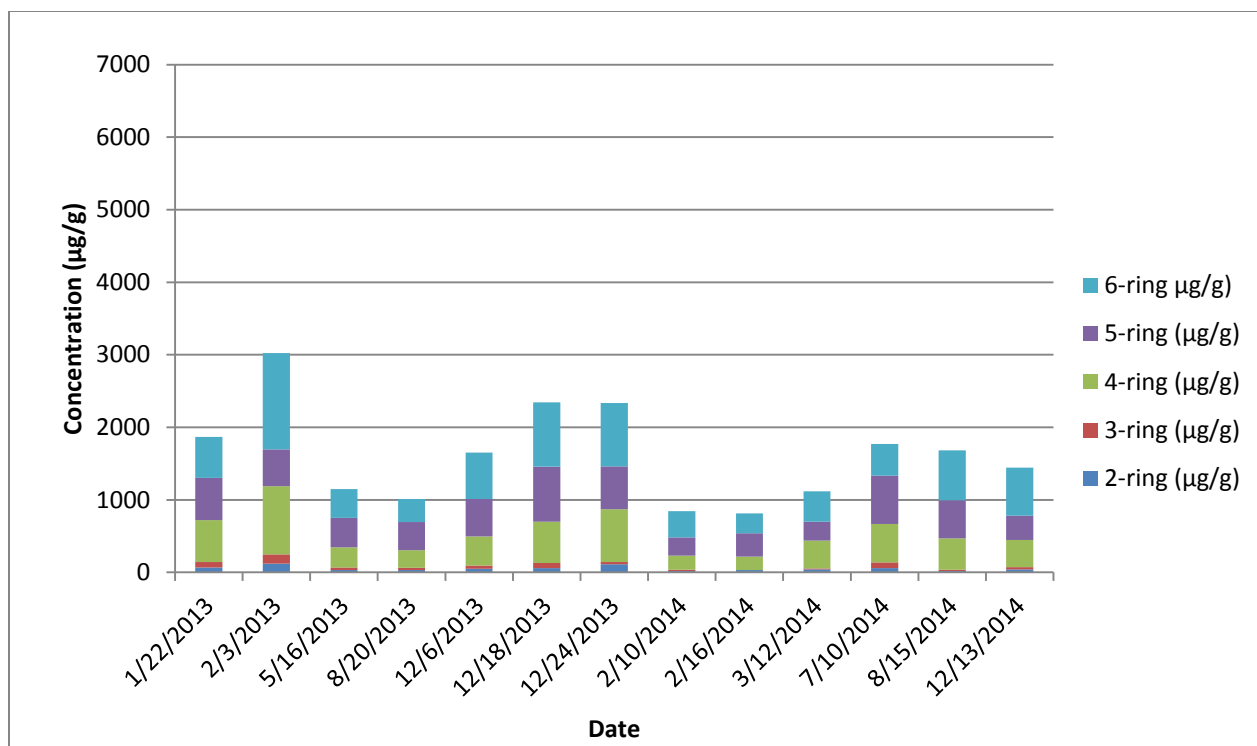


Figure 6. Concentration of PAHs in Moraine, grouped by number of rings

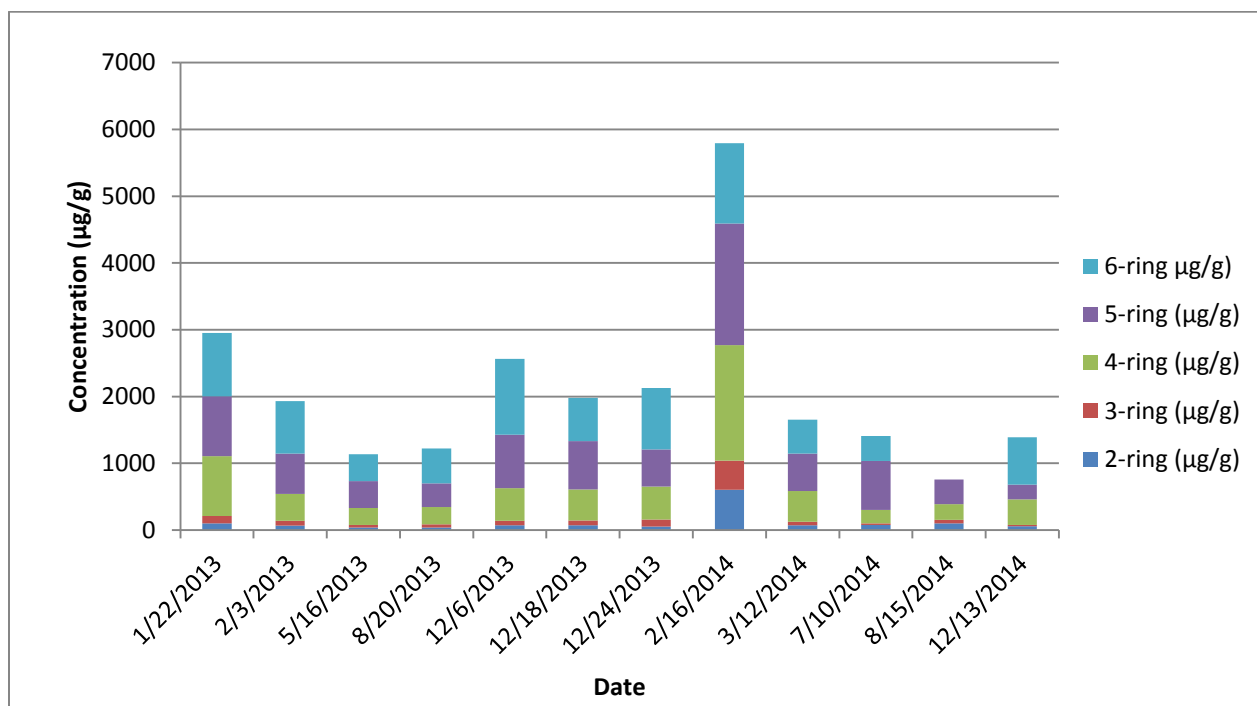


Figure 7. Concentration of PAHs in Yellow Springs, grouped by number of rings

Σ PAH concentrations ranged from 812 $\mu\text{g/g}$ to 3030 $\mu\text{g/g}$ (mass of PAHs/ PM_{10} mass) for Moraine and 758 $\mu\text{g/g}$ to 5790 $\mu\text{g/g}$ for Yellow Springs. The average and standard deviation Σ PAH for Moraine and Yellow Springs are $1620 \pm 660 \mu\text{g/g}$, and $2080 \pm 1320 \mu\text{g/g}$, respectively. The relative abundance of the PAHs generally increased with ring size as would be expected for PM_{10} samples. For Moraine, the abundance as a function of percent PAH, was as follows: 3-ring (2.72%) < 2-ring (3.26%) < 4-ring (27.7%) < 5-ring (29.0%) < 6-ring (37.3%). For Yellow Springs, the abundance as a function of percent PAH, was as follows: 3-ring (4.41%) < 2-ring (5.44%) < 4-ring (25.2%) < 5-ring (32.3%) < 6-ring (32.7%). When compared to the work done by Tomashuk et al, the values are largely different. For example, the PAH mass fraction of PM_{10} in Moraine had a range of 171 $\mu\text{g/g}$ to 641 $\mu\text{g/g}$, while the PAH mass fraction of PM_{10} in Yellow Springs was 77.4 $\mu\text{g/g}$ to 838 $\mu\text{g/g}$. Previously measured PAH concentrations in Moraine and Yellow Springs are shown to be much lower than current values. For example, the sum of 4-ring PAHs observed in Moraine in August 2009 was 1.756 $\mu\text{g/g PM}$ while the same analyte measured on August 2013 was 241.1 $\mu\text{g/g PM}$, a two hundred-fold increase over four years. This trend was repeated in December with a 2009 value of 1.426 $\mu\text{g/g PM}$ and a 2013 value of 401 $\mu\text{g/g PM}$.

By analyzing the Σ PAH concentrations per sample volume, the values are aligned more closely with the literature. The means and standard deviations of Moraine and Yellow Springs Σ PAH/sample air volume are $28.5 \pm 5.75 \text{ ng/m}^3$ and $32.4 \pm 35.2 \text{ ng/m}^3$. The tables of Σ PAH concentrations per sample volume for each location are given below.

Table 8. ΣPAH concentrations per sample volume for each date in Moraine

Moraine - Concentration given in ng/m ³							
	Total	6-ring	5-ring	4-ring	3-ring	2-ring	
01/22/13	25.419	7.706	7.913	7.858	1.008	0.934	
02/03/13	23.461	10.301	3.958	7.289	0.978	0.934	
05/16/13	34.293	11.935	12.084	8.302	0.955	1.017	
08/20/13	33.853	10.579	13.085	8.074	0.951	1.163	
12/06/13	33.502	12.983	10.427	8.139	0.959	0.994	
12/18/13	37.966	14.345	12.301	9.241	1.140	0.940	
12/24/13	23.304	8.732	5.865	7.262	0.346	1.099	
02/10/14	31.636	13.428	9.522	7.344	0.616	0.726	
02/16/14	22.294	7.483	8.880	5.065	0.000	0.867	
03/12/14	18.924	7.095	4.376	6.506	0.252	0.696	
07/10/14	31.691	7.849	11.904	9.496	1.355	1.087	
08/15/14	28.487	11.637	8.860	7.332	0.352	0.306	
12/13/14	25.725	11.826	5.941	6.697	0.554	0.707	
Average	28.50	10.45	8.85	7.59	0.73	0.88	
Standard Deviation	5.75	2.47	3.09	1.16	0.40	0.23	

Table 9. ΣPAH concentrations per sample volume for each date in Yellow Springs

Yellow Springs - Concentration given in ng/m ³							
	Total	6-ring	5-ring	4-ring	3-ring	2-ring	
12/13/14	22.502	11.501	3.577	6.172	0.298	0.953	
08/15/14	7.244	0.000	3.535	2.228	0.524	0.956	
07/10/14	15.676	4.144	8.148	2.252	0.296	0.837	
03/12/14	23.252	7.124	7.893	6.473	0.737	1.025	
02/16/14	142.322	29.561	44.718	42.491	10.709	14.843	
12/24/13	19.651	8.491	5.142	4.543	0.977	0.498	
12/18/13	25.555	8.351	9.351	6.012	0.915	0.927	
12/06/13	28.806	12.772	8.983	5.467	0.781	0.803	
08/20/13	26.503	11.334	7.733	5.573	0.995	0.868	
05/16/13	23.446	8.349	8.228	5.303	0.761	0.805	
02/03/13	29.746	12.105	9.281	6.199	1.137	1.024	
01/22/13	24.115	7.726	7.334	7.343	0.884	0.828	
Average	32.40	10.12	10.33	8.34	1.58	2.03	
Standard Deviation	35.15	7.10	11.02	10.87	2.89	4.04	

Dejean et al quantified atmospheric PAH in Toulouse, France, and reported Σ PAH at 22 ng/m^3 (Dejean, 2008). As molecular weight increases, the volatility of molecule decreases, and therefore the amount of 2- and 3-ring PAHs will not be representative of their true fraction in PM_{10} (Moyo, 2013). The sampling method also can confound the data. For the quantification of PAHs, there are two forms of sampling: active and passive. Active sampling, used in this study, involves the use of high-volume vacuums to draw air through a semi-permeable membrane – in this case, a quartz filter. Smaller PAHs, such as naphthalene, will pass through this filter at a higher rate than larger PAHs, such as pyrene, and will therefore skew results toward the larger PAHs (Tomashuk, 2012).

Tables H6 and H7 give the average winter and summer concentrations of PAHs for both sites. Winter mean Σ PAH values for Moraine and Yellow Springs are $27.9 \pm 5.73 \text{ ng/m}^3$ and $41.8 \pm 44.5 \text{ ng/m}^3$, respectively. Summer mean Σ PAH values for Moraine and Yellow Springs are $29.5 \pm 6.32 \text{ ng/m}^3$ and $19.2 \pm 7.80 \text{ ng/m}^3$, respectively. The difference in summer concentrations can be explained by the difference in activity in Moraine and Yellow Springs. The greater vehicular and train emissions that Moraine experiences during the summer will likely lead to higher PAH concentrations relative to rural Yellow Springs. The difference in winter concentrations can primarily be explained by a period of poor air quality from 2/16/14 to 2/22/14. On that date, Σ PAH for Yellow Springs was 142 ng/m^3 , 240% larger than the mean of 41.8 ng/m^3 . In Moraine during the same time period, the Σ PAH was 22.3 ng/m^3 , signifying a location-specific air quality event in Yellow Springs.

Tables H8 & H9 contain the individual PAH concentrations in $\mu\text{g/g PM}_{10}$ for both sites. Of particular interest is the concentrations obtained on 2/16/2014 in Yellow Springs: The largest

proportions of PAHs collected were: benzo[b]fluoranthene (23%), fluoranthene (14%), dibenz[a,h]anthracene (14%), pyrene (10%), and benzo[a]pyrene (9%). Moyo et al reported that a ratio of fluoranthene to the sum of fluoranthene and pyrene that is greater than 0.40 can be linked to pyrogenic sources as opposed to petrogenic sources (Moyo, 2013). The obtained ratio was 0.57, indicating that on 2/16/14, the PM contribution from PAHs primarily were created as a result of combustion processes. Yu et al reported that high concentrations of benzo[b]fluoranthene are also associated with pyrogenic sources, lending further evidence that the PAH load for the 2/16/14 date was due to the combustion of carbon sources other than petroleum (Yu, 2015). Another source apportionment study by Gao et al compared vehicular emission, coal combustion, and biomass burning markers to PAHs, and determined that larger ring PAHs are generated via coal combustion rather than vehicular emissions and combustion of biomass (Gao, 2015). The above listed high PAHs for the February 16th 2014 date are composed of 4-6 ringed PAHs, indicating that coal combustion, rather than wood smoke, contributed to the high PM spike event.

Table H8 provides the values for a set of PAH ratios used to develop bivariate plots. The values of indeno[1,2,3,-cd]pyrene (IcdP), benzo[ghi]perylene (BghiP), fluoranthene (Flt), pyrene (Pyr), Benz[a]anthracene (BaA), and chrysene (Chr) were first collected and then the following ratios were generated:

$$\text{Eq. 2: } \text{IcdP} / (\text{IcdP} + \text{BghiP}) \text{ vs. } \text{Flt} / (\text{Flt} + \text{Pyr})$$

$$\text{Eq. 3: } \text{BaA} / (\text{BaA} + \text{Chr}) \text{ vs. } \text{Flt} / (\text{Flt} + \text{Pyr})$$

The bivariate plots, shown below for Eq. 2 and Eq. 3, respectively, allow for the determination of PM sources using PAH abundance ratios (Yunker, 2002).

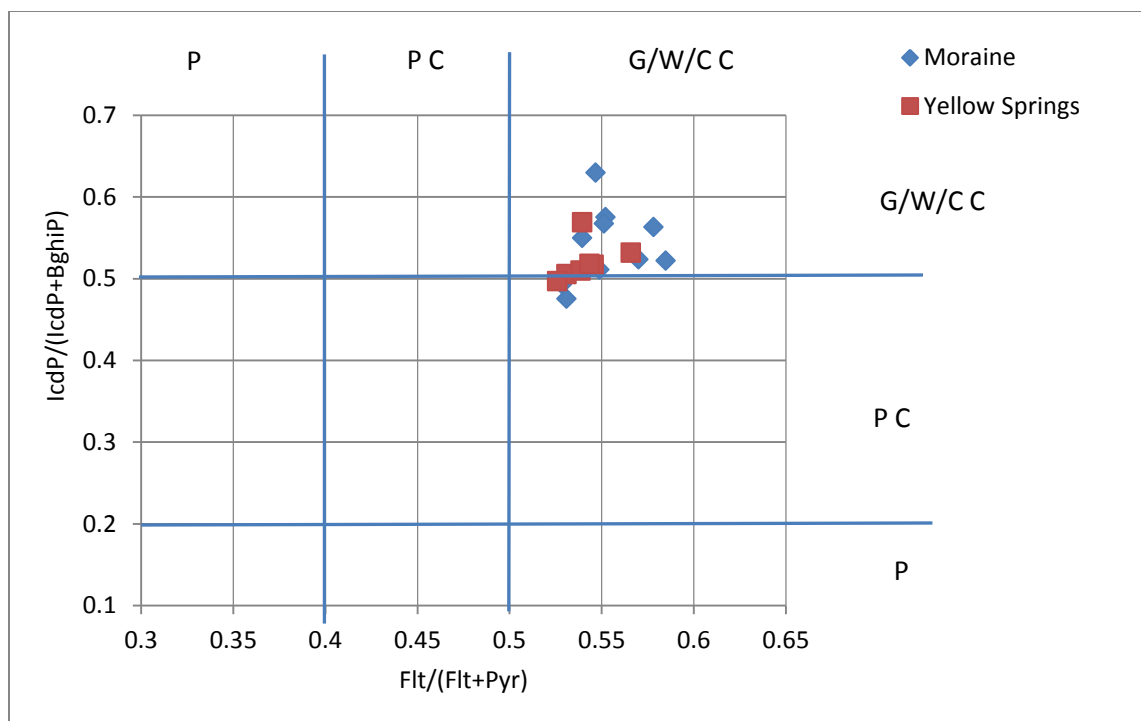


Figure 8. Bivariate plot of $IcdP/(IcdP+BghiP)$ vs. $Flt/(Flt+Pyr)$ for Moraine and Yellow Springs

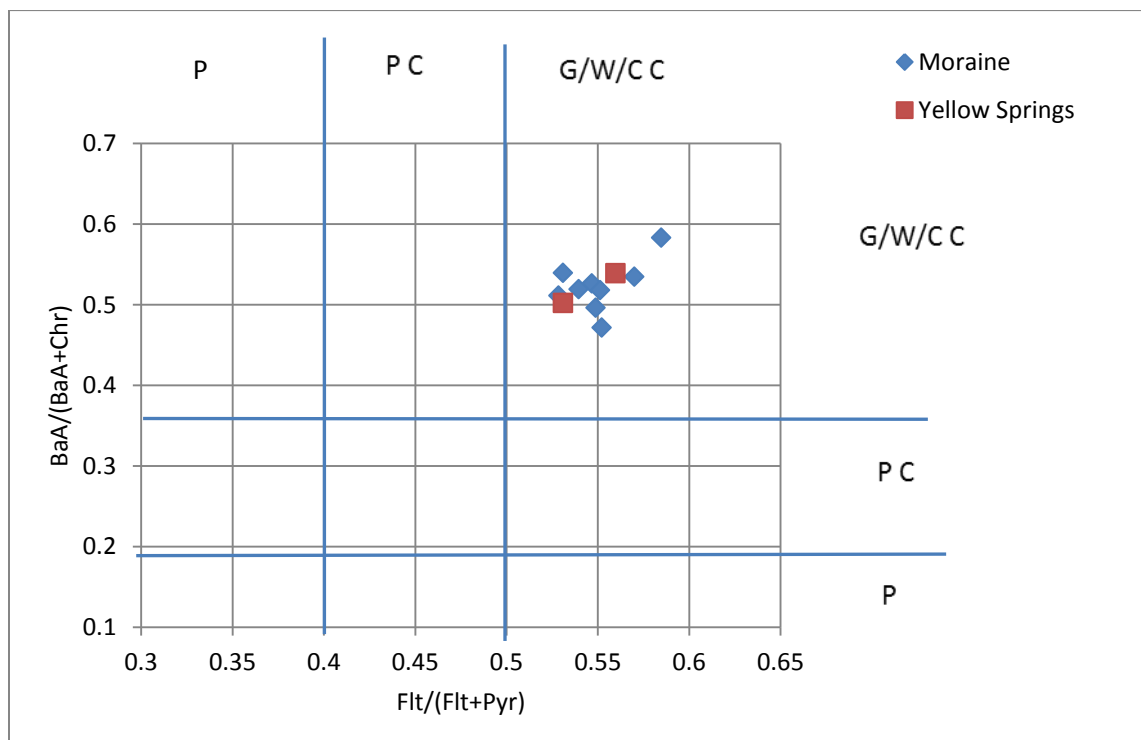


Figure 9. Bivariate plot of $BaA/(BaA+Chr)$ vs. $Flt/(Flt+Pyr)$ for Moraine and Yellow Springs

Unequal numbers of plotted points per site indicates that certain PAHs were not detected in all samples. In Figure 9, a separation in values is observed with Moraine having a higher value of $\text{Flt}/(\text{Flt}+\text{Pyr})$ relative to Yellow Springs. The February 16th, 2014 value was out of the scale of the bivariate plot, however, it was still within the grass/wood/coal combustion quadrant. The lower value of $\text{Flt}/(\text{Flt}+\text{Pyr})$ for Yellow Springs indicates a lower fraction of grass/wood/coal smoke compared to Moraine. Similarly, in Figure 8, a lower value of $\text{Flt}/(\text{Flt}+\text{Pyr})$ for the Yellow Springs samples indicates differences in the relative composition of grass/wood/coal smoke relative to Moraine. On each figure, the points with the highest value for $\text{Flt}/(\text{Flt}+\text{Pyr})$ were found in Moraine during the August sampling date, indicating the presence of a location-specific temporal trend. This region represents a higher portion of GWC combustion, which might be expected in the later summer months due to the increase in bonfires and cookouts in the region. For both figures, a similar ratio was obtained in Yellow Springs and Moraine on 12/24/13, indicating a shared effect on the air quality during that filter period. The clustering of ratios in both plots with lower $\text{Flt}/(\text{Flt}+\text{Pyr})$ values signifies that PAHs found in the air were predominantly created from petroleum and its combustion.

Weather Analysis

By comparing the $\text{PM}_{2.5}$ spike events to local weather data obtained from Weather Underground and radiosonde data obtained from the National Oceanic and Atmospheric Association (NOAA), possible weather-related PM effects were also investigated. Associating those dates to the $\text{PM}_{2.5}$ and PM_{10} data obtained from RAPCA and the concentrations of analytes determined in this study, the possibility of a temperature inversion occurring during the middle of February 2014 is suspected. In order to determine the presence of an inversion

event in the Dayton metro area, skew-t plots were obtained from the NOAA/ESRL database.

The skew-t plot provides temperature and dew point changes with respect to altitude. An inversion is likely to occur anywhere within the troposphere; however, in order for it to affect air quality, it must occur below 2 km (Wallace, 2006). If the temperature line (denoted by the red line on the right side on the radiosonde figures) decreases with respect to an increase altitude, an inversion had taken place on that date. This, coupled with other meteorological factors (such as wind speed and direction, temperature, and humidity) can support the notion that air quality was reduced by the stratification of air in the troposphere. Radiosonde figures and weather data for all PM_{2.5} spike events and the previous day can be found in Appendix D. Below is the radiosonde plot for February 12th-16th, 2014. The red line represents the temperature change with respect to height and the blue line represents the dew point change with respect to height. Altitude is given in units of thousands of feet (kft). On the right side of the plots, wind data is depicted using flags, with wind direction given by flag direction, and wind speed given by the length of the flag. The times given for the tables are 0000-1200 UTC and 1200-0000 UTC, which represent 8 p.m. – 4 a.m. and 04 a.m. – 8 p.m. local time.

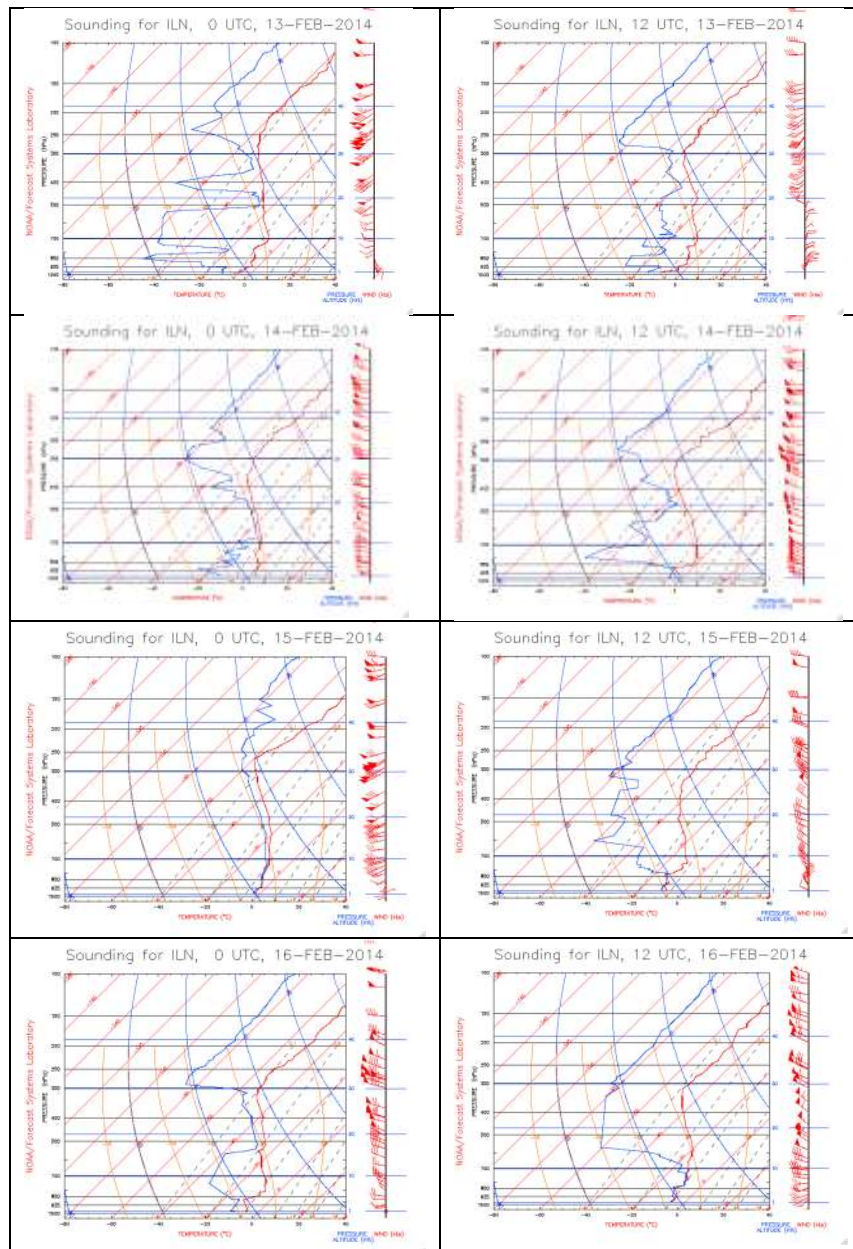


Figure 10. Radiosonde Figures for February 13-20, 2014 at 0000 UTC. Data was obtained from the NOAA/ESRL Radiosonde Database. Radiosonde data was obtained from <http://esrl.noaa.gov/raobs/> - Accessed on 9/3/2015.

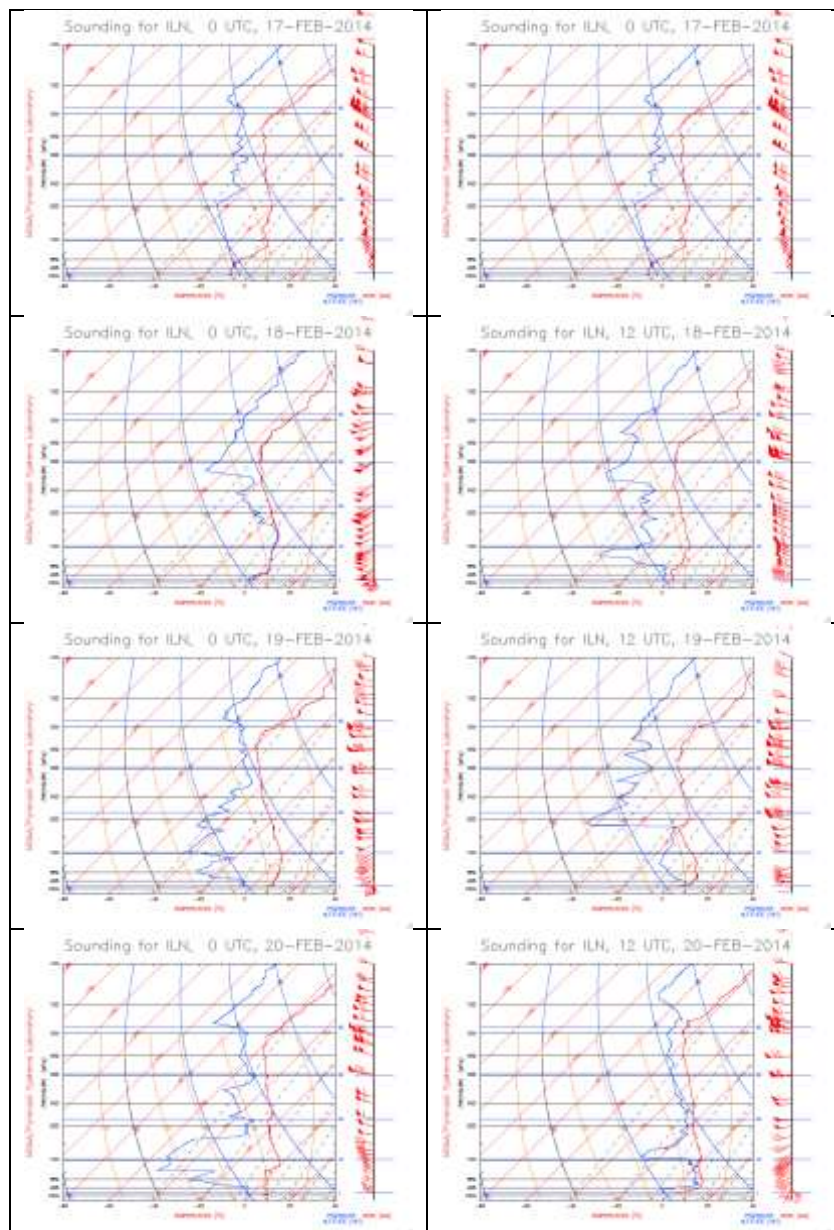


Figure 10 (continued)

As can be observed, the temperature decreased within the first 10 kft, indicating a temperature inversion. Weather data during that time period was marked by cold temperatures beginning on the 10th, low wind speeds and changing wind direction, and clear skies. Thus, the high PM_{2.5} spikes experienced during mid-February 2014 (which can be seen in Appendix C) can be linked to an inversion event. A filter was analyzed for the date range of

2/16/14-2/22/14, and the data for PM₁₀, PM_{2.5}, levoglucosan, ΣPAH, and selected metals compared to winter averages are given below.

Table 10. Filter Data for February 16th, 2014 compared to winter averages.

		Yellow Springs		Moraine	
		2/16/2014	Winter Average	2/16/2014	Winter Average
PM ₁₀	µg/ m ³	25.00	13.34	27.00	15.67
PM _{2.5}	µg/ m ³	25.40	11.62	26.20	13.11
Levoglucosan	ng/ m ³	< 0.06	0.540	0.221	0.657
ΣPAH	ng/ m ³	142.32	41.81	22.29	27.91
Fe	ng/ m ³	180.4	184.3	322.7	405.2
Si	ng/ m ³	893.0	550.4	677.0	547.3
Al	ng/ m ³	102.6	121.8	177.6	160.8
Ca	ng/ m ³	483.5	813.4	900.7	1608.1

As can be seen above, the concentrations for the selected date in Yellow Springs were significantly greater than their averages for PM₁₀, PM_{2.5}, ΣPAH, while the opposite is true for metals. In the case of Moraine, a similar effect was only observed with PM data and metal concentrations. The values during the month February 2014 fall within the EPA acceptable levels (< 35 µg/m³ for PM_{2.5} and < 50 µg/m³ for PM₁₀). While the levels in Yellow Springs & Moraine were below safe concentrations, they are higher than average, and therefore chemically and meteorologically support the argument that an inversion occurred during February 2014. According to the PAH data and source apportionment studies, the high PM concentration during the suspected inversion can be related to pyrogenic sources, including coal combustion. The obtained levoglucosan concentration for the spike date was below the limit of detection and therefore wood smoke can be eliminated as a possible cause for the high PM load. The metal concentrations were within normal ranges when compared to their winter

averages; thus their contribution to the PM₁₀ obtained on the filter was not the cause of the aberrance.

A PM_{2.5} spike event also occurred on May 17th, 2013, and in order to determine if an inversion was present that day, radiosonde and weather data was also obtained. Below are the radiosonde plots for May 16 and 17.

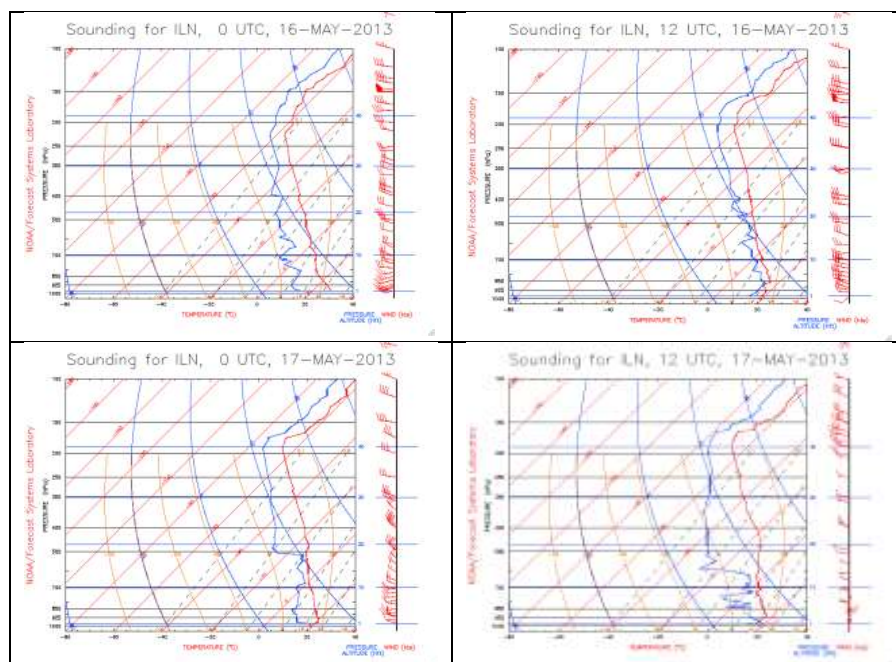


Figure 11. Radiosonde Figures for May 16-17, 2013. Data was obtained from the NOAA/ESRL Radiosonde Database. Radiosonde data was obtained from <http://esrl.noaa.gov/raobs/> - Accessed on 9/3/2015.

A lack of a temperature decrease within the first 10 kft indicates the absence of a surface temperature inversion. This is supported by the meteorological data as well, as these two days were characterized by high temperatures, rain, and relatively consistently high and non-variable winds. Therefore, the increase in particulate matter in the air on that date must be attributed to some other source. Of the selected dates for this study, the only temperature inversion that can be reasonably supported with the data is the one that occurred during

February of 2014. Similarly, the concentrations of $PM_{2.5}$ and PM_{10} fall within the acceptable levels regulated by the EPA and the analysis completed here demonstrate no large increase in PAH/levoglucosan/metal content in the PM.

The spike event witnessed during December of 2013 was investigated using radiosonde data as well, which can be found in Appendix D. The gradual decrease in temperature with respect to height and high wind speed is not consistent with a temperature inversion, though the meteorological characteristics were (high humidity, low wind speed, low temperature, & clear skies), representing a mixed bag of atmospheric data. One important caveat to note is that the radiosonde data obtained from NOAA comes from one weather balloon for the entire state. Small-scale inversions that do not fit the lapse rate requirement are entirely possible.

Conclusions

The use of three different analytical methods in high volume air filter samples allowed for the determination of PAHs, levoglucosan, and metal concentrations. When comparing the data with respect to time, the existence seasonal variations in PM could be supported or debated. Biomass burning markers such as levoglucosan and potassium should increase in the winter months as wood burning increases in frequency; this was not observed. In contrast to this finding, an increase in construction-related PM during summer months was observed as the concentration of iron during the summer was greater than that of winter. The analysis of two distinct locations also allowed for the analysis of particulate matter relative to city type.

The use of radiosonde data, wind conditions, humidity, and temperature along with chemical analyses also allowed for the qualitative assessment that an inversion event took place in February 2014. A recorded increase in PM_{2.5} concentrations during mid-February, a high observed concentration of ΣPAHs on the 2/16/14 sampling date, and the combination of low temperatures, weak and variable winds, and high humidity represent strong indicators for an inversion event occurring during mid-February 2014.

The use of levoglucosan, dust and trace metals, and PAHs provides a more comprehensive understanding of particulate matter in the Dayton metro area. The combination of these analytical methods, however, paints a more nebulous picture of the air quality in the Dayton area as there is little agreement. The need for larger data sets, specifically, a greater number of filter samples and locations will allow for more quantitative assessments to be drawn regarding the composition of particulate matter, its sources, and how it is distributed.

The impetus for this study, the December 14th, 2013 spike event, was found to not be a candidate for a temperature inversion date as it did not fit the methodology developed in this study. The need for more analysis, specifically a more comprehensive set of filter examination, may shed more light on the true cause for the aberrant weather event experienced in Yellow Springs.

References

1. Alves, C., Goncalves, C., Fernandes, A., Tarelho, L., Pio, C., 2011. Fireplace and woodstove fine particle emissions from combustion of western Mediterranean wood types. *Atmospheric Research*. 101, 692-700.
2. Amato, F. et al. 2014. Trends of road dust emissions contributions on ambient air particulate levels at rural, urban, and industrial sites in southern Spain. *Atmospheric Chemistry and Physics*. 14, 3533-3544.
3. Argyropoulos, G., Grigoratos, Th., Voutsinas, M., Samara, C. 2013. Concentrations and source apportionment of PM₁₀ and associated elemental and ionic species in a lignite burning power generation area of southern Greece. *Environ. Sci. Pollut. Res.* 20. 7214-7230.
4. Bachman, Megan. "Particulate Pollution Monitored - Cause of Spike Is Unknown." *Ysnews.com*. N.p., 20 Feb. 2014. Web. 8 Sept. 2015.
5. Bari, M., Baumbach, G., Kuch, B., Scheffknecht, G. 2009. Wood smoke as a source of particle-phase organic compounds in residential areas. *Atmospheric environment*. 43, 4722-4732.
6. Bari, M., Baumbach, G., Kuch, B., Scheffknecht, G. 2010. Temporal variation and impact of wood smoke pollution on a residential area in southern Germany. *Atmospheric Environment*. 44, 3823-3832.
7. Brown R. et al. 2008. Twenty-five years of nationwide ambient metals measurement in the United Kingdom: concentration levels and trends. *Environmental Monitoring and Assessment*. 142, 127-140.

8. Caseiro, A., Bauer, H., Schmidl, C., Pio, C., Puxbaum, H. 2009. Wood burning impact on PM₁₀ in three Austrian regions. *Atmospheric environment*. 43, 2186-2195
9. Chaloulakou, A., Kassomenos, P., Spyrellis, N., Demokritou, P., Koutrakis, P. 2003. Measurements of PM₁₀ and PM_{2.5} particle concentrations in Athens, Greece. *Atmos. Environ.* 37(5). 649-660.
10. Dejean, S., Ranaud, C., Meybeck, M., Della Massa, J., Simon, V. 2008. Polycyclic aromatic hydrocarbons (PAHs) in atmospheric urban area: monitoring on various types of sites. *Environmental Monitoring and Assessment*. 148, 27-37.
11. De Miguel, E. et al. 1997. Origin and patterns of distribution of trace elements in street dust: unleaded petrol and urban lead. *Atmospheric Environment*. 31 (17), 2733-2740.
12. Eagleman, J. 1985. *Meteorology: The atmosphere in action*. Wadsworth Publishing Company, Belmont.
13. Engel-Cox, J., Oanh, N., van Donkelaar, A., Martin, R., Zell, E. 2013. Toward the next generation of air quality monitoring: particulate matter. *Atmospheric Environment*. 80, 584-590.
14. Enz, J., Hofman, V., Thostenson, A. 2014. *Air Temperature Inversions: Causes, Characteristics and Potential Effects on Pesticide Spray Drift*. NDSU Extension Service. AE1705.
15. Fabbri, D., Torri, C., Simoneith, B., Marynowski, L., Rushdi, A., Fabianska, M., 2009. Levoglucosan and other cellulose and lignin markers in emissions from burning of Miocene lignites. *Atmospheric Environment*. 43, 2286-2295.

16. Galindo, N. Yubero, E., Nicolas, J.F., Crespo, J., Pastor, C., Carratala, A., Santacatalina, M. 2011. Water-soluble ions measured in fine particulate matter next to cement works. *Atmospheric Environment*. 45. 2043-2049.
17. Gao, B., Wang, X., Zhao, X., Ding, X., Fu, X., Zhang, Y., He, Q., Zhang, Z., Liu, T., Huang, Z., Chen, L., Peng., Guo, H. 2015. Source apportionment of atmospheric PAHs and their toxicity using PMF: impact of gas/particle partitioning. *Atmospheric Environment*. 103. 114-120.
18. Harrison, R., Tilling, R., Romero, M., Harrad, S., Jarvis, K. 2003. A study of trace metals and polycyclic aromatic hydrocarbons in the roadside environment. *Atmospheric Environment*. 37(17), 2391-2402.
19. Harrison, R., Yin, J. 2010. Chemical speciation of PM_{2.5} particles at urban background and rural sites in the UK atmosphere. *Journal of Environmental Monitoring*. 12, 1404-1414.
20. Al Jallad, F., Al Katheeri, E., Al Omar, M. 2013. Concentrations of particulate matter and their relationships with meteorological variables. *Sustain. Environ. Res.* 23(3). 191-198.
21. Jankowski, N., Schmidl, C., Marr, I., Bauer, H., Puxbaum, H. 2008. Comparison of methods for the quantification of carbonate carbon in atmospheric PM₁₀ aerosol samples. *Atmospheric Environment* 42, 8055-8064.
22. Kabir, E., Kim, K., Yoon, H. 2011. Trace metal contents in barbeque (BBQ) charcoal products. *Journal of Hazardous Materials*. 185, 1418-1424.

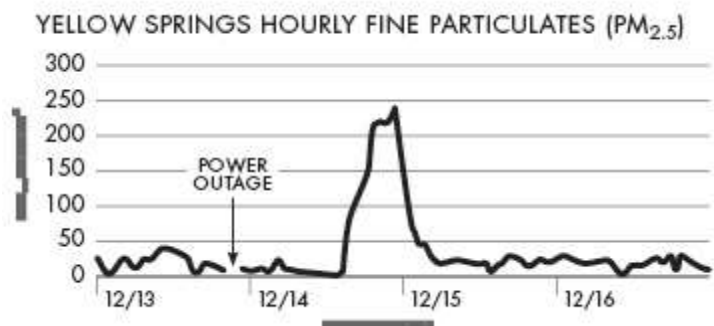
23. Karanasiou, A., Siskos, P., Eleftheriadis, K. 2009. Assessment of source apportionment by Positive Matrix Factorization analysis on fine and coarse urban aerosol size fractions. *Atmospheric Environment*. 43(21), 3385-3395.
24. Kassomenos, P. A., Paschalidou, A.K., Lykoudis, S., Koletsis, I. 2014. Temperature inversion characteristics in relation to synoptic circulation above Athens, Greece. *Environmental Monitoring and Assessment*. 186, 3495-3502.
25. Kolker, A. et al. 2013. Atmospheric mercury and fine particulate matter in coastal New England: Implications for mercury and trace element sources in the northeastern United States. *Atmospheric Environment*. 79, 760-768.
26. Li, C., Mi, H., Lee, W., You, W., Wang, Y. 1999. PAH emission from the industrial boilers. *Journal of Hazardous Materials*. A69, 1-11.
27. Lutgens, K., Tarbuck, E. 1986. *The Atmosphere: An Introduction to Meteorology*, 3rd ed. Prentice-Hall, Englewood Cliffs.
28. Manahan, S. 2009. *Environmental Chemistry*, 9th edition.
29. Moyo, S., McCrindle, R., Mokgalaka, N., Myburgh, J., Mujuru, M., Source apportionment of polycyclic aromatic hydrocarbons in sediments from polluted rivers. 2013. *Pure Applied Chemistry*. 85, (12), 2175-2196.
30. Naik, T., Canpolat, F., Chun, Y. Uses of CKD other than for flue gas desulfurization. CBU Report CBU-2003-35. September 2003.
31. National Oceanic & Atmospheric Administration, Radiosonde Database. www.esrl.noaa.gov/raobs/. 8 Sept. 2015.

32. Nilsson, B.A., 1994. Model of the relation between aerosol extinction and meteorological parameters. *Atmos. Environ.*, 28(5), 815-825.
33. Van Vlerah, J. Ohio EPA. (2014). What citizens need to know about national ambient air quality standards and nonattainment. Columbus, OH. Retrieved from epa.ohio.gov.
34. Papanastasiou, D.K. ,Melas, D., Kioutsioukis, I. 2007. Development and assessment of neural network and multiple regression models in order to predict PM levels in a medium-sized Mediterranean city. *Water Air Soil Pollut.*, 182(1-4), 325-334.
35. Rick, S., Wille, A., Steinbach, A. 2010. Determining saccharidic tracers in atmospheric aerosols. *Separation science*, 3 (5).
36. Ravindra, K., Sokhi, R., Grieken, R., Atmospheric polycyclic aromatic hydrocarbons: Source attribution, emission factors, and regulation. 2008. *Atmospheric Environment*, 42, 2895-2921.
37. Schmidl, C., Bauer, H., Dattler, A., Hitzenberger, R., Weissenboeck, G., Marr, I., Puxbaum, H. 2008. *Atmospheric Environment*, 42, 9070-9079.
38. Seaton, A., MacNee, W., Donaldson, K., Godden, D., 1995. Particulate Air pollution and acute health effects. *The Lancet*. 345, 176-178.
39. Simpson, C., Dills, R., Katz, B., Kalman, D. 2004. Determination of levoglucosan in atmospheric fine particulate matter. *Journal of the Air and Waste Management Association*. 54, 689-694.
40. Tomashuk, T. A., Truong, T. M., Mantha, M., McGowin, A. E. (2012) Atmospheric polycyclic aromatic hydrocarbon profiles and sources in pine needles and particulate matter in Dayton, Ohio, USA. *Atmospheric Environment*, 51, 196-202.

41. United States Environmental Protection Agency Federal Register. 2015. Fine Particulate Matter National Ambient Air Quality Standards: State Implementation Plan Requirements; Proposed Rule. Vol. 80, No. 55.
42. United States Environmental Protection Agency. Health assessment document for diesel exhaust. 2000. Washington, D.C., United States Environmental Protection Agency, EPA/600/8-90/057E.
43. Urban, R. et al. 2012. Use of levoglucosan, potassium, and water-soluble organic carbon to characterize the origins of biomass-burning aerosols. *Atmospheric Environment*. 61, 562-569.
44. Urban, R. et al. 2014. Sugar markers in aerosol particles from an agro-industrial region in Brazil. *Atmospheric Environment*. 90. 106-112.
45. Van der Merwe, P. et al. 2015. Sourcing the iron in the naturally fertilized bloom around the Kerguelen Plateau: particulate trace metal dynamics. *Biogeosciences*. 12, 739-755
46. Vihma, T., Kilpelainen, T., Manninen, M., Sjoblom, A., Jakobsen, E., Palo, T., Jaagus, J., Maturilli, M. 2011. Characteristics of temperature and humidity inversions and low-level jets over Svalbard Fjords in Spring. *Advances in Meteorology*. 2014, 1-14
47. Wallace, J., Hobbs, P. 2006. *Atmospheric Science: An Introductory Survey*, 2nd ed. Elsevier, Oxford.
48. Ward, T., Hamilton, R., Dixon, R., Paulsen, M., Simpson, C. 2006. Characterization and evaluation of smoke tracers in PM: results from the 2003 Montana wildfire season. *Atmospheric Environment*. 40, 7005-7017.
49. Weather Underground. www.wunderground.com, date accessed 08/19/2015.

50. Yin, J. et al., 2010. Source Apportionment of Fine Particles at Urban Background and Rural Sites in the UK Atmosphere. *Atmospheric Environment*. 44, 841-851
51. Yu, Y., Li, Y./ Guo, Z., Zou, H. 2015. Source apportionment of polycyclic aromatic hydrocarbons by positive matrix factorization in surface sediments of Taihu Lake, China. *Pol. J. Environ. Stud.* 24 (2). 793-799.
52. Yunker, M., Macdonald, R., Vingarzan, R., Mitchell, R., Goyette, D., Sylvestre, S. 2002. PAHs in the Fraser River basin: a critical appraisal of PAH ratios as indicators of PAH source and composition. *Organic Geochemistry*. 33, 489-515.
53. Zhang, H., Wang, Y., Hu, J., Ying, Q., Hu, X. (2015). Relationships between meteorological parameters and criteria air pollutants in three megacities in China. *Environmental Research* (140) 242-254.
54. Zhang, J., Wang, J., Hua, P., Krebs, P. (2015). The qualitative and quantitative source apportionments of polycyclic aromatic hydrocarbons in size dependent road deposited sediment. *Science of the Total Environment* (505) 90-101.

Appendix A – Yellow Springs News Article



Source: Regional Air Pollution Control Agency

Particulate pollution levels monitored— Cause of spike is unknown

By Megan Bachman

Published: February 20, 2014

A regional air pollution agency is investigating an unprecedented and potentially dangerous spike in air pollution in Yellow Springs in December when an exceedingly high concentration of lung-penetrating particles was recorded.

Air pollution monitors atop the John Bryan Community Center measured levels of the fine particulate PM_{2.5} at 240.5 millionths of a gram per cubic meter of air (µg/m³) on Saturday, Dec. 14, more than 20 times higher than the local average.

According to John Paul, administrator of the Dayton-area Regional Air Pollution Control Agency, that level is the highest concentration the agency has ever seen. The agency is now looking into the cause.

“This is something that caught our eye and we said ‘boy,’” Paul said this week, adding that fine particulates are the pollutant of most concern for the agency since they can “penetrate deeply into the lungs and stay there.”

Fine particulates are an inhalable mixture of solid particles and liquids emitted as dust and soot from power plants, industries, automobiles, smokestacks and fires. Breathing in fine particulates even for just a few hours or days can cause serious health effects, including premature death, heart attack,

strokes and respiratory symptoms like difficulty breathing, according to the U.S. Environmental Protection Agency, which regulates particulate pollution.

Once it secures funding and a university partner for the study, RAPCA plans to look at possible local causes for the spike, such as residential wood burning and large upwind emitters, including the Cemex cement production plant and Wright-Patterson Air Force Base, both in Fairborn.

On Dec. 14, measures of the pollutant PM_{2.5} departed from a normal local level of 10 µg/m³ starting at around 3 p.m. and lasted for 12 hours. Yellow Springs' 24-hour average of 71.7 µg/m³ triggered the rare EPA air quality index designation "Unhealthy," which is the fourth highest after "Good," "Moderate," and "Unhealthy for Sensitive Groups," according to RAPCA air pollution analyst Andy Roth. Only "Very Unhealthy" and "Hazardous" are higher.

"It a very rare occurrence to hit 'Unhealthy.' It's been some years," Roth wrote in an email this week, adding that the level "Unhealthy for Sensitive Groups" occurs about 12 times per year in the six-county area that RAPCA oversees. The Air Quality Index hit 155 on the day of the spike.

When local air quality reaches "Unhealthy," it is no longer just unsafe for sensitive populations such as the elderly, children and those with respiratory or heart disease to be outdoors, according to the EPA. At that level, everyone is at risk and should limit "prolonged exertion," because during physical activity particulates are inhaled more deeply into the lungs.

According to the American Lung Association's 2013 "State of the Air" report, even short-term exposure to fine particulates can kill.

"Deaths can occur on the very day that particle levels are high, or within one to two months afterward," according to the report. Short-term increases in particle pollution have been linked to increased mortality in infants and young children, increased heart attacks, increased hospitalization and emergency room visits for cardiovascular disease and strokes and increased severity of asthma attacks in children, the report said.

PM_{2.5} particulates, which are less than 2.5 microns in diameter or 1/30th the width of a single human hair, are particularly dangerous because they are small enough to enter the bloodstream and stay there, according to the EPA. Larger particulates, known as PM₁₀, can be expelled from the lungs by sneezing or coughing.

The particulate pollution spike did not violate EPA regulations and appears to be an anomaly, as Yellow Springs is not known to have poor air quality, according to Paul. In addition, the agency, which releases a daily air quality index forecast for the area and occasional air quality alerts, did not issue an alert because by the time the spike was noticed, the event was over, Paul said.

The EPA has a 24-hour standard of 35µg/m³ that is based upon annual peak pollution days averaged over three years. Alone, the 24-hour measure on Dec. 14 of 71.7 µg/m³ would not have been enough to trigger a violation. Yellow Springs' 24-hour 98th percentile level in 2012 was 20.2 µg/m³, according to an Ohio EPA report. The village also was below the EPA's annual standard of 12 µg/m³ (an average of hourly measures over the year) with an average of 9.58 µg/m³. Final figures from 2013 have yet to be released by the Ohio EPA.

Potential causes

To determine the cause of the air pollution spike, Paul said that RAPCA will first need to understand local weather conditions at the time, which can have a major impact on air quality. In fact, a rare meteorological event called an "ice fog" settled into the area on the evening of Dec. 14, which could have contributed to the high measures of pollution, Paul said.

"It could have been an extraordinary event air pollution-wise, but it's more likely an extraordinary event weather-wise, which allows the concentration of air pollutants that would normally be readily dispersed," Paul said. The temperature on Dec. 14 was in the low-30s.

RAPCA has also mostly ruled out area fires as a cause. According to Miami Township Fire-Rescue Chief Colin Altman this week, there were no local house fires or burn permits issued for that day.

To see if residential wood burning contributed to high particulate counts, Paul said the agency needs to review particulate data in the village over the last few years, compare measurements from summer and winter, chart weather patterns with the data and take samples from another local EPA monitor that is equipped with a filter. (The continuous 24-hour PM_{2.5} monitor that measured the spike does not save physical samples). If wood burning turns out to be the culprit, RAPCA would then encourage people to be sure to burn only clean, dry wood and regularly clean their wood stove or chimney, Paul said.

"We would point out the levels are still within the healthy range, but if you are outside and you do smell wood smoke, and if you have children that have asthma, you should avoid exposing yourself to that," he said.

RAPCA will also investigate a potential incident at the Cemex cement production plant off of Dayton-Yellow Springs in Fairborn by looking at the data from its pollution monitors, though Paul said he believes that is unlikely the cause since the plant is located so far away.

According to a statement this week from Cemex's corporate offices in Houston, Texas, the Fairborn plant, which continuously monitors its emissions in compliance with EPA regulations, reviewed its data for the months of November and December and reported "no exceedences."

Wright-Patterson Air Force Base, also in Fairborn, is another major upwind pollution source for Yellow Springs and will be examined, Paul said. According to Paul, the base is the largest polluter in the county as it burns coal to generate electricity at the base.

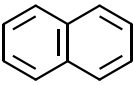
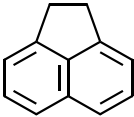
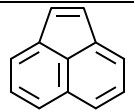
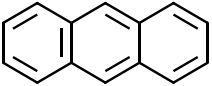
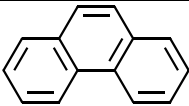
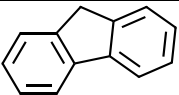
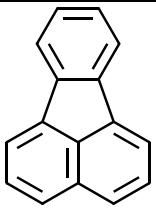
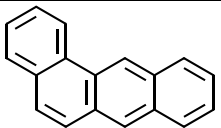
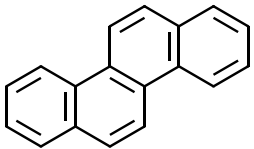
Two other events that may have contributed to the air pollution spike were a village-wide power failure on Friday, Dec. 13, that lasted from 8 to 11 p.m. and an accident on Interstate-70 on Friday evening that caused traffic to be re-routed through the village. Increased traffic, especially of diesel-burning semi-trucks, could increase PM_{2.5}, according to Roth. However, because the spike occurred 16 hours after these events, they may not be related, Roth wrote. Paul agreed.

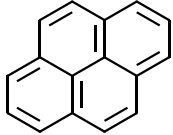
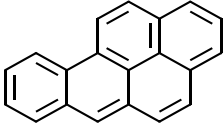
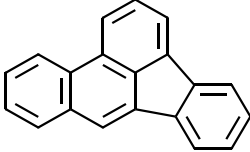
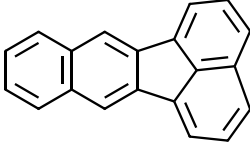
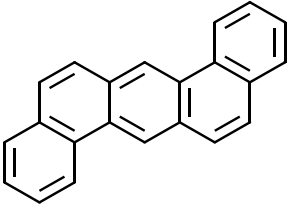
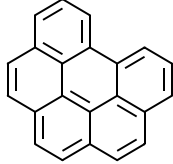
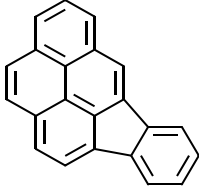
“It’s doubtful [they had an impact] unless diesel trucks were lined up for six hours,” Paul said. “A few hours of heavy but otherwise normal traffic is unlikely to have caused this.”

The possibility that the monitors malfunctioned is also being explored, according to Paul. Erroneous readings have happened before, though RAPCA has not yet been able to invalidate the Yellow Springs data.

As part of its investigation RAPCA will also look into another local PM_{2.5} spike to 234.5 µg/m³ that lasted just a few hours on Nov. 1.

Appendix B – Table of Polycyclic Aromatic Hydrocarbons

Polycyclic aromatic hydrocarbons	Number of rings	CAS #	Molecular weight (g/mole)	Structure
Naphthalene	2	91-20-3	128.17	
Acenaphthene	3	83-32-9	154.21	
Acenaphthylene	3	208-96-8	152.2	
Anthracene	3	120-12-7	178.23	
Phenanthrene	3	85-01-8	178.23	
Fluorene	3	86-73-7	166.22	
Fluoranthene	4	206-44-0	202.26	
Benz(a)anthracene	4	56-55-3	228.29	
Chrysene	4	218-01-9	228.29	

Pyrene	4	129-00-0	202.26	
Benzo(a)pyrene	5	50-32-8	252.32	
Benzo(b)fluoranthene	5	205-99-2	252.32	
Benzo(k)fluoranthene	5	207-08-9	252.32	
Dibenz(a,h)anthracene	6	53-70-3	278.35	
Benzo(g,h,i)perylene	6	191-24-2	276.34	
Indeno[1,2,3-cd]pyrene	6	193-39-5	276.34	

Appendix C – Filter Choice Data Tables & Graphs

Table 1. PM₁₀ filter selections*

Location	Start Date	PM Mass (g)	Air Volume (m ³)	PM Concentration (µg/m ³)
Moraine	01/22/13	0.02230	1640	13.60
Yellow Springs	01/22/13	0.01380	1688	8.18
Moraine	02/03/13	0.01250	1612	7.75
Yellow Springs	02/03/13	0.02270	1472	15.42
Moraine	05/16/13	0.04600	1543	29.81
Yellow Springs	05/16/13	0.03210	1555	20.64
Moraine	08/20/13	0.05060	1511	33.49
Yellow Springs	08/20/13	0.03460	1593	21.72
Moraine	12/06/13	0.03120	1539	20.27
Yellow Springs	12/06/13	0.01850	1647	11.23
Moraine	12/18/13	0.02570	1586	16.20
Yellow Springs	12/18/13	0.02120	1641	12.92
Moraine	12/24/13	0.01620	1624	9.98
Yellow Springs	12/24/13	0.01550	1678	9.24
Moraine (secondary)†	02/10/14	0.06290	1675	37.55
Moraine	02/16/14	0.04400	1602	27.47
Yellow Springs	02/16/14	0.04050	1648	24.58
Moraine	03/12/14	0.02620	1546	16.95
Yellow Springs	03/12/14	0.02230	1586	14.06
Moraine	07/10/14	0.02780	1553	17.90
Yellow Springs	07/10/14	0.01730	1552	11.15
Moraine	08/15/14	0.02630	1552	16.95
Yellow Springs	08/15/14	0.01500	1570	9.55
Moraine	12/13/14	0.02840	1595	17.81
Yellow Springs	12/13/14	0.02670	1648	16.20

*PM₁₀ start dates are given. The run time for each filter was six days.

† A co-located sampler filter was used for this analysis.

Table 2. PM₁₀ Filter Date Ranges and PM_{2.5} Spike Dates

PM ₁₀ Date Ranges	PM 2.5 Spike Dates & Locations & Concentrations (µg/m ³)
1/22/13-1/27/13	*
2/3/13-2/8/13	2/5 - 25.7 (M)
5/16/13-5/21/13	5/17 - 26.2 (M)
8/20/13-8/25/13	*
12/6/13-12/11/13	*
12/18/13-12/23/13	*
12/24/13-12/29/13	12/27 - 25.5 (M)
2/10/14-2/15/14	2/10 - 40.3 (YS), 2/11 - 26.3 (YS), 2/12 - 38.8 (YS), 2/13 - 32.9 (YS), 2/10 - 32.7 (M), 2/12 - 33.5 (M), 2/13 - 38.9 (M)
2/16/14-2/21/14	2/16 - 25.4 (YS), 2/16 - 26.2 (M)
3/12/14-3/17/14	
7/10/14-7/15/14	7/12 - 27.0 (YS), 7/12 - 25.8 (M)
8/5/14-8/20/14	8/18 - 26.8 (YS)
12/13/14-12/18/14	*

*No PM_{2.5} spikes occurred during these ranges

Figure 1. Particulate Matter Levels for the Yellow Springs Sampler Site from 2013-2015

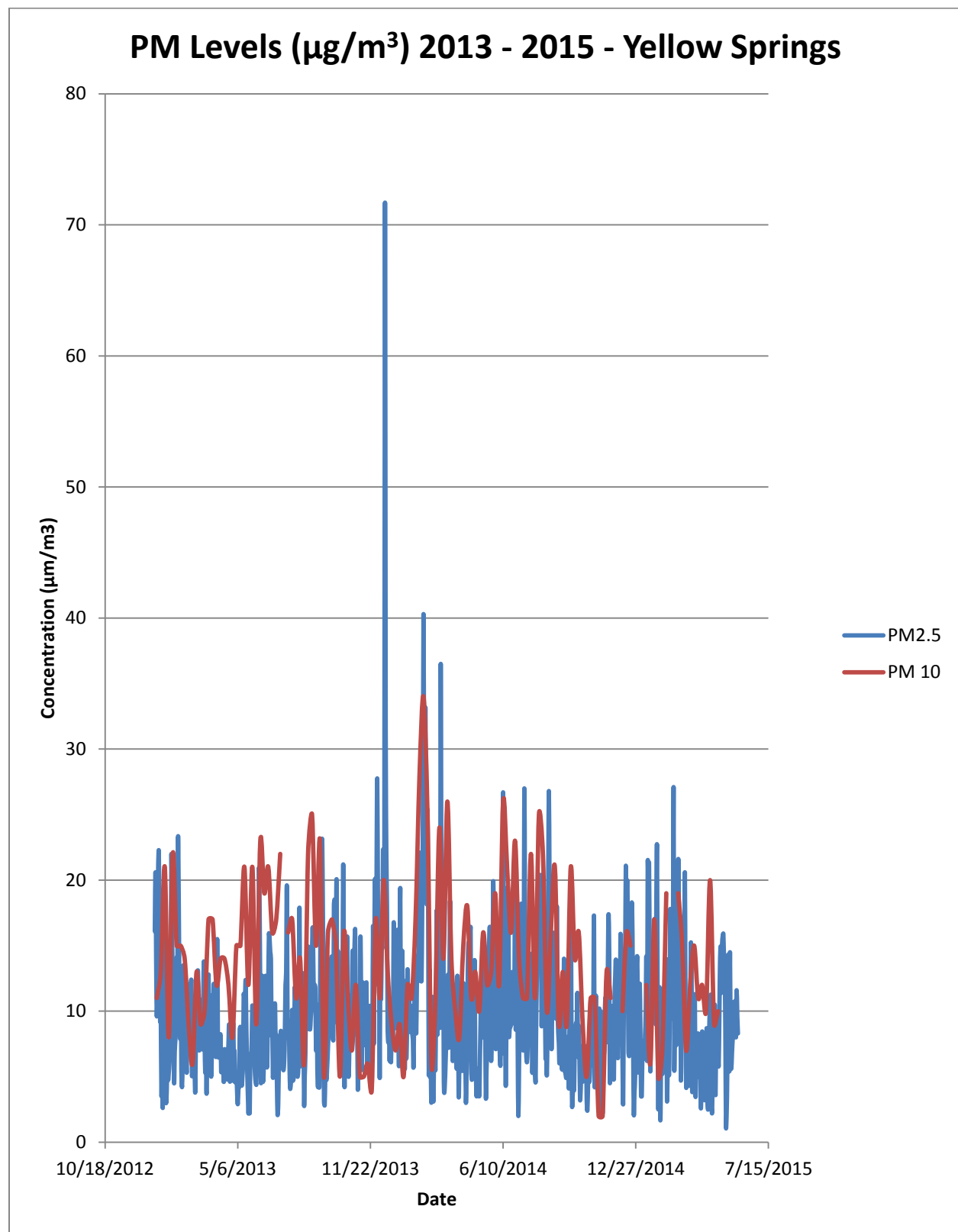
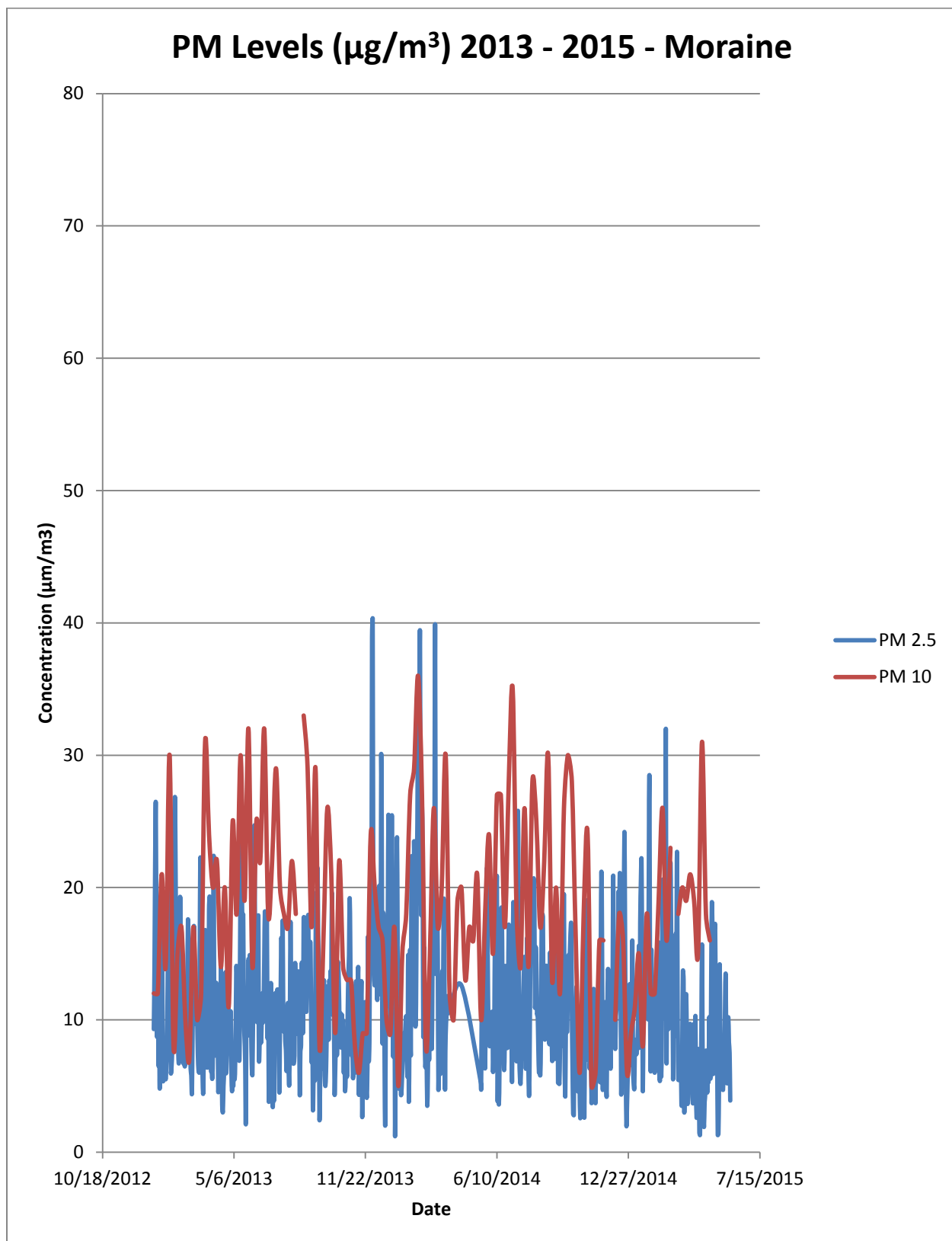


Figure 2. Particulate Matter Levels for the Moraine Sampler Site from 2013-2015



Appendix D – Weather and Radiosonde Data

Table 1. Weather data bracketing high PM2.5 dates. Weather data was obtained from www.wunderground.com – Accessed on 9/3/2015.

Sampling Dates - Moraine - KMGY	Mean Temperature (°F)	Mean Humidity (%)	Total Precipitation (in)	Wind Speed & Direction (mph)	Other Weather Notes
2/3/2013	20	75	0	8 (W)	snow
2/4/2013	24	86	0.01	7 (SSW)	Overcast, light snow
2/5/2013	30	83	0	5 (WNW)	Overcast, Scattered Clouds
5/16/2013	70	78	0.19	7 (SW)	Rain, and thunderstorm
5/17/2013	68	92	0.23	4 (SSE)	Fog, rain, thunderstorm
12/26/2013	32	63	0	11 (WSW)	Clear, mostly cloudy, scattered cloudy, partly cloudy
12/27/2013	37	64	0	7 (SSW)	Clear, Overcast, Mostly cloudy
2/9/2014	21	84	0.06	6 (W)	Fog, snow
2/10/2014	12	78	0	5 (NW)	Clear, Overcast, Mist
2/11/2014	8	71	0	4 (NE)	Clear, Haze
2/12/2014	14	65	0	9 (ENE)	Clear
2/13/2014	24	50	0	7 (West)	Clear, partly cloudy, Overcast

Table 1 continued

2/15/2014	22	75	0	9 (NW)	Snow, Haze, overcast, partly cloudy, mostly cloudy.
2/16/2014	21	84	0.01	7 (SW)	Light snow, Haze, Overcast, scattered clouds, mostly cloudy
7/11/2014	70	65	0	4 (NE)	Clear, Partly cloudy.
7/12/2014	74	69	0	5 (SSW)	Clear, Partly cloudy.
8/17/2014	70	90	0	3 (East)	Fog
8/18/2014	75	83	0.02	5 (ENE)	Overcast, Partly cloudy, Scattered cloudy, clear, Mostly cloudy

Table 2. Chosen Filter Dates & Weather Data for Yellow Springs Filter Samplers. Weather data was obtained from www.wunderground.com

Sampling Dates - Yellow Springs - KSGH	Mean Temperature (°F)	Mean Humidity (%)	Total Precipitation (in)	Wind Speed & Direction (mph)	Other Weather Notes
2/3/2013	18	78	0	10 (W)	Snow
2/4/2013	20	84	0.01	7 (SSW)	Fog, snow
2/5/2013	26	83	0	7 (WNW)	Snow
5/16/2013	67	76	0.02	9 (WSW)	Rain, thunderstorm
5/17/2013	66	77	0	5 (SSE)	Fog, rain, thunderstorm
12/26/2013	32	72	0	15 (WSW)	Haze, Clear, Overcast, Scattered clouds
12/27/2013	38	68	0	10 (SW)	Partly cloudy, clear, Overcast.
2/9/2014	20	89	0	6 (West)	Fog, rain, snow
2/10/2014	10	80	0	6 (WNW)	Clear, Haze, Most cloudy
2/11/2014	5	76	0	4 (North)	Clear, Haze.
2/12/2014	10	71	0	6 (ENE)	Clear, Light snow
2/13/2014	22	56	0	4 (West)	Clear, Partly cloudy, Mostly cloudy.
2/15/2014	20	78	0	10 (NW)	Snow
2/16/2014	20	88	0	7 (WSW)	Snow

Table 2 continued

7/11/2014	74	*	0.15	*	*
7/12/2014	74	*	0.15	*	*
8/17/2014	70	91	0	2 (SSE)	Fog, rain
8/18/2014	74	82	0	4 (ENE)	Light rain

- Values were not recorded on Weather Underground

Table 3. Radiosonde Figures for February 4-5, 2013. Data was obtained from the NOAA/ESRL Radiosonde Database. Radiosonde data was obtained from <http://esrl.noaa.gov/raobs/> - Accessed on 9/3/2015.

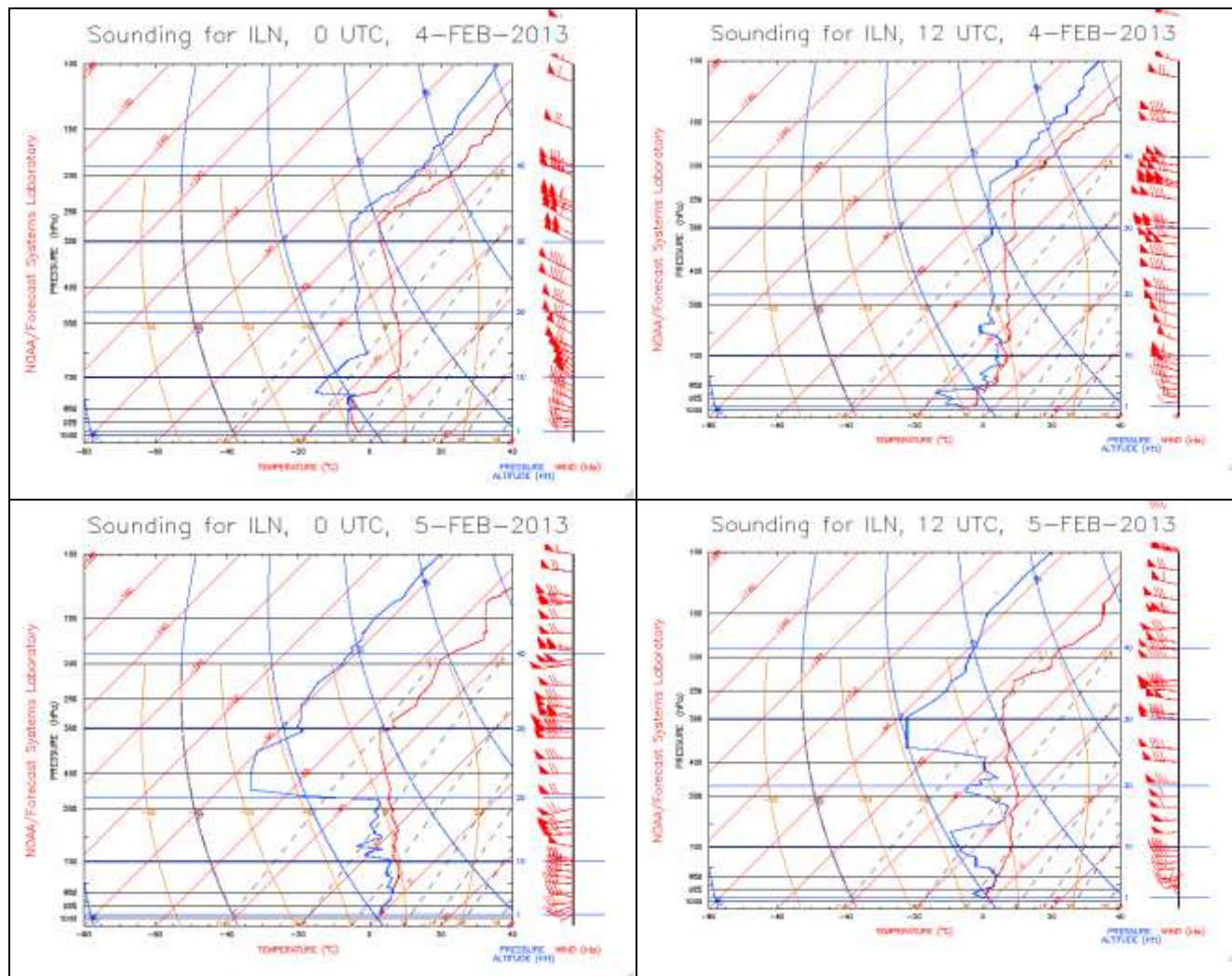


Table 4. Radiosonde Figures for May 16-17, 2013. Data was obtained from the NOAA/ESRL Radiosonde Database. Radiosonde data was obtained from <http://esrl.noaa.gov/raobs/> - Accessed on 9/3/2015.

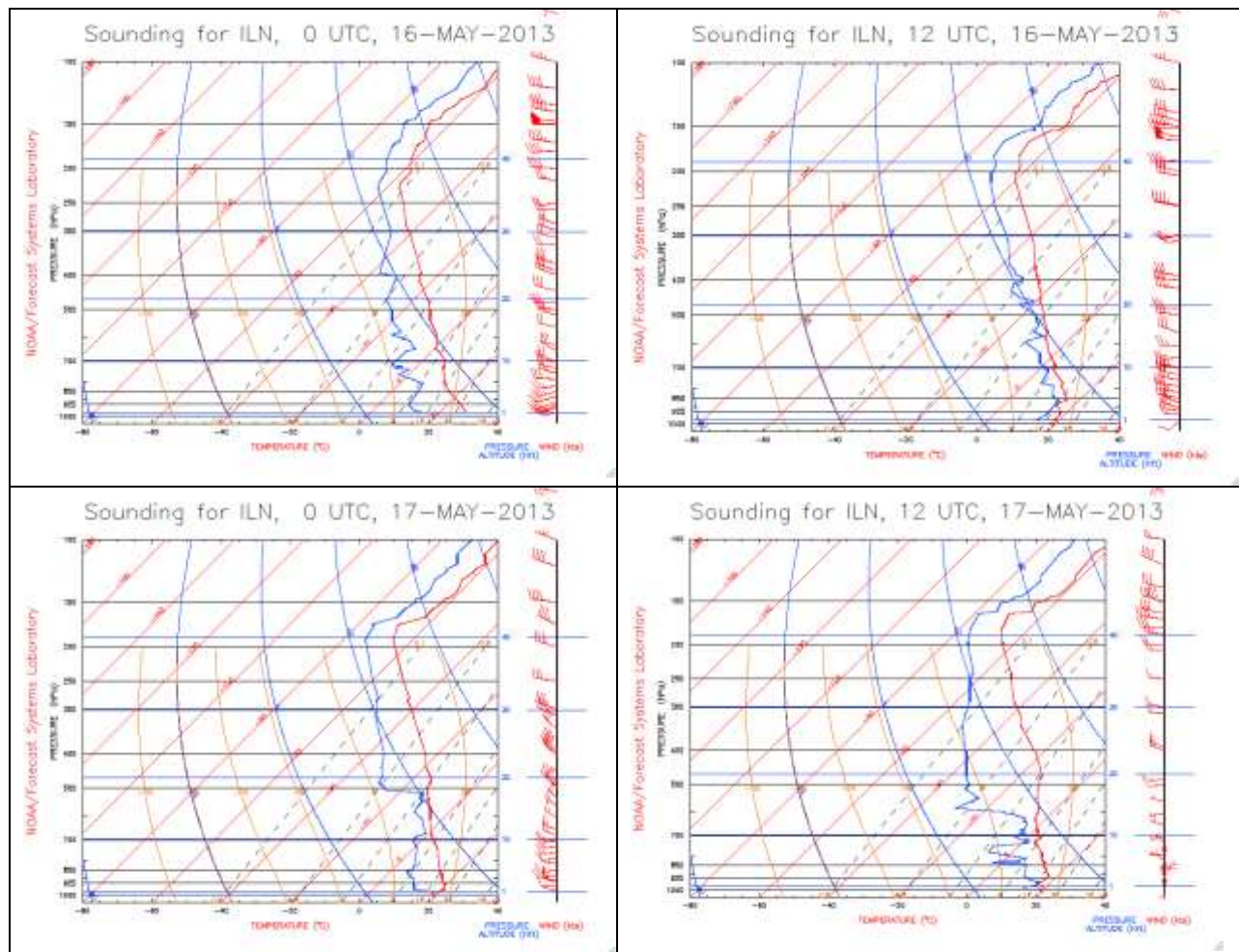


Table 5. Radiosonde Figures for December 13-14, 2013. Data was obtained from the NOAA/ESRL Radiosonde Database. Radiosonde data was obtained from <http://esrl.noaa.gov/raobs/> - Accessed on 9/3/2015.

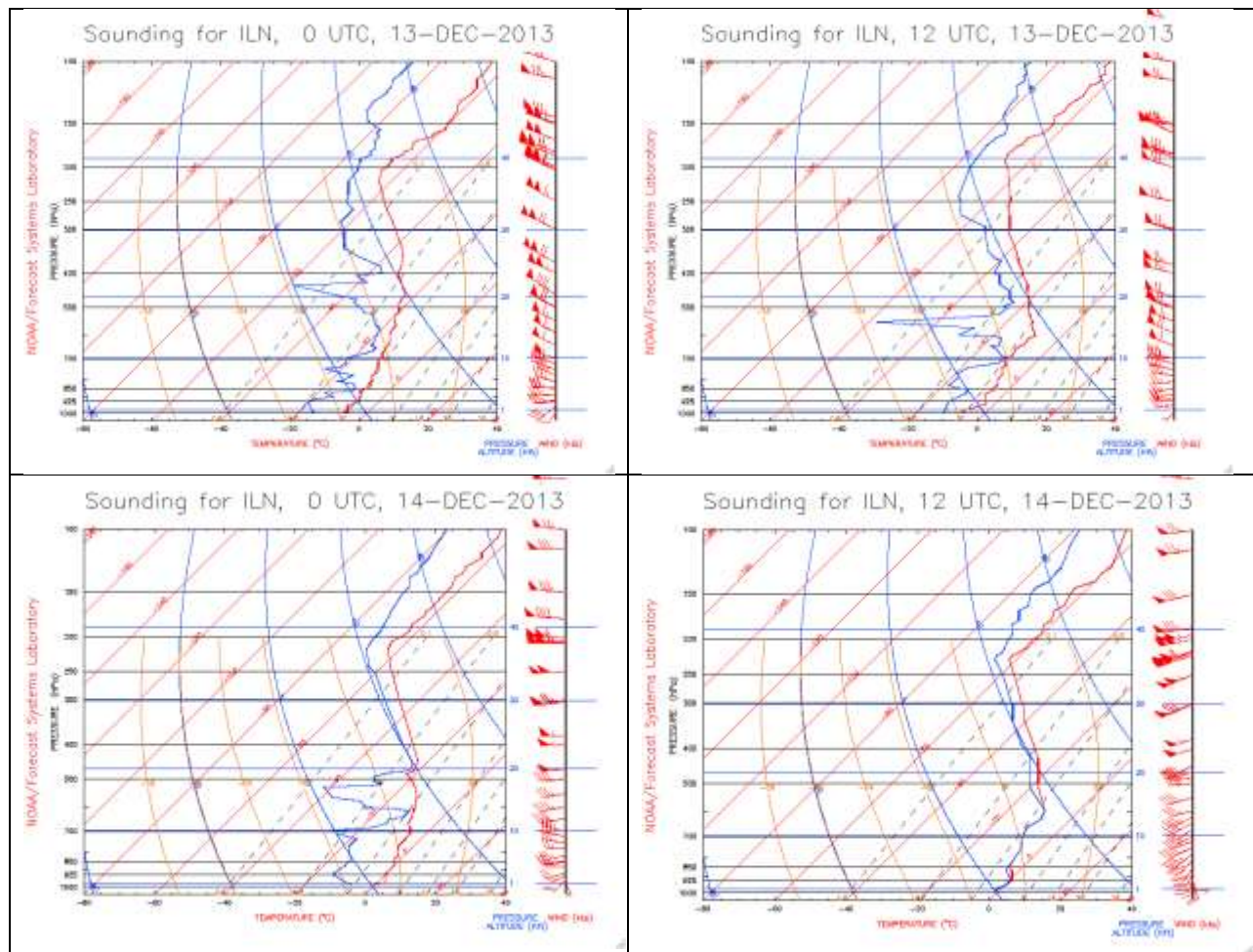


Table 6. Radiosonde Figures for December 26-27, 2013. Data was obtained from the NOAA/ESRL Radiosonde Database. Radiosonde data was obtained from <http://esrl.noaa.gov/raobs/> - Accessed on 9/3/2015.

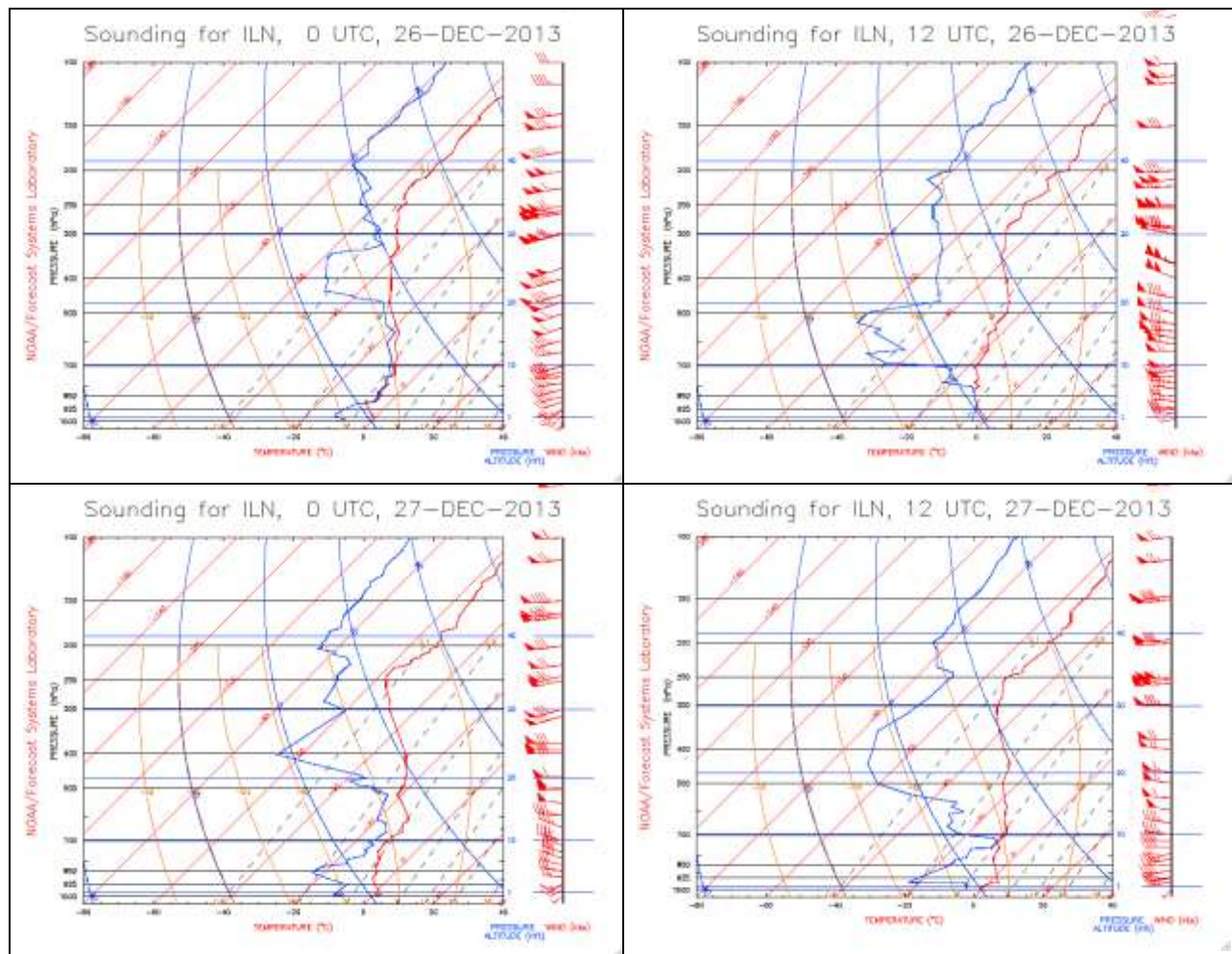


Table 7. Radiosonde Figures for February 9-13, 2014. Data was obtained from the NOAA/ESRL Radiosonde Database. Radiosonde data was obtained from <http://esrl.noaa.gov/raobs/> - Accessed on 9/3/2015.

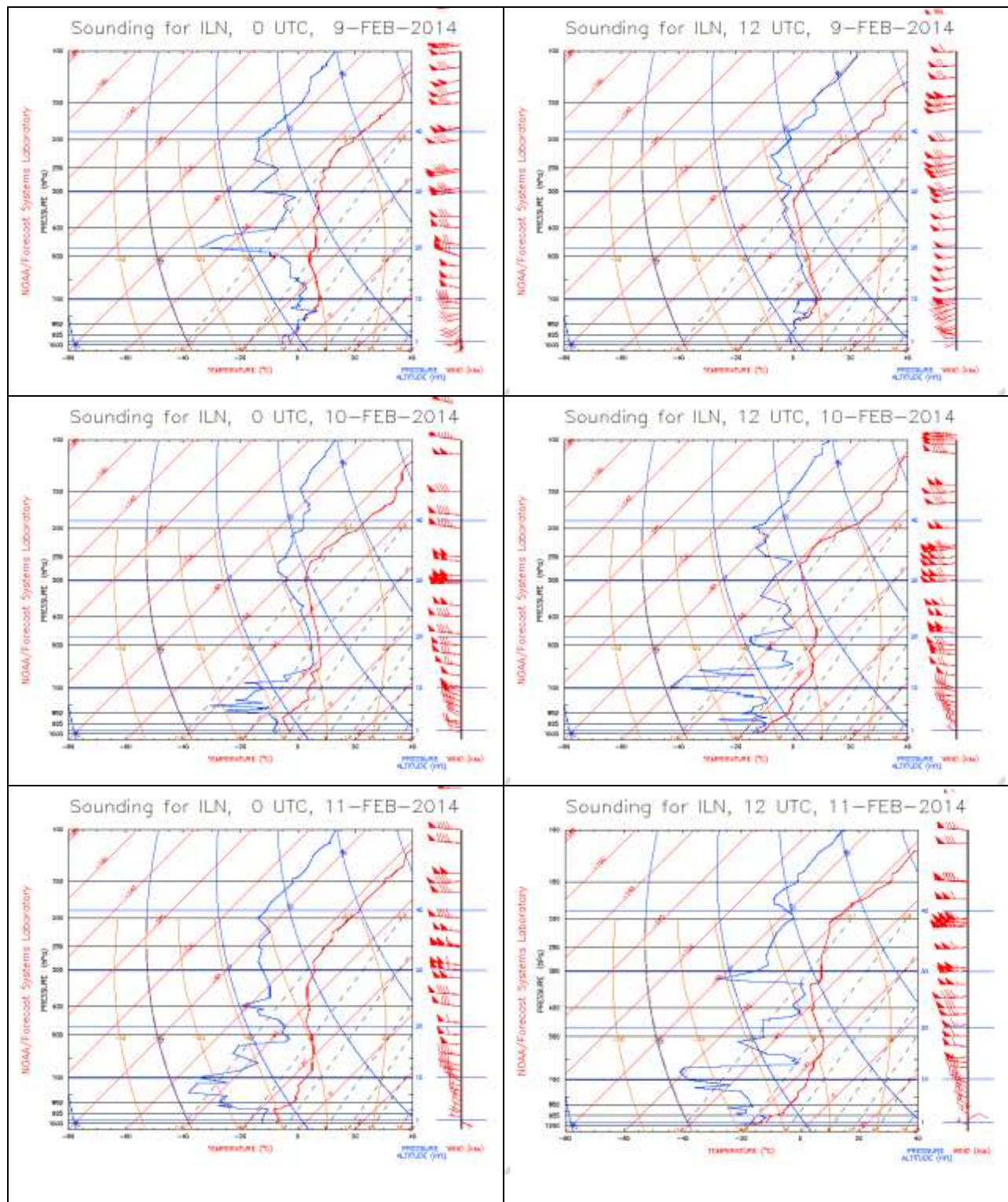


Table 7 continued

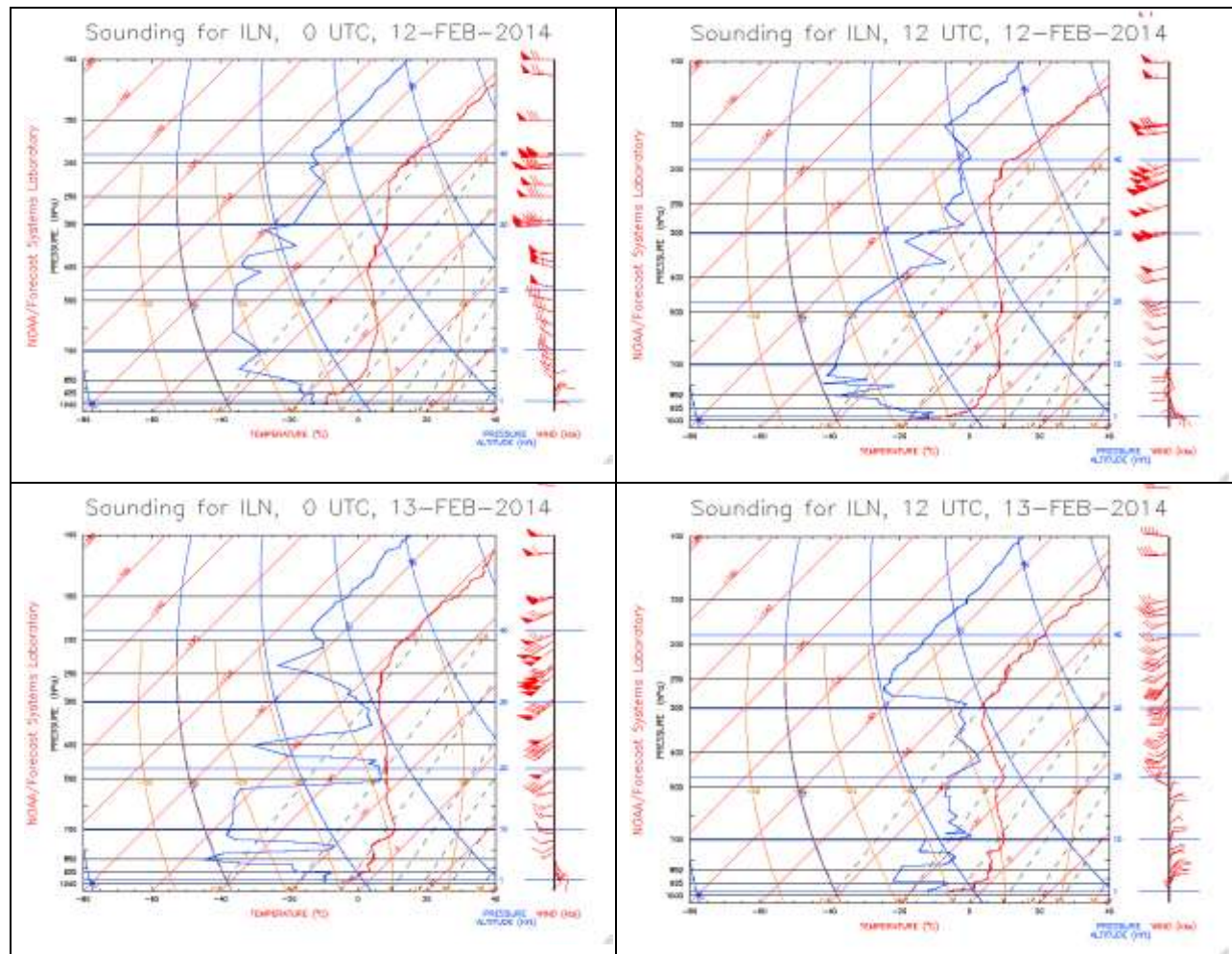


Table 8. Radiosonde Figures for February 15-16, 2014. Data was obtained from the NOAA/ESRL Radiosonde Database. Radiosonde data was obtained from <http://esrl.noaa.gov/raobs/> - Accessed on 9/3/2015.

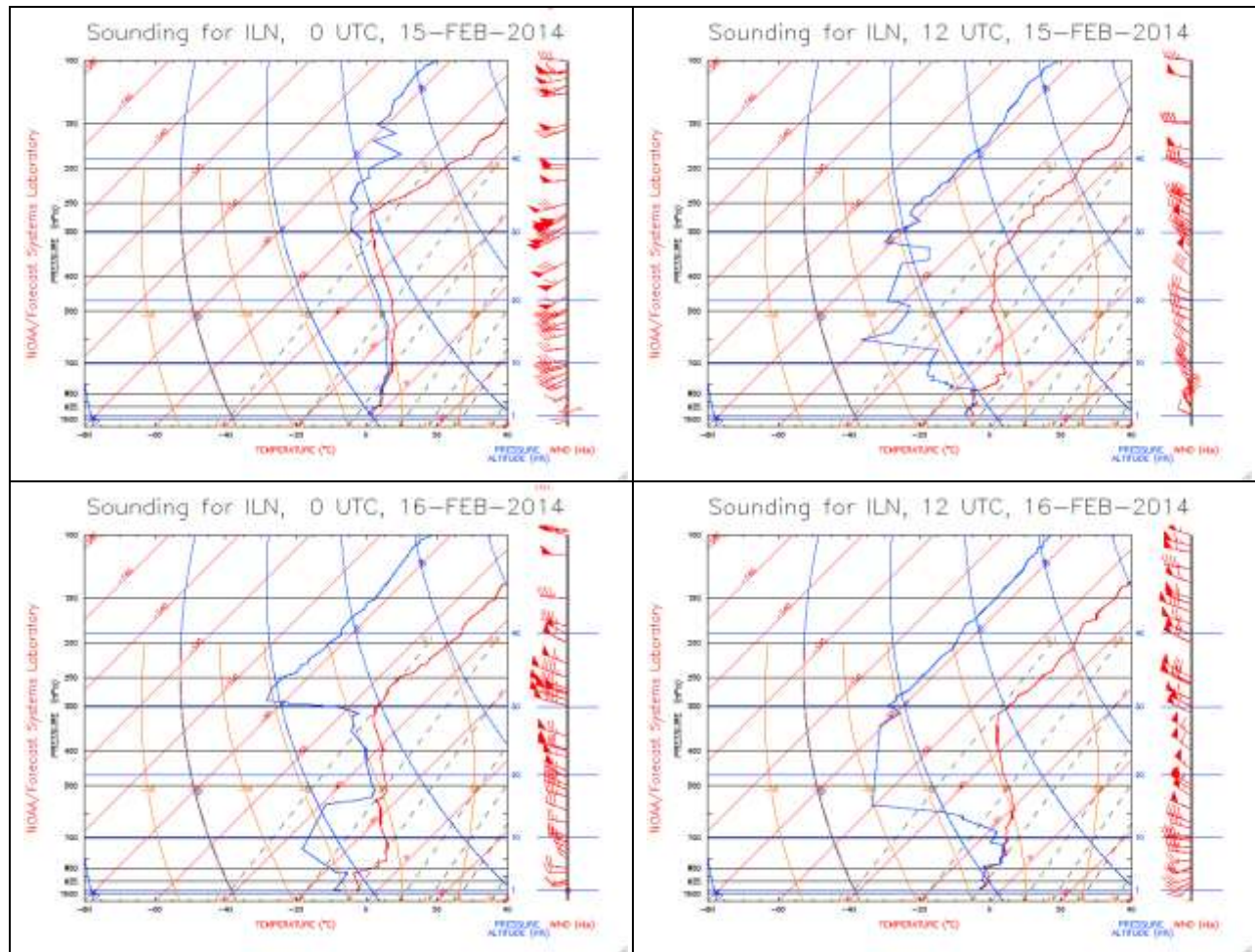


Table 9. Radiosonde Figures for July 11-12, 2014. Data was obtained from the NOAA/ESRL Radiosonde Database. Radiosonde data was obtained from <http://esrl.noaa.gov/raobs/> - Accessed on 9/3/2015.

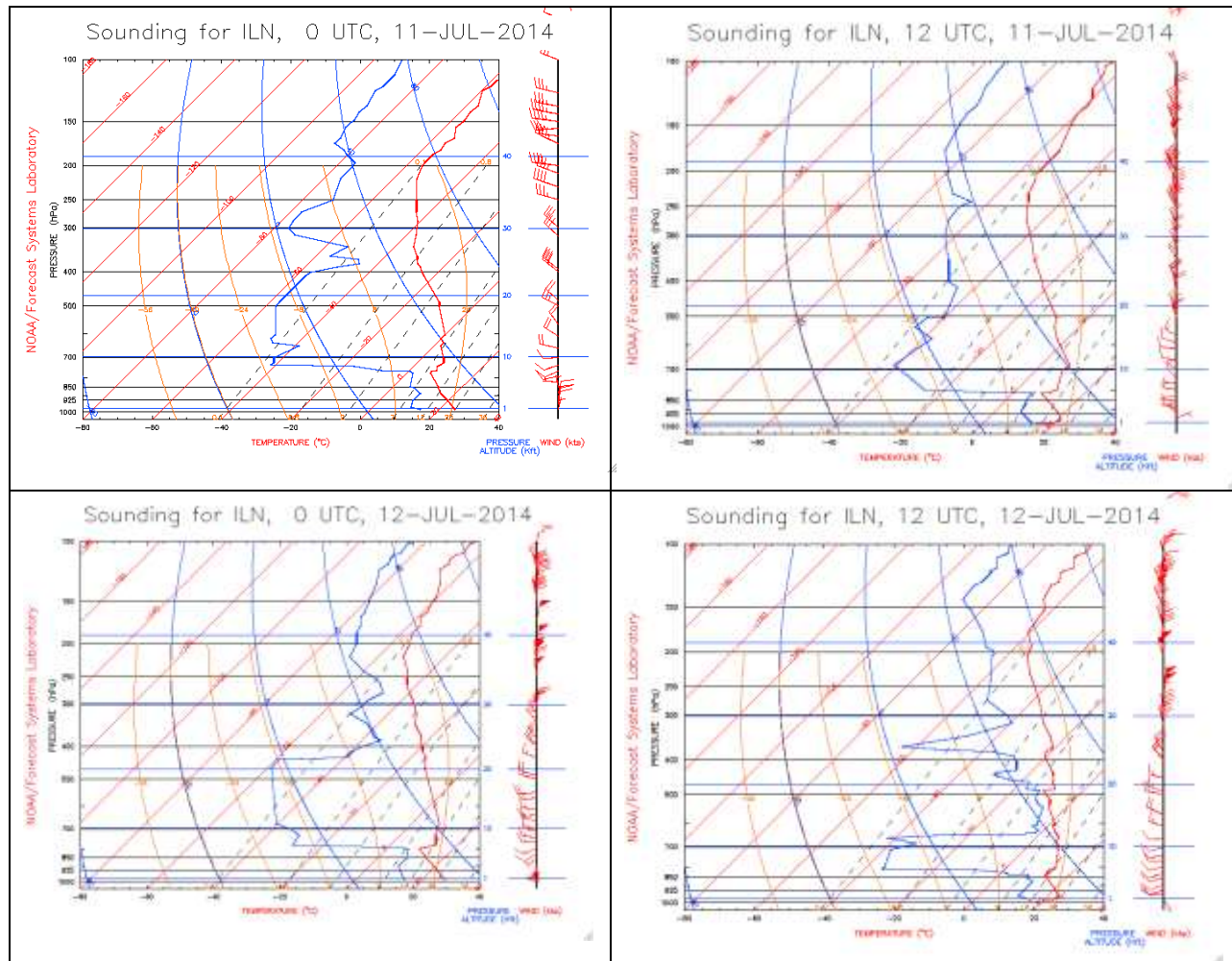
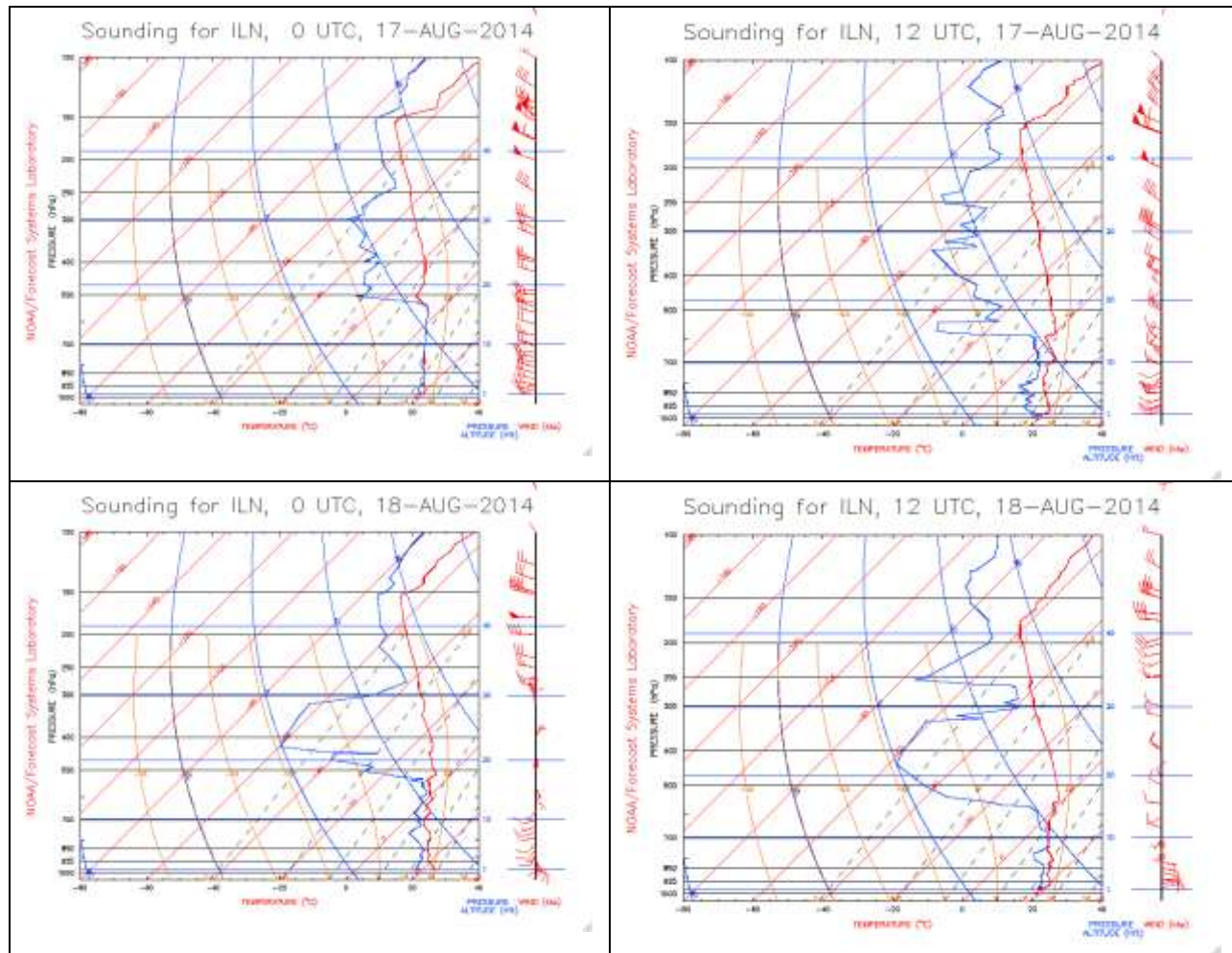


Table 10. Radiosonde Figures for August 17-18, 2013. Data was obtained from the NOAA/ESRL Radiosonde Database. Radiosonde data was obtained from <http://esrl.noaa.gov/raobs/> - Accessed on 9/3/2015.



Appendix E – Standard Operation Procedures

SOP 1.0

Acid Digestion and Analysis of Quartz Filter Samples for Determination of Metals by Inductively
Coupled Plasma – Optical Emission Spectrometry (ICP-OES)

Prepared by: Saagar Patel

7/26/15

A. Scope and Applicability

This method utilizes an analytical chemistry method to extract metals from quartz air-filters. Samples were collected over a six-day run, digested, filtered, and diluted prior to inductively coupled plasma analysis.

B. Summary of Method

This method applies to filter sample preparation for analysis by ICP-OES for metals.

C. Interferences

No interferences from the filter matrix has not yet been identified.

D. Safety

Proper lab techniques should be observed. PPE should be worn at all times. Extraction and sample prep should be done while wearing a lab coat, goggles, and gloves. The digestion process uses nitric acid, which is very acidic and dangerous. Any handling of nitric acid should be performed in the fume hood. When mixing acid and water, always add acid to water. If eye or skin contact occurs, flush with copious amounts of water. Immediately report any spills to appropriate personnel for proper cleanup. Unused nitric acid should be neutralized in the hood and additional hazardous waste should be disposed of properly.

E. Apparatus and Materials

Sample Collection

50-mL amber bottle with lid

X-acto Knife

Extraction

150mL beaker

Hot plate

10mL graduated cylinder

Fisher Scientific FS14H ultrasonic water bath

Filtration

100mL volumetric flask

Glass funnel

Whatman No. 41 filter paper or equivalent

F. Reagents and Chemicals

Trace metal grade nitric acid

18MΩ Resistivity Water

G. Sample Collection, Preservation and Handling

A 3.2 cm X 20.4 cm strip of the filter was cut using an x-acto knife and placed in an amber jar with lid and placed in a dark area until analysis.

H. Quality Control

An ASTM Type II water blank was prepared using the same methods applied to the sediment samples.

I. Sample Preparation Procedures

- a. Place samples in an oven to dry overnight.
- b. Remove the samples and place in a dessicator to cool. Place each sample in tared individual 150mL beakers and weigh each sample to the nearest 0.001 g.
- c. Add 10mL 1:1 HNO₃ to each beaker to create a slurry. Cover each sample with a watch glass and place beakers on a hot plate. Heat samples at 95 ± 5 °C for 1 hour.
- d. Allow the solutions to cool and decant the supernatant into a glass funnel with filter paper into a 100mL volumetric flask and dilute to the mark.
- e. Transfer a portion of the sample to a test tube for ICP-OES analysis.

J. Analytes

Analyte	Symbol	CAS No.	Wavelength (nm)
Aluminum	Al	7429-90-5	308.215
Barium	Ba	7440-39-3	493.409
Arsenic	As	7440-38-2	188.980
Calcium	Ca	7440-70-2	315.887
Copper	Cu	7440-50-8	324.754
Iron	Fe	7439-89-6	259.940
Manganese	Mn	7439-96-5	257.610
Magnesium	Mg	7439-95-4	279.079
Nickel	Ni	7440-02-0	231.604
Lead	Pb	7439-92-1	220.353
Potassium	K	7440-09-7	766.491
Selenium	Se	7782-49-2	196.099
Silicon	Si	7440-21-3	251.611
Sodium	Na	7440-23-5	588.995
Vanadium	V	7440-62-2	292.402
Zinc	Zn	7440-66-6	206.200

K. Calibration Standards

L. ICP-OES Analysis

M. Data Analysis

- a. Plot the intensity of each individual metal analyte versus the concentration to generate calibration curve equations.

- b. Determine the average and standard deviations for each analyte.
- c. Determine the concentration of each metal in the filters and report as mg/kg and percent of total mass.
- d. Limit of Detection (LOD) was determined by converting the lowest standard to concentration units using the calibration equation.

N. References

- 1. Alves, C. et al. 2011. Fireplace and woodstove fine particle emissions from combustion of western Mediterranean wood types, *Atmospheric Research*. 101, 692-700.
- 2. Chunlong Zhang, *Fundamentals of Environmental Sampling and Analysis*, Wiley-Interscience, 2007.
- 3. Acid Digestion of Sediments, Sludges, and Soils, USEPA Method 3050B, 1996.
- 4. Guidance on Evaluating Sediment Contamination Results, Standards and Technical Support Section, Ohio Environmental Protection Agency; Division of Surface Water, January 2010.

SOP 3.0

Preparation & Analysis of Samples & Standards for Levoglucosan by
Gas Chromatograph – Mass Spectrometry (GC/MS)

Prepared by: Saagar Patel

7/29/15

A. Scope and Applicability

This method is applicable to calibrated standards and treated samples prepared for Levoglucosan using the GC/MS

B. Summary of Method

This method uses a purchased sample of levoglucosan to prepare a set of 5 calibrated standards at concentrations of 333.3ppm, 166.7ppm, 83.3ppm, 16.6ppm, and 3.3ppm. These standards were analyzed using the GC/MS to generate a calibration curve, from which the sample concentrations can be calculated.

C. Interferences

Interferences with other anhydrosugar isomers, mannosan and galactosan, has been reported by literature. However, their concentrations are negligible.

D. Safety

Proper lab technique should be observed. Extraction and sample preparation should be done while wearing a lab coat and goggles. Gloves should be worn at all times. When derivitizing the levoglucosan, the procedure should be carried out in a fume hood. When using pyridine, the procedure should be carried out in the fume hood.

E. Apparatus and Materials

Sample Preparation

50-mL amber vial with lid
X-acto knife
Round Bottom Flask
Graduated Centrifuge Tube

Standard Preparation

GC Vials
GC Vial 400mL inserts
Pasteur Pipet & bulb

Equipment

Rotary Evaporator
Heating Block
Vortex
AE 240 Mettler Balance
FS14H Ultrasonicator
N₂ tank

F. Reagents and Chemicals

Solvents

Ethyl Acetate
Pyridine
Toluene

Reagents

Levoglucosan

BSTFA (w/ 1% TMCS)

G. Sample Preparation

1. Use an X-acto knife to cut a 3.2 cm x 20.4 cm strip from the air filter sample and place into a tared 100mL amber vial.
2. Weigh the sample and 30 mL of ethyl acetate into the amber and loosely close the lid.
3. Allow the sample to extract in a 150 W FS14H ultrasonicator from Fisher Scientific (Fair Lawn, NJ) for 30 minutes.
4. Collect the supernatant using a Pasteur pipette and transfer into a 500mL round bottom flask. Repeat this procedure three times to obtain a final volume of 90 mL ethyl acetate.
5. Rotovap the volume down to ~5 mL and transfer volume to a 10mL calibrated centrifuge tube and blow down the sample to exactly 2 mL using N₂ gas.
6. Withdraw 500 µL and place in a 2 mL vial. Blow down to dryness with N₂. Preserve the rest of the sample and place in fridge.
7. Resolute with 200 µL pyridine and add 100 µL BSTFA (with 1% TMCS) and vortex for 1 minute.
8. Heat sample on heating block at 78°C for 1 hour.
9. Blow sample down to near dryness and resolute in 300 µL toluene. Transfer to 400 µL vial insert.

H. Calibration Standards

- a. Place 1µL, 5 µL, 25 µL, 50 µL, 100 µL aliquots of levoglucosan in ethylacetate (from an original 1000 ppm standard solution) into 2 mL vials and bring to dryness with N₂ vapor.
- b. Resolute with 200 µL pyridine. Add 100 µL BSTFA (w/ 1% TMCS) to the vial and close it.
- c. Vortex each vial for 1 minute and heat at 78°C for 1 hour.
- d. Bring each sample to dryness with N₂ vapor.
- e. Resolute with 300 µL toluene. Transfer volume into a 400 µL vial insert.

I. GC/MS Analysis

- a. Analyze the standards and samples using a GC/MS at initial temperature of 50°C and ramp up to 300°C at 15°C/min.

- b. Use Selective Ion Monitoring – use m/z peaks of 73, 129, 147, 204, 217, and 333 at a retention time of 20.4 minutes to identify trimethylsilyl derivatives of levoglucosan.
- c. Plot the standard peak abundances on a Peak Area vs. Concentration (ng) graph and calculate the concentrations of those peaks for the samples using the calibration curve equation obtained from the standard dilutions.
- d. Limit of Detection (LOD) was determined by converting the lowest standard to concentration units using the calibration equation.

J. References

- a. Kuo LJ, Herbert BE, Louchouart P, Can levoglucosan be used to characterize and quantify char/charcoal black carbon in environmental media? *Organic Geochemistry*, 2008, 39, 1466-1478.
- b. Simpson CD, Dills RL, Katz BS, Kalman, DA, Determination of levoglucosan in atmospheric fine particulate matter, *Journal of the Air & Waste Management Association*, 2004, 54, 689-694.
- c. Bari MA, Baumbach G, Buch B, Scheffknecht G, Wood smoke as a source of particle-phase organic compounds in residential areas, *Atmospheric Environment*, 2009, 43, 4722-4732.
- d. Fabbri D, Chiavari G, Prati S, Vassura I, Vangelista M, Gas chromatography/mass spectrometric characterization of pyrolysis/silylation products of glucose and cellulose, *Rapid Communications in Mass Spectrometry*, 2002, 16, 2349-2355.

SOP 4.0

Preparation & analysis of Samples & Standards for PAH Analysis by
Gas Chromatograph – Mass Spectrometry

Prepared by: Saagar Patel

7/29/15

A. Scope and Applicability

This method is applicable to calibrated standards and treated samples prepared for PAH analysis using the GC/MS.

B. Summary of Method

This method uses a mixture of the EPA 16 PAH at 4000ppm to prepare five calibrated standards at concentrations of 1.0 ppm, 0.5 ppm, 0.2 ppm, 0.1ppm and 0.05ppm. The prepared standards and samples are analyzed with GC/MS to generate a series of calibration curves,

C. Interferences

The co-elution of chrysene and d12-chrysene prohibits quantitative values to be determined with respect to concentration. As such, obtained values from both analytes should be treated as qualitative.

D. Safety

Proper lab technique should be observed. Extraction and sample preparation should be done while wearing a lab coat and goggles. Any use of PAH standards should be done in a fume hood.

E. Apparatus and Materials

Sample & Standard Preparation

X-acto knife

100mL amber vial with lid

GC vials

400 µL GC vial insert

Round Bottom Flask

Instrumentation & Equipment

GC/MS

Mettler Balance

Ultrasonicator

F. Reagents and Chemicals

Hexane

Dichloromethane

N₂ tank

200-ppm mixed PAH standard (Accustandard, New Haven, CT) containing EPA 16 PAHs: naphthalene, acenaphthene, acenaphthylene, fluorene, phenanthrene, anthracene, fluoranthene, pyrene, benz[a]anthracene, chrysene, benzo[b]fluoranthene, benzo[k]fluoranthene, benzo[a]pyrene, dibenz[a,h]anthracene, benzo[ghi]perylene, indeno[1,2,3-cd]pyrene

4000-ppm mixed deuterated PAH standard (naphthalene-d8, acenaphthene-d10, phenanthrene-d10, chrysene-d10 and perylene-d12)

p-terphenyl (as internal standard)

G. Sample Preparation

- a. Use an Exacto[®] knife to cut sample into 3.2 cm x 20.4 cm strips.
- b. Weigh the strip in a tarred sample boat using a Mettler AE240S Balance (Mettler Instrument Corp, Highstown, NJ) and place into pre-weighed 100-mL amber glass vials.
- c. Then add 80 μ L of 100 μ g/mL deuterated mixed standard solution and allow each sample to sit for 20 minutes.
- d. Afterwards, add 60 mL of a 1:1 volume ratio of hexane/dichloromethane and allow sample to extract in a 150 W FS14H ultrasonicator from Fisher Scientific (Fair Lawn, NJ) for 10 minutes with the lid tightly screwed.
- e. Transfer the samples to 300 mL round-bottom flasks with aluminum foil coverings.
- f. Extract the sample twice using fresh aliquots of solvent, providing that the final volume does not exceed 180 mL.
- g. Rotovap the volume to 2-3 mL.
- h. Filter the extract through a 0.45 μ m PTFE syringe filter into a 10 mL calibrated centrifuge tube.
- i. Dilute the volume to 4.00 mL. Save 2.0 mL of the extract in sample vials and place in a dark space.
- j. Place 2.00 mL of the sample into GC vials and add 40 μ L of 25 ppm p-terphenyl as internal standard.
- k. Filter the extract through a 0.45 μ m PTFE syringe filter into a 10 mL calibrated centrifuge tube.

H. Sample Analysis

1. Analyze the standards and samples using a GC/MS (splitless mode) with ultrapure helium as the carrier gas under the following ramp conditions:
 - Initial temperature of 40 °C with a 5 minute hold
 - Ramp up to 180°C at 10°C/min with a 5 minute hold
 - Ramp up to 250°C at 10°C/min with a 5 minute hold
 - Ramp up to 320°C at 10°C/min with a 5 minute hold
2. Use Selective Ion Monitoring – use the following table of m/z peaks and retention times to identify the 16 PAH's, 6 dPAH's and p-terphenyl.

Polycyclic aromatic hydrocarbons	Structure (# of rings)	Molecular weight (g/mole)	CAS #	Retention Time (s)
Naphthalene	2	128.17	91-20-3	14.340
Acenaphthene	3	154.21	83-32-9	18.562
Acenaphthylene	3	152.2	208-96-8	18.113
Anthracene	3	178.23	120-12-7	23.909
Phenanthrene	3	178.23	85-01-8	23.623
Fluorene	3	166.22	86-73-7	19.886
Fluoranthene	4	202.26	206-44-0	28.760
Benzo(a)anthracene	4	228.29	56-55-3	33.707
Chrysene	4	228.29	218-01-9	33.560
Pyrene	4	202.26	129-00-0	29.471
Benzo(a)pyrene	5	252.32	50-32-8	39.658
Benzo(b)fluoranthene	5	252.32	205-99-2	38.558
Benzo(k)fluoranthene	5	252.32	207-08-9	38.674
Dibenz(a,h)anthracene	6	278.35	53-70-3	42.801
Benzo(g,h,i)perylene	6	276.34	191-24-2	43.261
Indeno[1,2,3-cd]pyrene	6	276.34	193-39-5	42.701

Deuterated Polycyclic aromatic hydrocarbons	Structure (# of rings)	Molecular weight (g/mole)	CAS #	Retention Time (s)
Acenaphthene-d10	3	164.17	15067-26-2	18.483
Chrysene-d12	4	240.12	1719-03-5	33.614
1,4-Dichlorobenze-d4	1	150.95	3855-82-1	11.281
Naphthalene-d8	2	136.14	1146-65-2	14.293
Perylene-d12	6	264.15	1520-96-3	39.852
Phenanthrene-d10	3	188.09	1517-22-2	23.507
p-terphenyl	3	230.30	92-94-4	30.315

3. Plot the standard peak abundances on a Peak Area vs. Concentration (ng) graph and calculate the concentrations of those peaks for the samples using the calibration curve equation obtained from the standard dilutions.
4. To calculate the concentration of PAHs in the filter,
 - Sum the nanogram concentrations derived from the calibration curve calculations for the 16 PAHs.
 - Multiply the concentration by the size ratio of the filter sample used to the whole filter to obtain a mass concentration of the full filter.
 - Divide by the mass of the filter to obtain a PAH/filter ratio.
5. To calculate the concentration of PAHs in the air passed through the filter,
 - Take the full-filter mass of PAH and divide by the total volume of air (in m³)
6. Limit of Detection (LOD) was determined by converting the lowest standard to concentration units using the calibration equation.

I. References

- a. Bojes, H.K., Pope, P. G., Characterization of EPA's 16 priority pollutant polycyclic aromatic hydrocarbons (PAHs) in tank bottom solids and associated contaminated soils at oil exploration and production sites in Texas. *Regulatory Toxicology and Pharmacology*, 2007, 47, 3, 288-295.
- b. McGowin, A., Patel, S. PM Filter Extraction and Analysis. RAPCA Report. 2014. 1-2
- c. Tomashuk, T.A., Truong, T. M., Mantha, M., McGowin, A.E., Atmospheric polycyclic aromatic hydrocarbon profiles and sources in pine needles and particulate matter in Dayton, Ohio, USA. *Atmospheric Environment*, 2012, 51, 196-202.

Appendix F – Concentrations of Levoglucosan

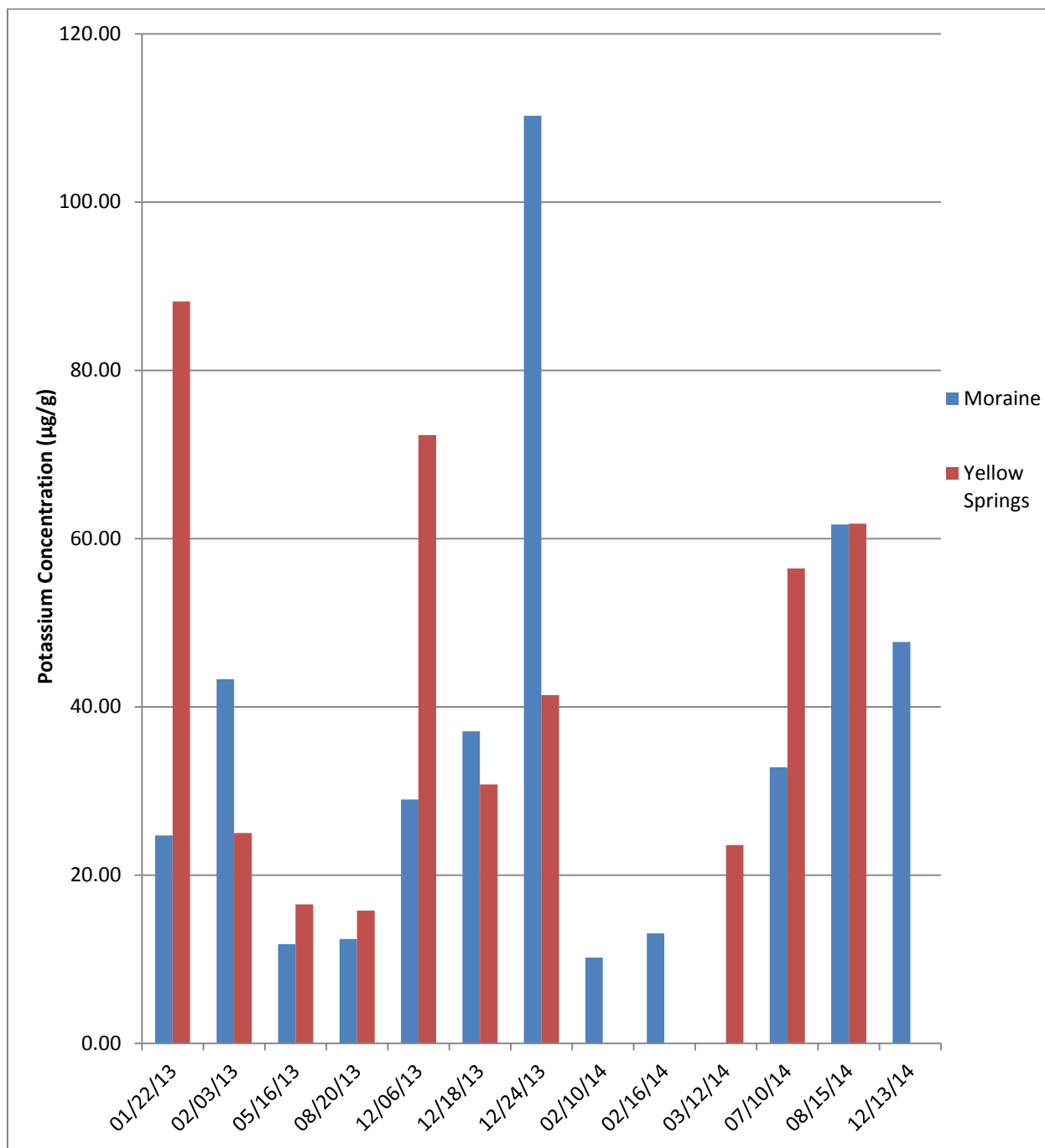
Table 1. Levoglucosan Concentration over time by site

Dates	Moraine (µg/g)	Yellow Springs (µg/g)
01/22/13	24.72	88.17
02/03/13	43.27	24.99
05/16/13	11.79	16.50
08/20/13	12.39	15.78
12/06/13	28.98	72.28
12/18/13	37.10	30.77
12/24/13	110.27	41.38
02/10/14	10.19	*
02/16/14	13.06	†
03/12/14	†	23.56
07/10/14	32.80	56.45
08/15/14	61.66	61.77
12/13/14	47.70	‡
* No filter was received from RAPCA † Sample was below limit of detection ‡ Sample was lost in spill - no result		

Table 2. Average Levoglucosan Values by Site

	Average (µg/g)	Standard Deviation (µg/g)
Moraine	39.4	31.6
Yellow Springs	46.9	27.1
	Summer Average (µg/g)	Summer Standard Deviation (µg/g)
Moraine	29.7	23.5
Yellow Springs	37.6	24.9
	Winter Average (µg/g)	Winter Standard Deviation (µg/g)
Moraine	39.4	31.6
Yellow Springs	51.5	27.4

Figure 1. Levoglucosan concentrations over time by site



Appendix G – Concentrations of Metals over time

Table 1. Concentrations of Metals in Moraine

Analytes (µg/g)											
	3/12/14	2/16/14	2/10/14	12/24/13	12/18/13	12/6/13	8/20/13	5/16/13	2/3/13	1/22/13	Date
7/10/14	10500	6470	5280	12900	13200	5570	11300	14400	1320	1760	Al
14100	*	*	*	46.2	*	*	*	*	*	*	As
158200	48730	32790	35760	117600	95900	41850	118200	54520	161000	337000	Ca
6067	2435	3088	3105	8630	6192	3864	7761	3801	4332	10960	Cu
59078	18700	11748	15014	24150	41777	16868	66142	32287	27399	40763	Fe
27170	15380	12930	9958	26690	17610	16430	13980	13880	26750	22780	K
6567	†	†	†	†	†	†	18040	†	†	28440	Mg
338.9	*	*	385.5	*	1419	*	674.8	577.6	*	417.8	Mn
135550	222800	165400	183000	234600	411600	267000	57350	72840	527500	243800	Na
*	*	*	*	*	*	*	80.07	*	*	484.3	Pb
43590	22640	24650	24240	23010	32950	22200	17000	19640	50120	50980	Si
*	*	*	*	*	*	*	*	*	4490	*	Sr
4807	2483	2031	2093	5281	4732	2998	5988	2116	4262	4047	Zn

Table 1 continued

Zn	31690	3008
Sr	*	*
Si	40670	27860
Pb	22.04	*
Na	123600	104800
Mn	527.9	*
Mg	29010	†
K	21510	15040
Fe	69549	18432
Cu	7630	4490
Ca	194300	48210
As	*	*
Al	16800	6300
	8/15/14	12/13/14
* Concentrations were below limit of detection = 0.01000ppm		
† Concentrations were below limit of detection = 0.1000ppm		

Table 2. Concentration of Metals in Yellow Springs

Analytes (µg/g)					
Zn	4134	2592	2204	3346	
Si	42930	36100	25140	25820	
Pb	*	*	54	527	
Na	309900	141400	100700	77910	
Mn	*	*	133	*	
K	30560	17660	18510	13990	
Fe	21830	10790	28470	14120	
Cu	6070	1640	5868	4300	
Ca	205950	42880	58310	35240	
As	*	*	2772	*	
Al	19240	7532	19250	5731	
Date	1/22/13	2/3/13	5/16/13	8/20/13	

Table 2 continued

4890	5644	4274	1452	6913	4602	6452	3646
49410	64390	00951	36340	08743	02120	40850	02120
*	*	*	*	*	*	*	*
175800	294200	006792	003500	005481	006300	006900	024621
*	*	*	*	*	*	*	*
25300	18840	00003	04730	02791	02130	26320	04740
17950	19720	01441	342	0206	02061	21900	02801
10640	2328	8626	4224	3213	5695	4344	1241
51220	74920	01369	06961	08963	06994	83260	01124
*	*	*	*	*	*	*	*
10280	11900	02131	9714	9915	9436	06911	5316
12/6/13	12/18/13	12/14/2/21	4/19/14	4/12/21/3	4/10/14	8/15/14	4/13/14
* Concentrations were below limit of detection = 0.01000ppm							

Table 3. Concentration of Potassium in Moraine and Yellow Springs

Moraine (µg/g)		Yellow Springs (µg/g)	
1/22/2013	22780	1/22/2013	30558
2/3/2013	26754	2/3/2013	17662
5/16/2013	13877	5/16/2013	18512
8/20/2013	13978	8/20/2013	13991
12/6/2013	16427	12/6/2013	25305
12/18/2013	17605	12/18/2013	18843
12/24/2013	26693	12/24/2013	30046
2/10/2014	9958	2/10/2014	*
2/16/2014	12930	2/16/2014	14725
3/12/2014	15380	3/12/2014	16722
7/10/2014	27168	7/10/2014	23130
8/15/2014	21512	8/15/2014	26324
12/13/2014	15045	12/13/2014	16739
* No filter was obtained for Yellow Springs			

Figure 1. Concentration of potassium vs. time

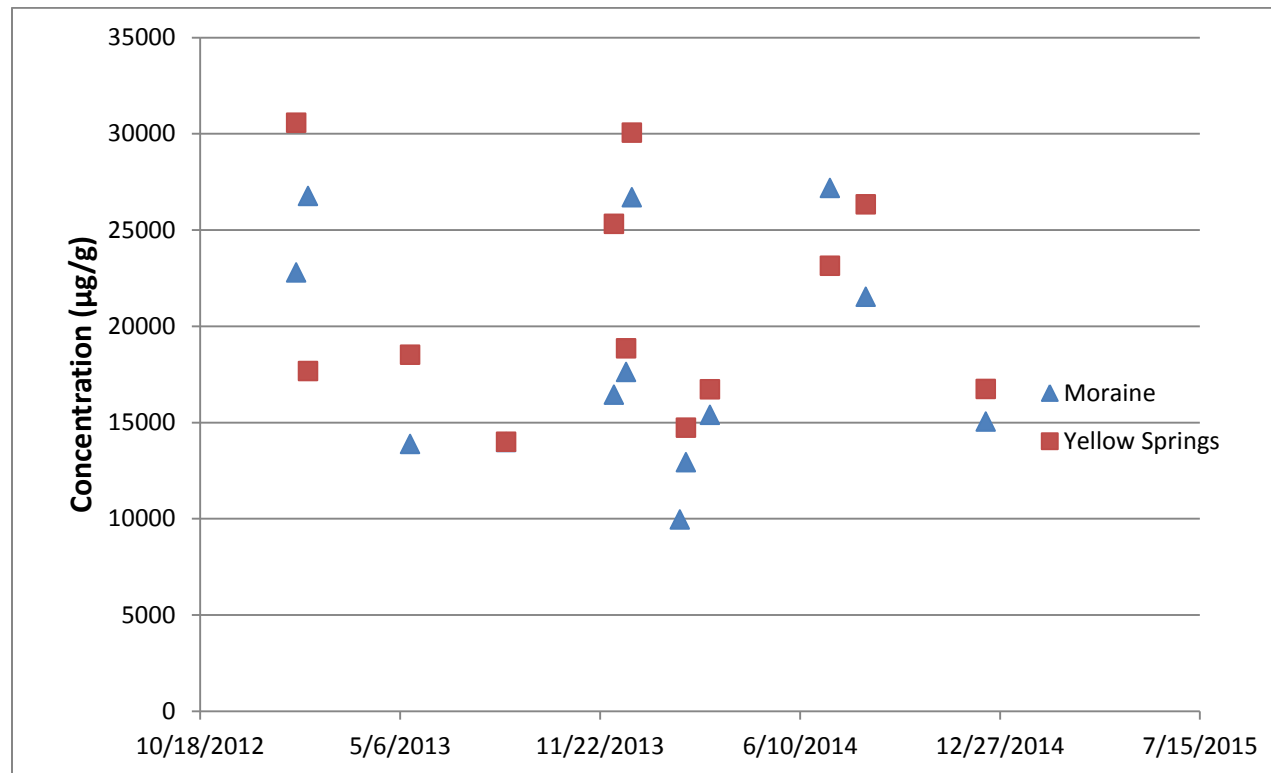


Figure 2. Concentration of aluminum over time

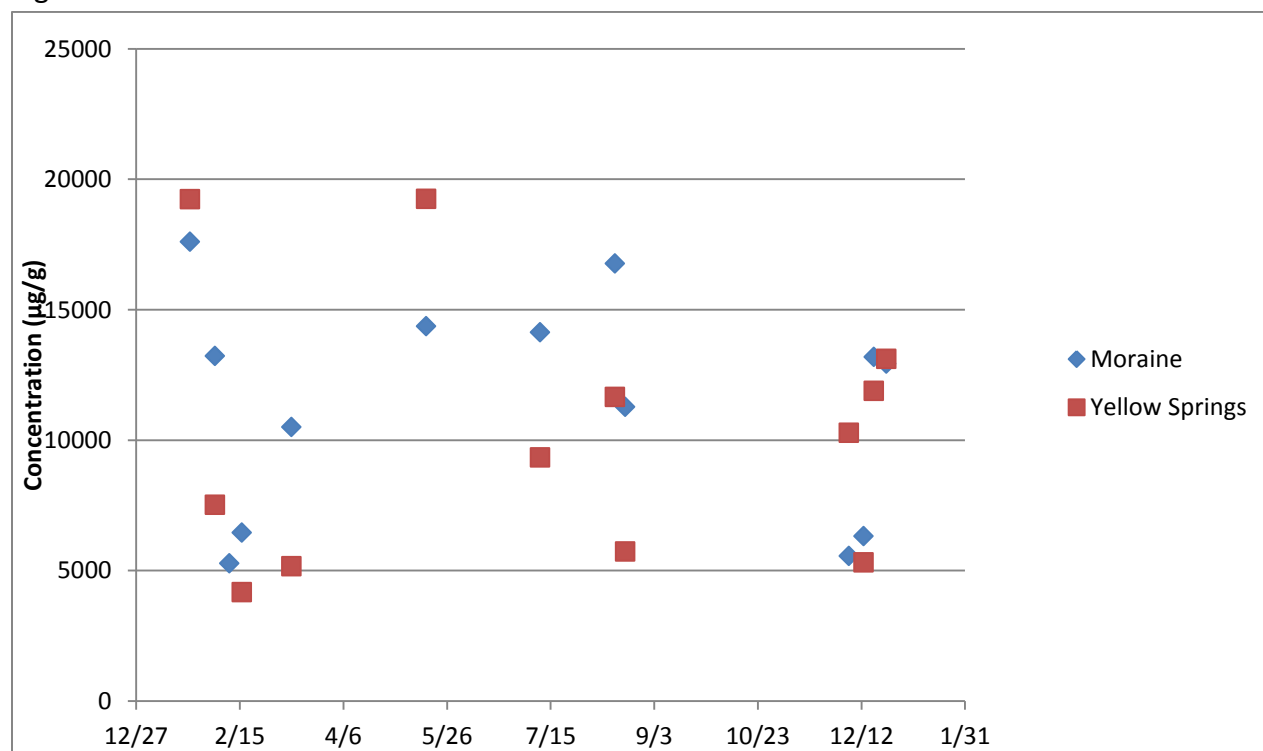


Figure 3. Concentration of calcium over time

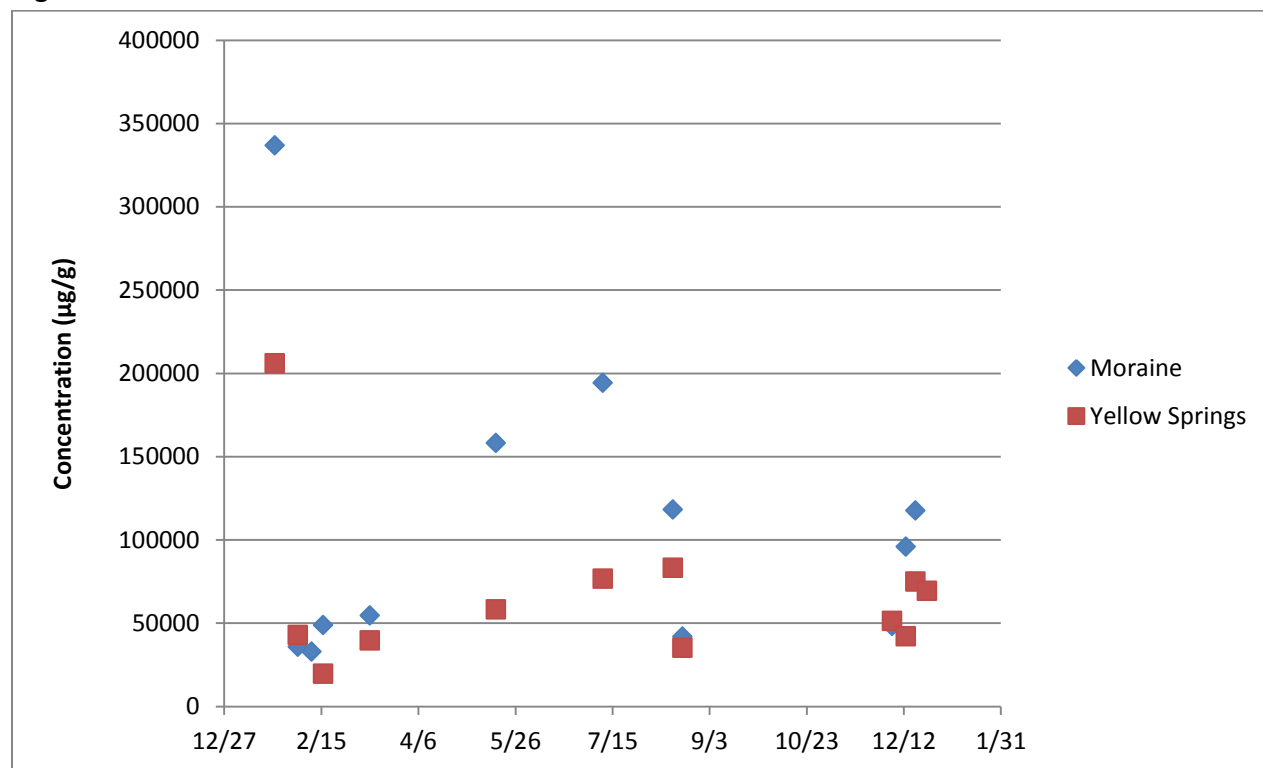


Figure 4. Concentration of copper over time

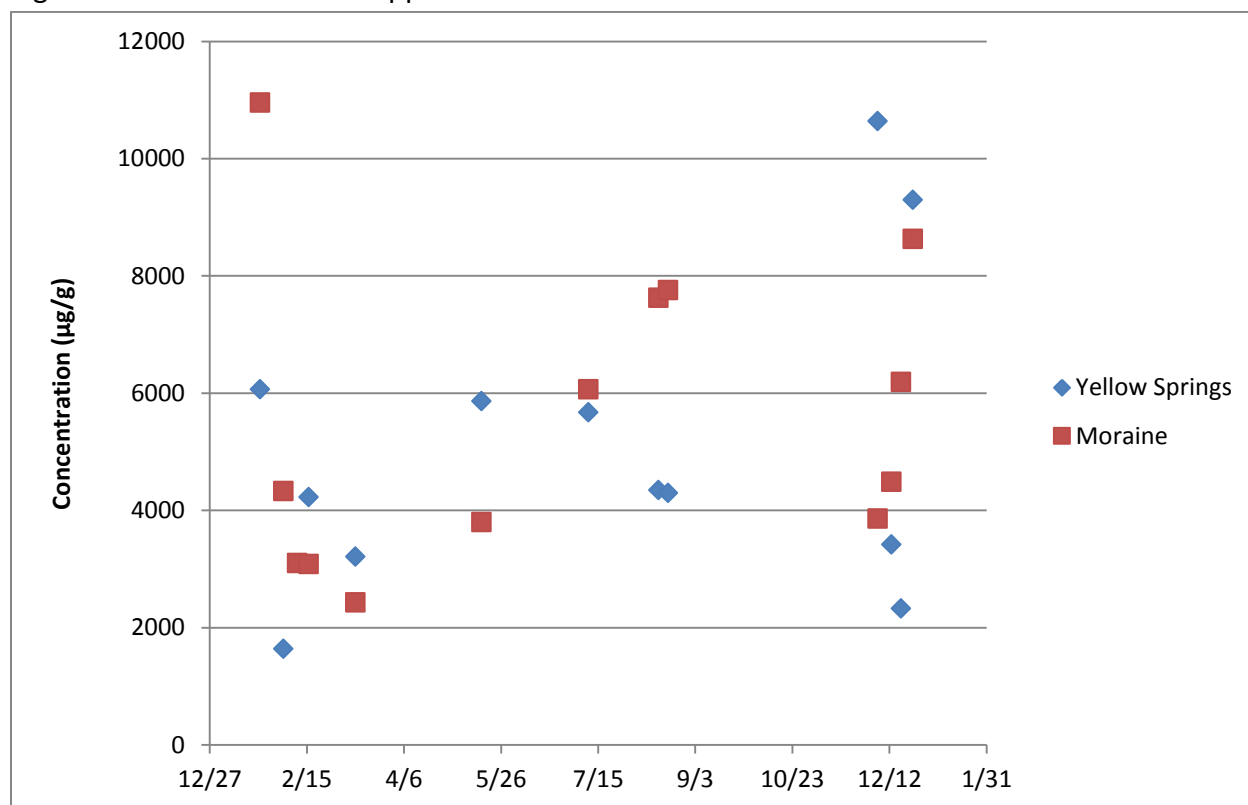


Figure 5. Concentration of iron over time

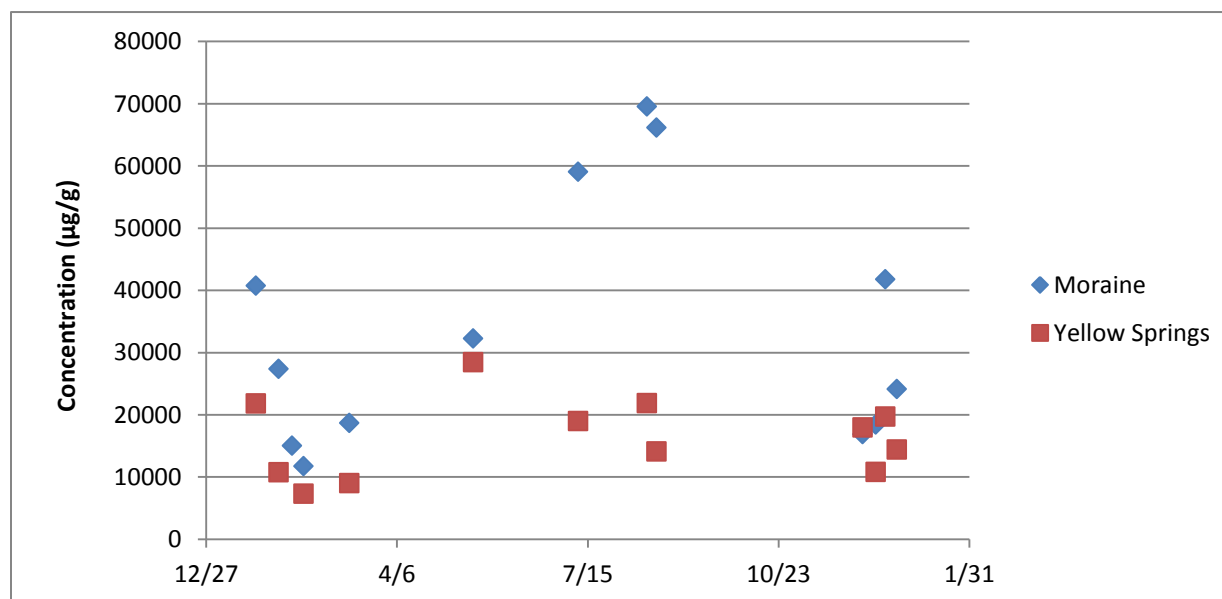


Figure 6. Concentration of silicon over time

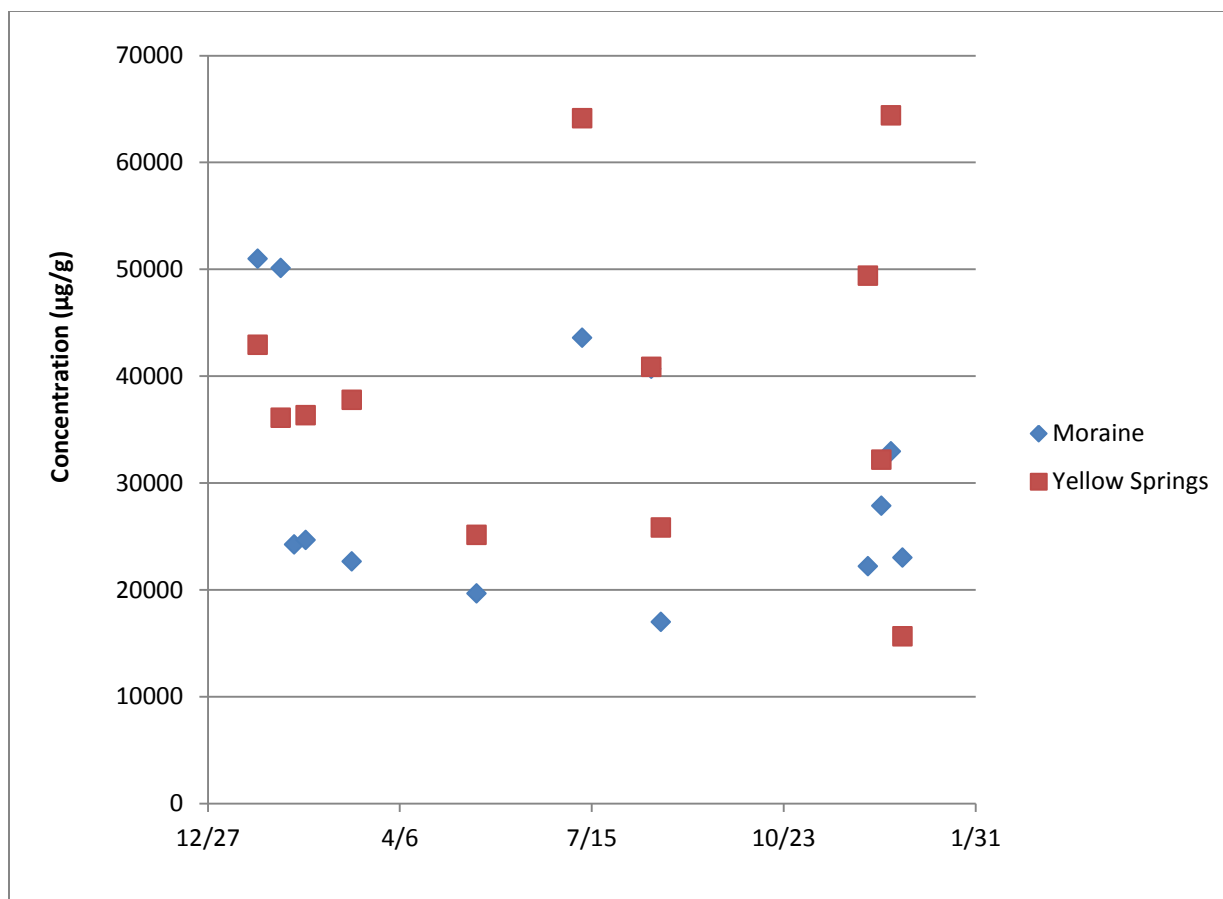


Figure 7. Concentration of sodium over time

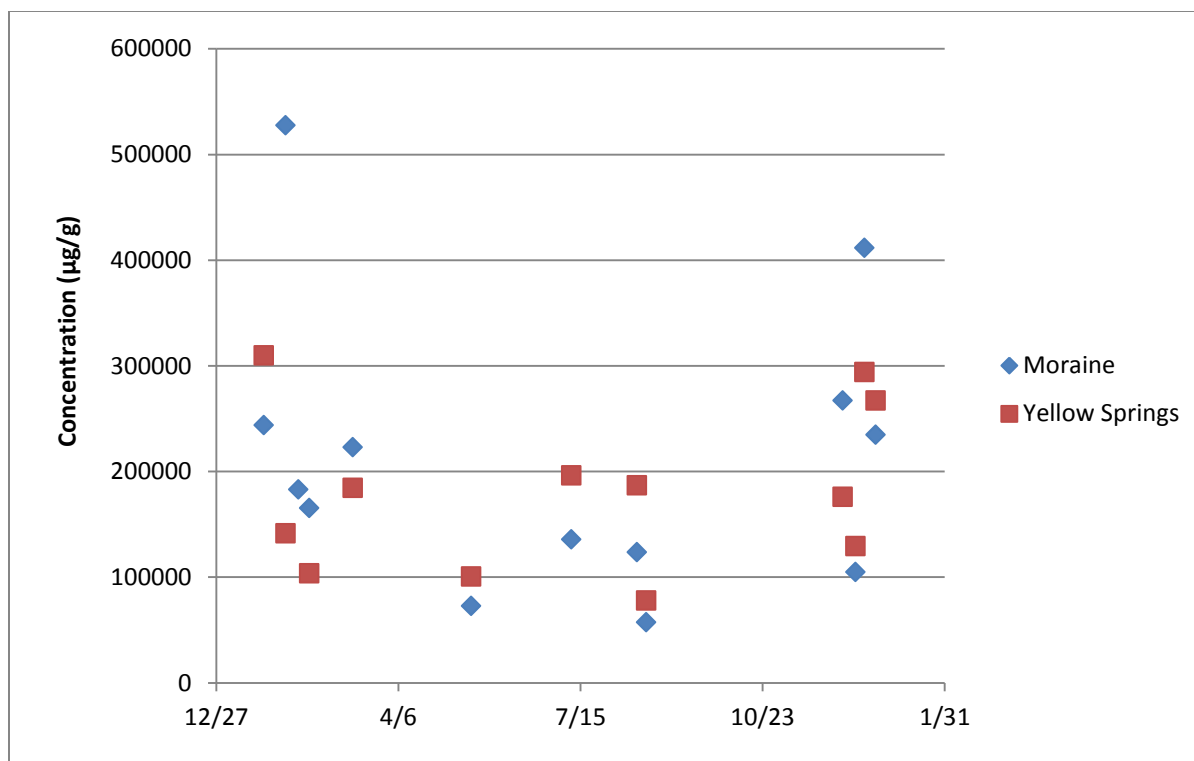
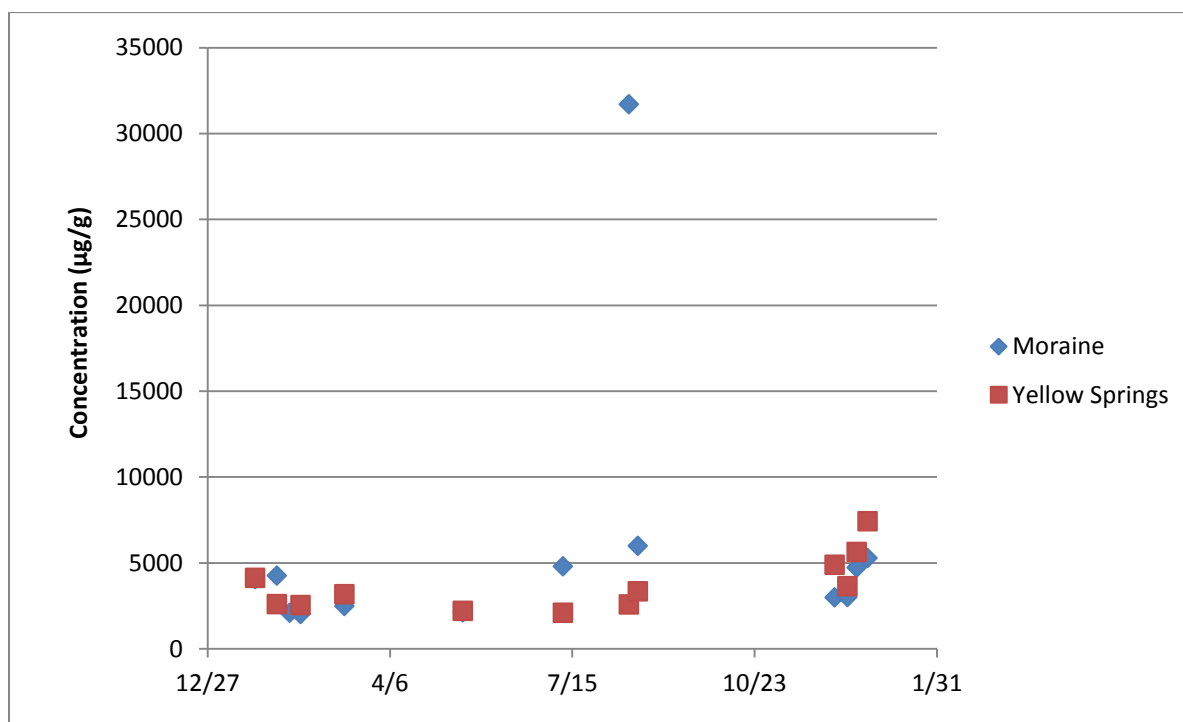


Figure 8. Concentration of zinc over time



Appendix H- Concentrations of PAHs

Table 1. Concentration of PAHs in Moraine, grouped by number of rings

Total (µg/g)	6-ring µg/g	5-ring (µg/g)	4-ring (µg/g)	3-ring (µg/g)	2-ring (µg/g)	
1869	566.7	581.9	577.9	74.16	68.69	01/22/13
3025	1328	510.4	940.0	126.2	120.5	02/03/13
1150	400.3	405.3	278.5	32.04	34.12	05/16/13
1011	315.9	390.7	241.1	28.41	34.74	08/20/13
1653	640.4	514.3	401.5	47.29	49.03	12/06/13
2343	885.2	759.1	570.3	70.33	58.01	12/18/13
2336	875.4	587.9	728.0	34.69	110.19	12/24/13
842.4	357.6	253.6	195.6	16.40	19.32	02/10/14
811.7	272.4	323.3	184.4	0.00	31.55	02/16/14
1117	418.6	258.2	383.9	14.85	41.06	03/12/14
1770	438.5	665.0	530.5	75.69	60.72	07/10/14
1681	686.7	522.8	432.7	20.79	18.08	08/15/14
1445	664.2	333.6	376.1	31.12	39.72	12/13/14

Table 2. Concentration of PAHs in Yellow Springs, grouped by number of rings

12/13/14	58.85	18.37	380.9	220.8	709.9	1389
08/15/14	100.1	54.86	233.2	370.0	0.00	758.2
07/10/14	75.09	26.54	202.0	730.9	371.7	1406
03/12/14	72.92	52.40	460.4	561.3	506.6	1654
02/16/14	603.97	435.77	1729.0	1819.6	1202.87	5791
12/24/13	53.89	105.79	491.8	556.7	919.2	2127
12/18/13	71.72	70.85	465.3	723.8	646.4	1978
12/06/13	71.51	69.56	486.7	799.7	1137.03	2564
08/20/13	39.97	45.82	256.6	356.0	521.8	1220
05/16/13	38.99	36.86	256.9	398.6	404.5	1136
02/03/13	66.38	73.73	402.0	601.8	784.9	1929
01/22/13	101.3	108.2	898.2	897.1	945.0	2950
	2-ring (µg/g)	3-ring (µg/g)	4-ring (µg/g)	5-ring (µg/g)	6-ring µg/g)	Total (µg/g)

Table 3. Means and standard deviations of PAH concentrations by site and ring-size

	Moraine		Yellow Springs	
	Average ($\mu\text{g/g}$)	Standard Deviation ($\mu\text{g/g}$)	Average ($\mu\text{g/g}$)	Standard Deviation ($\mu\text{g/g}$)
2-ring	52.75	31.62	112.9	155.9
3-ring	43.99	34.27	91.56	111.9
4-ring	449.3	219.0	521.9	423.0
5-ring	469.7	157.2	669.7	414.5
6-ring	603.9	295.5	679.2	345.3
Total	1620	660	2075	1324

Table 6. Winter Concentrations of PAHs in Moraine and Yellow Springs

Winter Concentrations (ng/m ³)				
	Moraine		Yellow springs	
	Average	Standard Deviation	Average	Standard Deviation
2-ring	0.900	0.132	2.839	5.296
3-ring	0.800	0.293	2.243	3.742
4-ring	7.362	1.202	11.175	13.835
5-ring	8.101	2.740	12.626	14.323
6-ring	10.850	2.683	12.930	7.606
Total	27.913	5.730	41.814	44.457

Table 7. Summer Concentrations of PAHs in Moraine and Yellow Springs

Summer Concentrations (ng/m ³)				
	Moraine		Yellow springs	
	Average	Standard Deviation	Average	Standard Deviation
2-ring	0.854	0.354	0.898	0.091
3-ring	0.773	0.462	0.663	0.264
4-ring	7.942	1.117	4.366	1.989
5-ring	10.062	3.550	7.107	2.007
6-ring	9.819	2.217	6.190	4.316
Total	29.450	6.316	19.224	7.797

Table 8. Concentration of Individual PAHs per sample in Moraine

Moraine	01/22/13	02/03/13	05/16/13	08/20/13	12/06/13	12/18/13	12/24/13	02/10/14	02/16/14	03/12/14	07/10/14	08/15/14	12/13/14
PM Mass (g)	0.02230	0.01250	0.04600	0.05060	0.03120	0.02570	0.01620	0.06290	0.04400	0.02620	0.02780	0.02630	0.02840
	ug/g	ug/g	ug/g	ug/g	ug/g	ug/g	ug/g	ug/g	ug/g	ug/g	ug/g	ug/g	ug/g
naphthalene	17.99	33.57	9.80	9.28	16.43	17.23	24.19	4.98	5.68	3.28	27.46	-5.19	5.83
acenaphthylene	50.69	86.94	24.32	25.46	32.59	40.77	86.01	14.34	25.87	37.78	33.26	23.28	33.90
acenaphthene	31.94	56.43	13.90	11.63	20.91	36.37		16.40			53.89	8.10	31.12
fluorene	42.22	69.73	18.15	16.78	26.37	33.95	34.69			14.85	21.80	12.69	
phenanthrene	32.08	57.23	15.55	14.14	22.93	27.84	44.16	11.37	16.26	27.31	25.73	27.20	
anthracene	71.66	128.67	33.59	31.13	50.87	61.30						43.40	
fluoranthene	100.71	143.02	54.43	74.73	68.87	123.95	170.43	42.44	51.59	71.63	149.63	71.18	70.28
pyrene	88.99	127.61	45.13	54.51	58.78	100.57	128.59	34.54	41.76	55.28	102.03	50.53	57.78
chrysene	131.00	236.27	61.45	66.61	96.19	135.61	179.06	51.67		110.07	136.54	100.17	124.92
benzo[a]anthracene	153.49	247.18	68.33		103.84	121.00	205.77	55.54	74.80	119.63	116.53	140.20	123.12
benzo[b]fluoranthene	139.01	182.78	139.69	145.32	162.44	270.59	221.29	78.34	85.46	99.75	215.60	135.01	165.69
benzo[k]fluoranthene	191.99	327.60	109.05	100.98	147.07	196.80		70.17	95.89	158.44	164.40	188.23	167.95
benzo[a]pyrene	250.92		156.60	144.43	204.82	291.73	366.63	105.06	141.95		285.00	199.58	
indeno[1,2,3-cd]pyrene	269.47	493.86	252.02	177.87	265.12	393.10	458.38	142.07				259.86	252.09
dibenz[a,h]anthracene		326.30			158.03	201.86		107.13	122.07	171.38	198.28	188.93	170.77
benzo[g,h,i]perylene	297.22	508.27	148.31	138.05	217.28	290.27	416.99	108.38	150.37	247.25	240.20	237.90	241.32

Table 9. Concentration of Individual PAHs per sample in Yellow Springs

Yellow Springs	01/22/13	02/03/13	05/16/13	08/20/13	12/06/13	12/18/13	12/24/13	02/10/14	02/16/14	03/12/14	07/10/14	08/15/14	12/13/14
PM Mass (g)	0.01380	0.02270	0.03210	0.03460	0.01850	0.02120	0.01550		0.04050	0.02230	0.01730	0.01500	0.02670
ug/g	ug/g	ug/g	ug/g	ug/g	ug/g	ug/g	ug/g		ug/g	ug/g	ug/g	ug/g	ug/g
naphthalene	26.81	17.85	8.99	10.01	22.10	22.73			303.33	13.60	22.82	23.17	11.38
acenaphthylene	74.45	48.53	30.00	29.96	49.41	48.99	53.89		300.64	59.32	52.28	76.93	47.47
acenaphthene	44.25	33.84	15.76	23.66	28.44	31.59	67.17		435.77	31.84			
fluorene	63.93	39.88	21.10	22.16	41.11	39.26	38.63			20.56	26.54	54.86	18.37
phenanthrene	51.84	31.52	22.29	20.68	38.67	33.75	46.16		17.66	32.08	41.35	47.69	26.79
anthracene	112.21	72.03	44.71	43.68	81.60	74.46							
fluoranthene	139.02	84.82	53.87	57.72	109.55	117.06	133.14		804.73	81.36	90.23	102.55	65.46
pyrene	122.81	76.47	46.16	48.06	93.50	98.32	102.16		601.52	65.17	70.40	82.95	51.50
chrysene	235.10	137.16	89.86	86.45	163.36	141.76	210.39			139.05			109.31
benzo[a]anthracene	237.23								305.12	142.74			127.88
benzo[b]fluoranthene	191.36	150.60	84.79	77.36	218.95	204.45	181.02		1307.92	119.83	163.13		
benzo[k]fluoranthene	301.61	192.65	129.18	119.61	234.66	210.70				187.28	236.10		
benzo[a]pyrene	404.08	258.58	184.62	159.04	346.11	308.64	375.63		511.70	254.22	331.70	370.01	220.81
indeno[1,2,3-cd]pyrene	477.63	284.65	206.26	200.52	462.72	334.79	488.94						251.77
dibenz[a,h]anthracene		212.02		133.96	323.78				826.34	220.87			210.59
benzo[g,h,i]perylene	467.40	288.28	198.19	187.34	350.52	311.64	430.25		376.52	285.78	371.73		247.54

Table 10. Ratios of indeno[1,2,3,-cd]pyrene (IcdP), benzo[ghi]perylene (BgHiP), fluoranthene (Flt), pyrene (Pyr), Benz[a]anthracene (BaA), and chrysene (Chr) for Moraine and Yellow Springs

Yellow Springs				Moraine			
BaA/ (BaA+Chr)	Flt/ (Flt+Pyr)	IcdP/ (IcdP+BghiP)	BaA/ (BaA+Chr)	Flt/ (Flt+Pyr)	IcdP/ (IcdP+BghiP)		
0.5022	0.5310	0.5054	0.5395	0.5309	0.4755	01/22/13	
	0.5259	0.4968	0.5113	0.5285	0.4928	02/03/13	
	0.5385	0.5100	0.5265	0.5467	0.6295	05/16/13	
	0.5457	0.5170		0.5782	0.5630	08/20/13	
	0.5395	0.5690	0.5191	0.5395	0.5496	12/06/13	
	0.5435	0.5179	0.4715	0.5521	0.5752	12/18/13	
	0.5658	0.5319	0.5347	0.5700	0.5236	12/24/13	
			0.5180	0.5513	0.5673	02/10/14	
0.5065			0.5208			03/12/14	
			0.4605			07/10/14	
			0.5833	0.5848	0.5221	08/15/14	
0.5392	0.5597	0.5042	0.4964	0.5488	0.5109	12/13/14	

Appendix I – Discussion on Experimental Issues

The analysis of levoglucosan required copious amounts of solvent and an inordinate amount of time for work-up when compared to the analysis of metals and PAHs. This was due to the necessity of having two solvent swaps and two periods of time where solution concentration was reduced using nitrogen gas. Due to the relatively difficult process involved, it is likely that the final concentration of levoglucosan is lower than what originally came off of the filters. This effect could be reduced if another form of work-up was used. The procedure employed in this project was indicative of popular techniques in the field. However, newer techniques involve using LC-MS or IC-PAD which would reduce workup time and cost and be a greener procedure.

The analysis of PAHs is dependent upon the sampling technique. In order to obtain a more realistic sample of PAHs in the environment, passive sampling and active sampling must be used in tandem. Therefore, the use of only active sampling methods in this project prevents the data being obtained from being completely accurate.

The decision to analyze metals was made after observing the importance of potassium concentrations in source apportionment studies. The determination of the many trace metals could be eliminated in further studies as the concentrations obtained did not add to the knowledge about air quality in the Dayton area.